SMD 2024

THE SWEDISH MECHANICS DAYS

GOTHENBURG 17–19 JUNE

The conference series *Svenska Mekanikdagarna* (Swedish Mechanics Days) has been arranged by the Swedish National Committee for Mechanical Engineering since 1974.

Here, you find the proceedings of the 28th edition of the Swedish Mechanics Days (SMD2024) hosted at Chalmers University of Technology in Gothenburg on 17–19 June 2024.

Organising Committee:

Fredrik Larsson
Niklas Andersson
Lars Davidson
Magnus Ekh
Mikael Enelund
Peter Folkow
Ragnar Larsson

SMD 2024 collaborators:

City of Gothenburg

CHALMERS UNIVERSITY OF TECHNOLOGY | Area of Advance MATERIALS SCIENCE

Studentlitteratur

CHALMERS UNIVERSITY OF TECHNOLOGY | Area of Advance TRANSPORT

The Odqvist Lecture 2024

Gasser T. C.: Vascular biomechanics and its translation into modern health care 5

Plenary Lectures

Pons A.: "Entomechanics" - the mechanics and multiphysics of insects 6
Sebben S.: High-fidelity simulations to access the aerodynamic performance of road vehicles 7
Wallin M.: Strategies for topology optimization beyond linear elasticity 8

Bio-Mechanics

Carlsson J.: The role of boundary conditions in crack propagation in cortical bone 9
Christierson L.: Simulation of healthy patient-specific mitral valves using fluid-structure interaction: validation against in vivo data 10
Gustafsson A.: Automatic crack detection for fracture testing of compact bone 11
Holmberg J.: Finite element prediction of screw pull-out failure using bone-like polyurethane foam 12
Li P.: Pulsatile breathing conditions effects on a simplified three-dimensional human soft palate 13

Fluid Mechanics

Abali B. E.: Filling of thermosetting polymers during curing 14
Bhardwaj S.: On the convergence of cylindrical shock wave 15
Davidson L.: Improving an explicit algebraic stress model using neural network 16
Hederberg H.: Large-scale fluid-structure interaction topology optimization of a hydraulic system component 17
Lindborg E.: Rayleigh-bénard convection at high Rayleigh number and low aspect ratio 18
Mark A.: Simulation of viscoelastic flows applied to hemming 19
Moosavi A.: Flow disturbing structures for air-cooled battery thermal management systems 20
Thore C.: Multiphysics topology optimization for optimal internal cooling 21

Mechanical and Vehicle Engineering

Delmotte H.: Blast response of composite plates in barrel experiment 22
Deylaghian S.: Study of electric and friction braking at low-speeds 23
Johansson A.: Performance analysis of a hydrogen fuelled composite cycle aeroengine 24
Pai Y.: Fault diagnosis of single rotor system using rigid-flexible hybrid modelling 25

Solid Mechanics

Afshar R.: Methodology for evaluation of long-term mechanical properties of polymers 26
Andersson B.: Simulation-based assessment of railhead repair welding process parameters 27
Ansin C.: Efficient simulation of evolving plasticity in rails using reduced order modelling 28
Assis Da Silva G.: Stress-constrained topology optimization with the augmented Lagrangian method 29
Auenhammer R.: Predicting the stress response and failure of natural fibre composites with generative adversarial networks based on x-ray computed tomography three-dimensional images 30
Auth K. L.: Gradient-enhanced phase-field crystal plasticity modeling of ductile failure in polycrystals 31
Ayanoglu M.: Modeling bending stiffness of single-face honeycomb core sandwich specimens 32
Bharali R.: An arc-length method for phase-field fracture models 33
Biel A.: Delamination of paperboard effects of in-plane straining 34
Blixt K.: Exploring grain boundaries in crystalline materials through the phase field crystal method 35
Boman G.: Reduced order multiscale modeling of paperboard 36
Börjesson E.: Variationally consistent homogenisation of plates 37
Dahlberg C.: Neutron imaging of hydrogen embrittlment and serendipity due to experimental constraints 38
Dahlin C.: Modular simulation approach for case hardening of steel 39
Edefors G.: The constitutive response of textile reinforced concrete shells from computational homogenization 40
Granlund G.: Large-scale elasto-plastic topology optimization 41
Gulfo L.: Voxel-based mesostructure modelling of tow-based discontinuous composites for finite element analysis . . . 42
Gustafsson D.: Fatigue life estimation of punched and trimmed specimens 43
Halilovic A.: Fracture toughness characterization of high strength martensitic steels subjected to hydrogen 44
Haveroth G. A.: Optimizing scanning strategies for additive manufacturing processes 46
Hertelendy K.: Explicit and implicit simulation of UD-fibre composites loaded in compression 47
Hård D.: Multi-material topology optimization of EAP and electrodes 48
Jacobsson E.: A level set approach to modelling diffusional phase transformations under finite strains: an application to Cu_6Sn_5 formation 49
Jonsson S.: Studying the rate effects on plane stress fracture toughness in press hardening steel sheets 50
Katsivalis I.: Compressive properties of tow-based discontinuous composites 51
Klein D. V.: Effects of toughness variations in ringhals 4 pressurizer weld on brittle fracture toughness 52

Larsson C.: Modelling and calibration of structural battery full cells . . . 53
Larsson F.: Mechanical testing of a novel thick UHSS intended for warm forming . . . 54
Larsson J.: Influence of temperature gradients and microstructure on hot-rolled sheet and strip . . . 55
Larsson R.: Subscale modelling of metal cutting . . . 56
Lee J.: Particle swarm optimization of a tripod shaped support structure for preliminary design of floating offshore wind turbines . . . 57
Liu L.: Mesostructural characterisation and modelling of closed-cell foams: impacts of cell anisotropy and cell wall thickness profile . . . 58
Meyer K. A.: Modeling mortar as a reactive porous medium and calibration via in-situ xrct experiments . . . 59
Möglich A.: Crack propagation analysis in electroactive polymers using a phase field fracture model . . . 60
Oddy C.: Is it damage, plasticity, rate dependence or all of the above? characterising and modelling the non-linear behaviours of 3D-fabric reinforced composites . . . 61
Olsson E.: Fatigue strength assessment of press hardened chassis members . . . 62
Piiroinen P.: Noisy boundaries and stochastic saltation matrices . . . 63
Rydefalk C.: Lateral variations in ZD-properties of liquid packaging paperboard . . . 64
Safranoglou V.: Notched performance of tow-based discontinuous composites . . . 65
Sandin O.: Using the particle finite element method for predicting optimum shear cutting clearance . . . 66
Strömberg N.: A two-players game for multi-scale topology optimization of static and dynamic compliances of TPMS-based lattice structures . . . 67
Suarez L.: Simulation of brittle fracture: an application for comminution . . . 68
Subasic M.: Corrosion fatigue of hollow cylindrical specimens in simulated LWR environment . . . 69
Talebi N.: Simulation methodology for predicting initiation of surface cracks in railway rails . . . 70
Tavares Da Costa M. V.: Four-point bending in paper-based sandwich beams: experimental and modelling aspects . . . 71
Tkachuk A.: Impact stress in a rock drilling machine piston . . . 72
Tkachuk M.: Discrete network model for irreversible deformation of needle-punched nonwoven fabrics . . . 73
Tojaga V.: Toward simulating fracture in large particle systems . . . 74
Ullrich A.: Modelling of industrial applications with a DEM-FEM coupling algorithm . . . 75
Vieira Lima F.: Studying hydromechanics of heterogenous porous sandstone using advanced experiments and digital twin modelling . . . 76
Wang S.: A non-local gurson model with two fracture-mechanism associated length scales . . . 77

Sound and Vibration

Boström A.: Ultrasonic attenuation in polycrystalline materials . . . 78
Yang B.: Nonlinear dynamics of multilayer graphene considering size effects . . . 79

Teaching and Education in Mechanics

Mousavi M.: Mixed reality for educating mechanical engineers . . . 80

Miscellaneous

Dalai B.: Material characterization of a high pressure die cast secondary aluminum alloy . . . 81

VASCULAR BIOMECHANICS AND ITS TRANSLATION INTO MODERN HEALTH CARE

T. Christian Gasser[1]

[1]*Department of Engineering Mechanics, Division of Material and Structural Mechanics, KTH Royal Institute of Technology, Stockholm, Sweden*

Regardless great advances in diagnose, prevention, and treatment of cardiovascular diseases, they remain the leading cause of death and disability worldwide. As the transport of blood and substances therein via a pressurized system, constitutes the primary function of the cardiovascular system, it is not surprising that mechanics is fundamental to the understanding of cardiovascular health and disease. An incredibly large body of literature therefore reports the subtitle coupling between mechanical factors, such as stress and strain, and biological responses, such as gene expression and tissue growth [1,2,3]. In addition, fracture, a process fundamental to the understanding of material properties and the design of man-made structures, is also intimately linked to the development of vascular pathologies and clinical events, such as stroke and cardiac infarction.

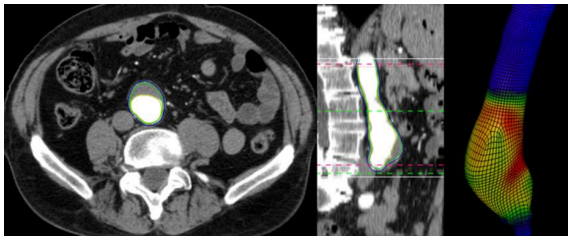

Figure 1: Semi-automatic AAA wall stress computation directly from Computed Tomography-Angiography (CT-A) images [7].

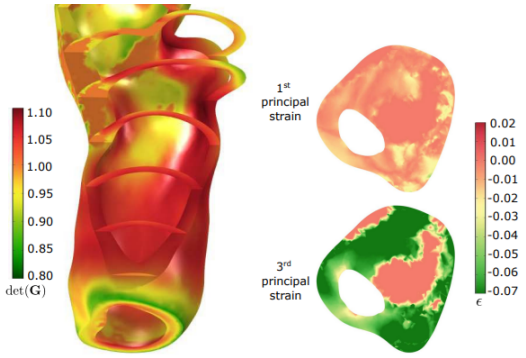

Figure 2: Biomechanical parameters of an atherosclerotic carotid artery [6]. Determinant of the growth tensor indicating local volume change (left) and first and third principal residual strain (right).

This Odqvist lecture summarizes our laboratories' efforts in studying different aspects of vascular tissue biomechanics, most of which towards assessing the life-threatening risk carried by abdominal aortic aneurysms (AAA) (see Figure 1) or atherosclerotic carotid blood vessels (see Figure 2), respectively. The development of numerical tools [4,5,6] together with clinical studies [7,8] and novel laboratory experiments [9] (see Figure 3) determines our efforts in the characterization of vascular tissue properties and the study of clinically relevant problems.

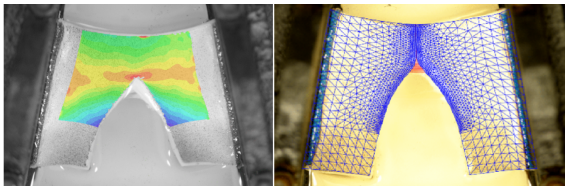

Figure 3: Symmetry-constraint Compact Tension (symconCT) test to explore the fracture properties of aortic wall tissue [9]. Digital Image Correlation (DIC) full-field strain measurements (left) and FEM predictions using a cohesive fracture model (right) are superimposed on the test specimen.

Regardless first translations of vascular biomechanics research into clinical applications [9], much more basic (university) research is needed to better understand how biomechanical and biological factors interact, information that then helps to design patient-individual therapies and better medical devices.

References

[1] M. Bäck, et al. Spotlight Review, Cardiovasc Res, 99, 2013.
[2] T.C. Gasser. Vascular Biomechanics. Springer. DOI 10.1007/978-3-030-70966-2, 2021.
[3] T. Seime, et al. Cells 18, 2022.
[4] C. Miller et al. J Mech Phys Solids, 169, 2022.
[5] A. Buckler, et al. Art. Throm. Vasc. Biol., 41, 2021.
[6] A. Mastrofini, et al. Ann Biomed Engrg. 2024.
[7] T.C. Gasser, et al. Eur J Vasc. Endovasc Surg, 40, 2010.
[8] M. Lindquist Liljeqvist, et al. Sci Rep, 11, 2021.
[9] M. Alloisio, et al. Acta Biomat 167, 2023.
[10] ARTEC, https://www.artecdiagnosis.com/

Corresponding author email: gasser@kth.se

"Entomechanics"—the mechanics and multiphysics of insects

A. Pons[1]

[1]*Division of Fluid Dynamics, Department of Mechanics and Maritime Sciences, Chalmers University of Technology, Gothenburg, Sweden*

Nobody who has swatted a fly, trod through a cloud of midges, or been bitten by a tick has failed to be impressed—and possibly infuriated—by the extraordinary mechanical capabilities of insects. Over an evolutionary history spanning over three hundred million years, insects have lived, walked and flew at scales ranging from less than a millimetre to over half a metre. Insects are now found everywhere on Earth's surface: on every continent; at every terrain altitude, and even out on the open ocean. They comprise over half of all terrestrial species, yet at the same time, their biodiversity is threatened by pesticide use, habitat loss, and climate change—in ways that we still do not fully understand.

Entomology, the study of insects, is replete with challenging problems in mechanics: across structural mechanics, aerodynamics, biomechanics, and more. Tackling these problems not only gives us insight into ecology and evolution; but also opens pathways to advances in theoretical and applied mechanics, and in robotics. In this talk, we'll survey problems and advances in "entomechanics"—including:

- The counterintuitive properties of resonance in strongly damped oscillators, and how these properties yield insight into the mechanics of the insect flight drivetrain [1] (Fig. 1).
- Work-loop techniques for analysing energy-efficiency in forced oscillators: how these techniques allow us to prove new theoretical results in linear and nonlinear systems, and can explain previously-unexplained features of insect wingbeat patterns [2,3].
- The highly-adapted behaviour of insect flight muscle: how these muscles can be characterised as active viscoelastic structures and how insect wingbeats arise from self-oscillation [4].
- The paradox of rate-independent damping models of insect exoskeleta, and how these models lead to open problems in the study of integral transforms.
- And, finally, the ways in which we can leverage advances in entomechanics to improve insectoid robot designs (Fig. 2)

In overview: the mechanics and multiphysics of insects is more than only an interesting new area to apply engineering techniques. It pushes us toward new theoretical results and new analysis methods; forges new connections between mechanics and fundamental challenges in zoology, ecology and biodiversity conservation; and raises the prospect of unique robot designs.

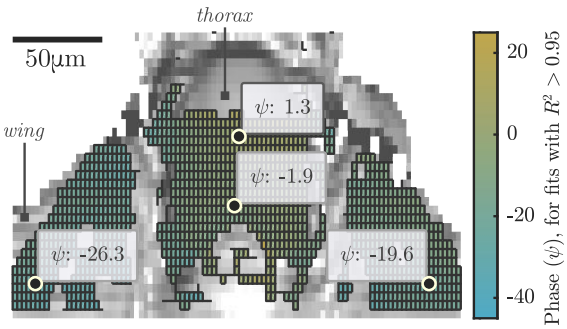

Figure 1: Phase relationships though the flight motor of a hawkmoth (*Agrius convolvuli*) revealed via laser profilometry [1].

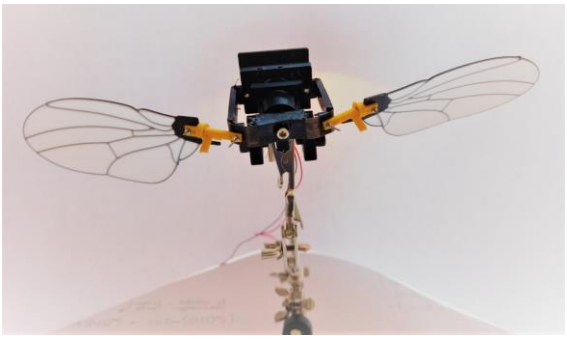

Figure 2: Insectoid robot at CHALMERS.

References

[1] Pons, A., and Beatus, T., 2022, "Distinct Forms of Resonant Optimality within Insect Indirect Flight Motors," J. R. Soc. Interface, 19(190).

[2] Pons, A., Perl, I., Ben-Dov, O., Maya, R., and Beatus, T., 2023, "Solving the Thoracic Inverse Problem in the Fruit Fly," Bioinspir. Biomim., 18(4), p. 046002.

[3] Pons, A., and Beatus, T., 2023, "Band-Type Resonance: Non-Discrete Energetically Optimal Resonant States," Nonlinear Dyn., 111(2), pp. 1161–1192.

[4] Pons, A., 2023, "The Self-Oscillation Paradox in the Flight Motor of *Drosophila Melanogaster*," J. R. Soc. Interface, 20(208), p. 20230421.

Corresponding author email: arion@chalmers.se

HIGH-FIDELITY SIMULATIONS TO ACCESS THE AERODYNAMIC PERFORMANCE OF ROAD VEHICLES

S. Sebben[1], A. Brandt[2]

[1]*Department of Mechanical and Maritime Sciences, Chalmers University of Technology, Gothenburg, Sweden*
[2]*China Euro Vehicle Technology AB, Gothenburg, Sweden*

Legislations and customers awareness of the negative effects of transportation on the global climate are driving the development of more energy efficient vehicles. One of the key factors influencing energy efficiency is the aerodynamic drag. Although streamlined cars are desirable from an efficiency perspective, they might impair instabilities which can be perceived as a vehicle nervous to drive. The assessment of driving stability of a vehicle is often done on test tracks in late project phases when a prototype is available. Late design changes are costly, and with demands on shorter lead time to launch new products, vehicle manufactures require robust virtual tools for earlier assessment of stability.

In this work, high-fidelity numerical simulations of a full-scale vehicle at relevant Reynolds number and realistic driving conditions are performed using a hybrid turbulence model and the commercial CFD code Ansys Fluent. The dynamics of the base wake and the temporal fluctuations of the aerodynamic lift are analysed and coupled to the driver's perception of stability for two versions of a roof spoiler. For the simulations, unstructured, hexahedral dominated meshes of 200-300 million cells with 10 to 15 prism layers on the vehicle surfaces and ground were used with second order temporal and spatial discretization schemes. Mesh and time dependence studies were conducted and considered a compromise between lead time and accuracy.

From prior field tests, it was known that the baseline spoiler caused stability issues, while the improved spoiler had good performance at high speeds. From simulations, both spoilers showed time-averaged lift coefficients within the set requirements. However, the CFD analysis revealed the importance of considering the unsteady rear lift fluctuations, C'_{lr}, as these could be associated with frequencies prone to induce the vehicle instabilities observed on the road. Figure 1 shows that the baseline spoiler (blue) experiences higher amplitude of fluctuations in the sensitive frequency range for vehicle dynamics (0.5-2 Hz), particularly with yaw (only 5 deg shown here).

The unsteady vertical base pressure gradient was monitored on several positions at the vehicle base and is plotted as probability density function (PDF) in Figure 2. It shows that the wake of the baseline spoiler (blue) has two states, H and L, representing the wake dynamics that generates high and low rear lift forces. The improved spoiler (red) has only one state with a higher vertical base pressure, indicating more upwash, and thus lower rear lift. This behaviour was connected to the driver's perception of instability during field tests. The lateral base pressure gradient was also monitored but showed a single state.

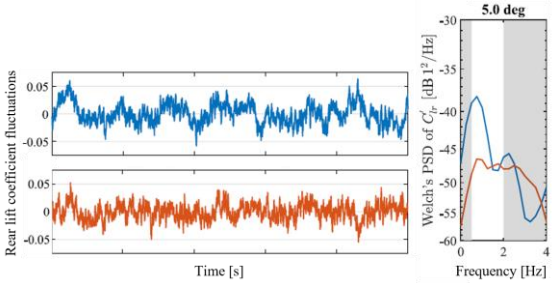

Figure 1: Rear lift fluctuations for the baseline spoiler (blue) and the improved spoiler (red) for 5 deg flow angle, and Welch's PSD frequency response [1].

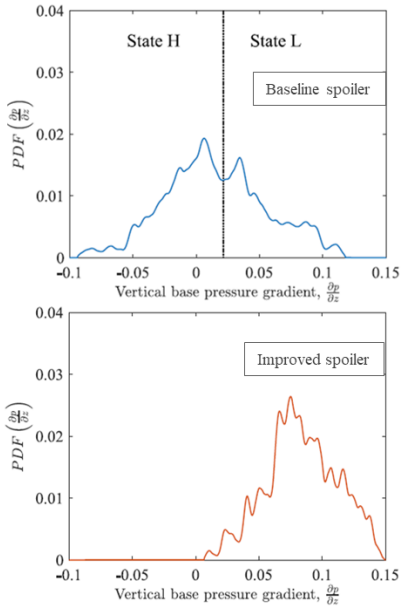

Figure 2: Probability density function of the vertical base pressure gradient at 5 deg [1].

Finally, the improved spoiler increased drag for all flow angles, but with a lower sensitive to yawed flow.

References

[1] Brandt, A., Sebben, S., and Jacobson, B., Base wake dynamics and its influence on driving stability of passenger vehicles in crosswind. *J Wind Engineering and Industrial Aerodynamics*, https://doi.org/10.1016/j.jweia.2022.105164

Corresponding author email: simone.sebben@chalmers.se

STRATEGIES FOR TOPOLOGY OPTIMIZATION BEYOND LINEAR ELASTICITY

Mathias Wallin[1]

[1]*Division of Solid Mechanics, Lund Institute of Technology, Lund, Sweden*

During the last three decades there has been a tremendous development of numerical methods tailored for optimal design of materials and structures. Topology optimization (TO) has been applied problems at the engineering scale as well as to design of micro-structures to render exotic properties such as materials with negative Poisson's ratio and negative thermal expansion on the macro-scale. The method has not only been applied to elastic problem but it has also proven to be useful to design structures optimal for thermal, fluid and wave propagation. Even though non-gradient based optimization algorithms do exist they have due to their large computational cost not won widespread acceptance and methods that rely on gradient information are dominating. In the first part of the talk a short overview of the basic concepts needed to perform a topology optimization will be presented. Ingredients that will be introduced are: design representaion, material interpolation, regularization, sensitivity analysis and opimization solver.

Complex, non-linear path-dependent and transient response of engineering structures can today numerically be modeled with good accuracy. For linear systems, this modeling has for a long time successfully been combined with computational design optimization. The combination of non-linear modeling and numerical design optimization is, however, less established. In the present talk we discuss some recent steps taken to close the gap between modeling of non-linear modeling and numerical optimization. Topics that will be discussed include:

Topology optimization of non-linear elastic structures. The generalization to from small strain elasticity to finite strain elasticity is non-trivial. One issue is the generalization of the 'stiffness' which is non unique. In the talk, we will discuss the influence of the stiffness measure definition. Another issue that needs to be addressed is the question of how to model the void elements such that they do not detoriate the convergence of the state solve. A number of examples including stress and eigenvalue constraints that demonstrate the possibility to optimization hyper-elastic will be discussed.

Toplogy optimization of transient problems. When the load duration is short, transient effects can play a significant role. This phenomena will be demonstrated via design of multimaterial compliant fast sensors that are modeled using coupled thermo-hyperelasticity. The required gradients needed for the design updates are based on the adjoint sensitivity methods which will be discussed in detail. An example of a compliant mechanism optimized for different load durations is shown in Fig. 1.

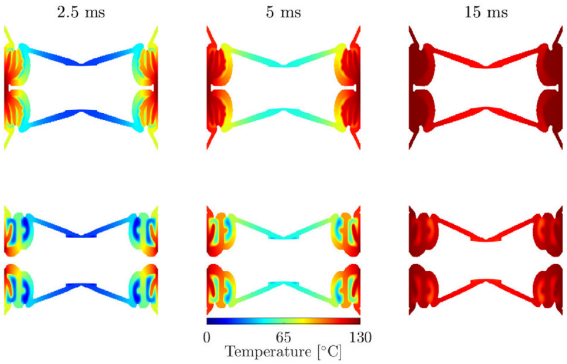

Figure 1: Compliant gripper optimized under transient conditions. From Granlund et al. 2023.

Toplogy optimization of irreversible structures. In the final part of the talk we will discuss TO of irreversible materials and structures. The optimization will be used to design structures that are optimized for maxium energy absorbtion, minimal peak plasticity and structures with a tailored response. Due to the significant computational cost associated with the optimization problem we will discuss efficient large scale implementations that allows optimization of high resolution designs.

Corresponding author: mathias.wallin@solid.lth.se

THE ROLE OF BOUNDARY CONDITIONS IN CRACK PROPAGATION IN CORTICAL BONE

J. Carlsson, O. Karlsson, H. Isaksson, A. Gustafsson

Department of Biomedical Engineering, Lund University, Lund, Sweden

Normal ageing, as well as diseases, have adverse effects on the quantity and quality of bone in our skeletons. To identify patients with increased fracture risk, it is important to understand how ageing affects the damage mechanisms in bone.

Computational fracture mechanics is a useful tool to investigate the effect of changes in bone quality and their relation to bone fracture susceptibility. To develop meaningful computational models, validation by comparison to experimental studies is vital. Experimental results are typically obtained from notched three-point bend tests, whereas most computational studies to date consider pre-cracked plates under tensile displacement boundary conditions, often on geometries whose edges measure only about 1 mm, cf. e.g. [1]. Our objective is to investigate the impact of the boundary conditions upon strain distributions and crack paths in finite element simulations of fracture of cortical bone.

We investigate fracture of cortical bone microstructures numerically using phase-field finite element models implemented in Abaqus [2]. The microscale models consist of 1.2x1.2 mm cross sections of human compact bone tissue. The different microstructural features: osteons (containing the hollow haversian canal), cement lines and interstitial matrix (Fig. 1) have been segmented by hand [3] and assigned individual mechanical properties. Each geometry contains a pre-crack of 0.1 mm length. The models are subjected to either tensile displacement boundary conditions or embedded in a beam of homogeneous linear elastic material of similar elastic modulus as the microscale model subjected to notched three-point bending.

The results show that the associated fracture behaviours differ between the two sets of boundary conditions. The stress singularity of the crack tip is more pronounced in the embedded models, which also affects the observed crack paths (Fig. 1). This is important, as a good agreement between experimental and simulated boundary conditions enables further studies into the properties of the constituents of the cortical bone microstructure, as well as the role of this microstructure in bone fragility.

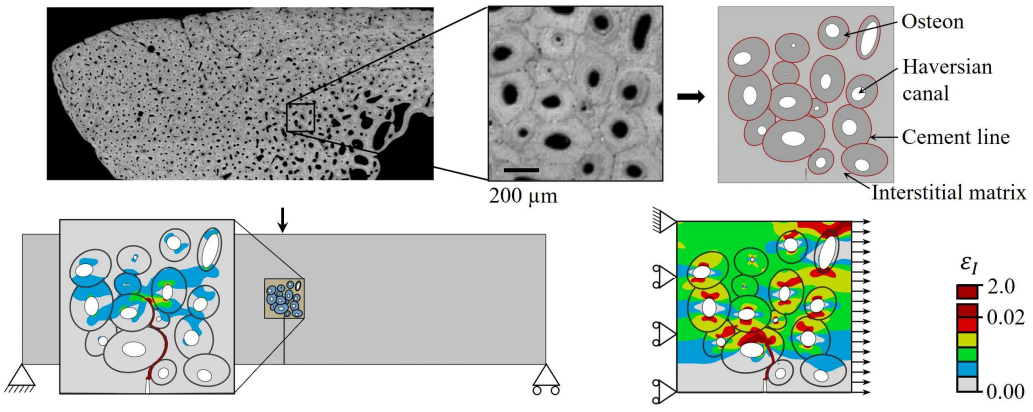

Figure 1: Top: Workflow for creating the microscale models by segmentation, by Gustafsson et al. [3]. Bottom: Boundary conditions and contours of first principal strain during crack propagation for the two sets of boundary conditions. (Colourbar refers to all contour plots.)

References

[1] Maghami, E., Josephson, T.O., Moore, J.P., Rezaee, T., Freeman, T., Karim, L., Najafi, A.R. Fracture behavior of human cortical bone: Role of advanced glycation end-products and microstructural features. *Journal of Biomechanics,* 110600, (2021).

[2] Karlsson, O. *The investigation of crack propagation in cortical bone using a phase field fracture approach.* Master's thesis in Biomedical Engineering. Lund University (2022).

[3] Gustafsson, A., Wallin, M., Isaksson, H. Age-related properties at the microscale affect crack propagation in cortical bone. *Journal of Biomechanics*, 95, 109326, (2019).

Corresponding author email: jenny.carlsson@bme.lth.se

Simulation of Healthy Patient-specific Mitral Valves using Fluid-Structure Interaction: Validation against in vivo Data

L. Christierson[1,3], P. Frieberg[2], H. Isaksson[3], J. Revstedt[4], P. Liuba[1] and N. Hakacova[1]

[1]*Dep. of Clinical Sciences Lund, Pediatric Heart Center, Skåne Univ. Hospital, Lund University, Sweden*
[2]*Dep. of Clinical Sciences Lund, Clinical Physiology, Skåne Univ. Hospital, Lund University, Sweden*
[3]*Dep. of Biomedical Engineering, Lund University, Sweden*
[4]*Dep. of Energy Science, Lund University, Sweden*

Heart valve disease is commonly identified as a contributor to heart failure. Specifically, the mitral valve (MV) is subjected to the highest loads within the heart, and when affected by structural abnormalities or ventricular dysfunction due to heart disease, stenosis or insufficiency can arise [1]. Distinguishing the underlying factors contributing to valve pathologies and predicting the outcomes of valve interventions remains challenging [2]. Simulation models have the possibility to enhance our understanding of valvular dynamics and predict the outcomes of valve repair. Previous research has demonstrated the accuracy of fluid-structure interaction (FSI) simulations for clinical applications [3]. The aim of this study is to further develop and validate the computational framework, using FSI, to simulate patient-specific mitral valves to investigate the velocity through the valve, the valvular dynamics, and the valve leaflet strain. The simulation results will be validated against echocardiography (Echo) data.

Ten (n=10) healthy volunteers, aged 19 ± 10.3 years, have so far been recruited. The patient-specific MV geometry was obtained from 3D Echo data with an automated segmentation process (4D MV assessment, TOMTEC Imaging Systems GmbH) and inserted into a generic left heart model. The 0.8 mm thick valve leaflets were meshed using first-order tetrahedral elements and the flow domain was meshed using hexahedral elements, using the Chimera overset method to allow large deformations of the valve. The contraction of the heart was numerically modeled by applying a patient-specific mass flow boundary condition at the apex of the heart, derived from the ventricular volume change. The boundary at the MV was set to a zero-pressure outlet and the boundary at the aortic valve was set to a zero-pressure boundary during systole and to a wall condition during diastole. The FSI coupling was created with the software Star-CCM+ and Abaqus/Standard. The MV tissue and chordae tendineae were modeled as linear elastic with Young's modulus of 1 MPa and 22 MPa. The Carreau model was employed to model the blood viscosity behavior, assuming laminar flow. The blood density was set to 1060 kg/m^3 and modeled as compressible to ensure numeric stability.

Results show satisfactory agreement of the valvular dynamics during the systolic phase, 0-29 % of the cardiac cycle, compared with Echo data, Fig. 1. The simulated valve starts to close after the filling phase of diastole at 45 % of the cardiac cycle when it is expected to close at the next contraction. The maximum valve opening differs by 9 %, and the mean trans-valvular velocity differs by 18 % compared to Echo data, Fig. 1. Further improvements lie in the material modeling of the MV, for improved estimation of the valve opening and thus, the velocity estimation. We believe the model has the potential to predict person-to-person differences in patient-specific simulations.

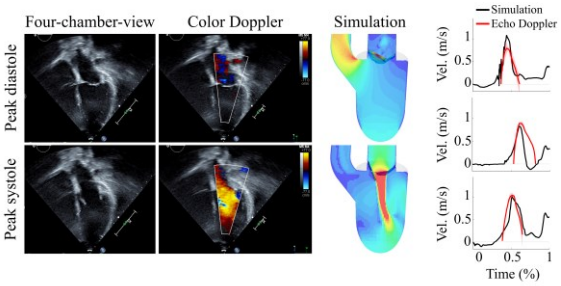

Figure 1: The images show the comparison of the simulation results against Echo data for the velocity distribution at peak systole and peak diastole. The graphs show the velocity through the valve measured by Echo Doppler (red) and computed by the simulations (black) for three of the cases.

References

[1] Wood, A. et al, Mitral valve reconstruction in a pediatric population: Late clinical results and predictors of long-term outcome, *J. Thorac. Cardiovasc. Surg.*, 130, 66-73, (2005)

[2] Chandran, K., Role of Computational Simulations in Heart Valve Dynamics and Design of Valvular Prostheses. *Cardiovasc Eng Technol*, 1, 18-38, (2010)

[3] Christierson, L. et al, Validation of fluid-structure interaction simulations of the opening phase of phantom mitral heart valves under physiologically inspired conditions, *Comput. Biol. Med.,* 171, 108033 (2024)

Corresponding author email: lea.christierson@med.lu.se

AUTOMATIC CRACK DETECTION FOR FRACTURE TESTING OF COMPACT BONE

A. Gustafsson[1], G. Galteri[1,2], A. Barakat[1], J. Engqvist[3], L. Grassi[1], L. Cristofolini[2], H. Dejea[1], H. Isaksson[1]

[1]*Department Biomedical Engineering, Lund University, Sweden*
[2]*Department Industrial Engineering, Alma Mater Studiorum-University of Bologna, Italy*
[3] *Division of Solid Mechanics, Lund University, Sweden*

Age and degenerative diseases compromise the integrity of bone and increase the risk of fracture. Understanding bone fragility requires unraveling the links between fracture resistance and bone composition and structure. Standards methods for fracture testing that use empirical relationships to estimate crack length from unloading compliance are not well-suited for bone [1]. Alternative methods typically require manual identification of the crack tip from microscopy images, which is both non-standardized and time consuming [1]. We therefore explored an optical method for automatic crack detection [2] and analyzed how fracture resistance relates to bone microstructure (Fig. 1B). We combined fracture testing with high resolution imaging and hypothesized that crack tortuosity is correlated to fracture resistance.

Notched beam specimens (2x4x25mm) were cut from compact cow bone in three orientations (Fig. 1A): LT (n=10), RT (n=10) and TL (n=9). The initial notch was sharpened with a scalpel (1.47±0.16 mm). Three-point bending tests (span=16 mm) to failure were performed (Instron 8511) [1,3] in combination with 2D-Digital Image Correlation (Vic 2D, Correlated Solution, image acquisition 1 Hz).

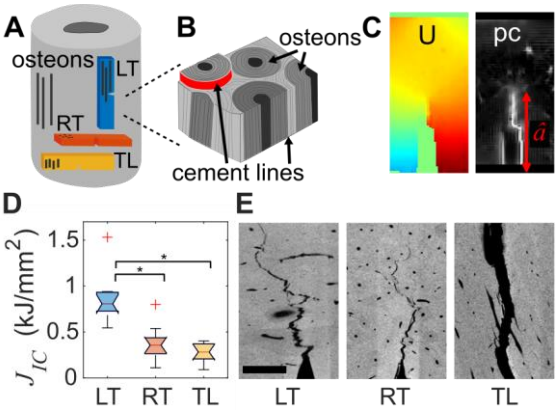

Figure 1: **A**) Notched beam specimens in three orientations: LT, RT, TL. **B**) Compact bone tissue reinforced with osteons. **C**) Automatic crack detection ($\hat{a}$) using phase congruency (pc) analysis of the displacement field (U). **D**) Critical fracture energy for crack initiation (J_{IC}). **E**) Representative crack paths. Scalebar 500 µm.

Fracture toughness (J-R-curve) was analyzed following ASTM E1820 and [1], where crack growth was automatically tracked based on the phase congruency (pc) of the displacement field (Fig. 1C) [2]. A subset of 17 specimens were scanned with high resolution x-ray tomography post-testing (Zeiss Xradia, voxel size 6.5 µm) to analyze the crack tortuosity. Data were compared using linear mixed-effect models.

We show that pc analysis combined with 2D-Digital Image Correlation can be used to automatically track stable crack extension in cortical bone during testing. Fracture toughness was significantly higher in LT specimens compared to the other tissue orientations (Fig. 1D). Crack tortuosity, as illustrated in Fig. 1E, was significantly different for all three groups (LT > RT > TL) and correlated to fracture resistance (R^2=0.52). Yet, RT and TL had similar fracture toughness albeit the higher crack tortuosity in RT. This shows that crack deflections around osteons in RT, following the weak cement line interfaces, are not efficient toughening mechanisms (Fig. 1E). Importantly, this data set enables future validation of computational models that precedes current literature. Using e.g. phase field models [4], we will strive to explore physical failure mechanisms, which will substantially contribute to our understanding of bone fracture.

References

[1] Dapaah, D., and Willett, T., A critical evaluation of cortical bone fracture toughness testing methods, *JMBBM*, 134:105419, 2022

[2] Cinar, A.F. et al, An autonomous surface discontinuity detection and quantification method by digital image correlation and phase congruency, *Opt Laser Eng*, 96:94-106, 2017

[3] Yadav, R.N. et al, Effect of ageing on micro-structure and fracture behavior of cortical bone as determined by experiment and Extended Finite Element Method (XFEM), *Med Eng Phys*, 93:100-112, 2021.

[4] Gustafsson, A., and Isaksson, H., Phase field models of interface failure for bone application - evaluation of open-source implementations, *Theor Appl Fract Mech*, 121, 2022.

Corresponding author email: anna.gustafsson@bme.lth.se

FINITE ELEMENT PREDICTION OF SCREW PULL-OUT FAILURE USING BONE-LIKE POLYURETHANE FOAM

A. Azeez[1], J. Xu[2], M. Calmunger[2], D. Wezenberg[3], J. Schilcher[3], J. Stålhand[1], LJ. Holmberg[1]

[1]*Division of Solid Mechanics, IEI, Linköping University, Linköping, Sweden*
[2]*Division of Engineering Materials, IEI, Linköping University, Linköping, Sweden*
[3]*Division of Surgery, Orthopedics and Oncology, BKV, Linköping University, Linköping, Sweden*

Osteoarthritis is a leading cause of disability in elderly. Around 25% of the Swedish population over 45 is affected and need total hip replacement. In revision surgery, screws are required for a stable fixation and osseointegration [1]. Screw pull-out failure lead to fixation loss. Thus, understanding and prediction of screw pull-out is necessary to the development of improved fixation. In this work, nonlinear explicit finite element (FE) analysis is utilised to predict experimental pull-out tests of titanium screw, Stryker 6.5mm low profile hex screw, in a bone-like solid rigid polyurethane foam, Sawbones® of 0.32 g/cc density. Tensile and compressive tests were performed using dog-bone specimens made of the polyurethane foam, see Figure 1. The data from these tests were necessary to calibrate a nonlinear hyperelastic material model for foam.

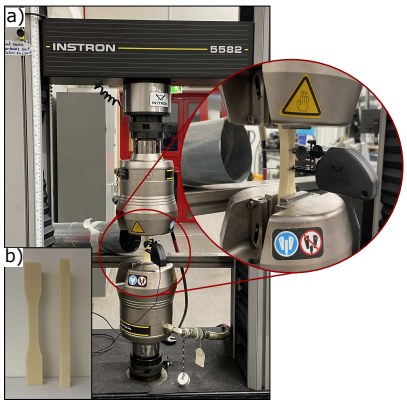

Figure 1: a) Instron 5582 testing rig used for all the experimental tests. b) Dog-bone specimen.

The FE model consisted of a cylindrical foam with a screw inserted at the middle, see Figure 2. Only the screw threads inside the foam were modelled as shown in Figure 2b. The cylindrical foam was clamped at the outer ring area while the sectioned screw head was fixed in the transverse directions to avoid bending. Pull-out force was applied on the screw using a reference node and contact condition was added between screw and foam (Figure 2). To predict the thread failure, a damage criterion was set to remove elements of the foam when the maximum principle stress pass a threshold value defined from the tensile tests. Linear tetrahedron element were used with very fine mesh near threads. To reduce simulation run-time, both mass and time scaling were utilised.

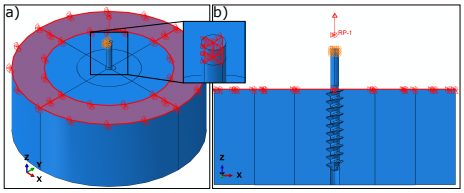

Figure 2: FE model of the screw pull-out showing: a) boundary conditions and b) side cut view.

The results obtained from the simulations are shown in Figure 3 where comparable pull-out force to the experimental tests can be seen. The foam damage at the maximum screw pull-out force is shown in Figure 4.

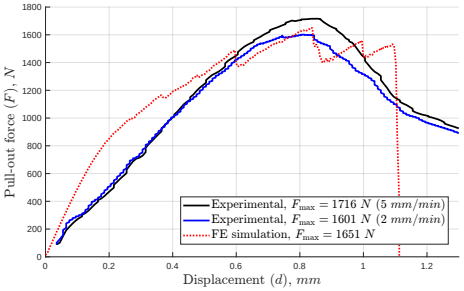

Figure 3: Experimental and FE predicted screw pull-out force versus axial displacement.

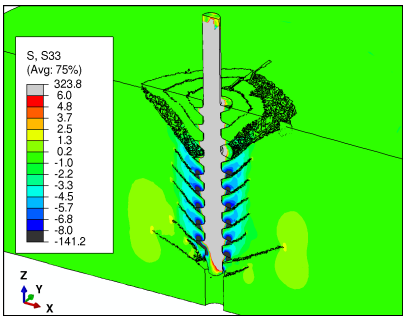

Figure 4: Side cut view of FE model showing stress field and element deletion at the maximum pull-out load.

References

[1] Pilliar, R., Lee, J., Maniatopoulos, C., Observations on the effect of movement on bone ingrowth into porous-surfaced implants. Clin. Orthop. Relat. Res., 208, 108–113, (1986)

Corresponding author: joakim.holmberg@liu.se

PULSATILE BREATHING CONDITIONS EFFECTS ON A SIMPLIFIED THREE-DIMENSIONAL HUMAN SOFT PALATE

P. Li[1], M. Laudato[1], M. Mihaescu[1]

[1]*Department of Engineering Mechanics, FLOW, KTH Royal Institute of Technology, Osquars Backe 18, Stockholm, 10044, Sweden*

Obstructive Sleep Apnea Syndrome (OSAS) manifests as airflow obstruction during sleep, primarily due to the collapse of the upper airway's soft tissues. One common symptom of patients with such sleep-induced apnea is the vibration or collapse of the flexible tissue of the upper airway. Understanding the mechanical behavior of soft palate under airflow conditions is crucial for developing effective clinical interventions. In-vivo measurements are usually challenging. A three-dimensional fluid-structure interaction (FSI) model for the human uvula-palatal system relevant to OSAS based on simplified geometries is utilized in the present study. Numerical simulations are performed to evaluate how gravitational forces and varying pulsatile breathing patterns affect the soft palate's oscillatory behavior. Additionally, the vortex dynamics and the structural frequency response are examined for the coupled fluid-structure system. This research provides insights into the biomechanical phenomena influencing OSAS and supports the design of novel therapeutic strategies.

Corresponding author: penl@kth.se

FILLING OF THERMOSETTING POLYMERS DURING CURING

B. Emek Abali[1] and Sara Florisson[1]

[1]*Division of Applied Mechanics, Dept. of Materials Science and Engineering, Uppsala University, Uppsala, Sweden*

Epoxy based polymers are used in lightweight applications for their low weight and high mechanical stiffness properties. The material, as a resin mixed with hardeners, starts curing under specific conditions by an exothermal chemical reaction. This so-called thermosetting polymer hardens while curing builds a network of polymer chains. Hence, a viscous fluid flow becomes a solid with an increase of degree of cure. Such a phase change, incorporating curing related temperature deviation, is an irreversible process.

Such a system is solved by fulfilling balances of mass, momentum, and energy. Their constitutive equations stem from thermodynamics. Herein, for a viscous fluid flow and temperature, we incorporate non-equilibrium thermodynamics and motivate a thermodynamically compatible evolution equation used for the degree of cure [1].

Temperature and degree of cure are coupled directly and even a measurement procedure may be developed to measure materials response during curing [2]. For a large structure filled with epoxy, the filling procedure may take some time such that the hardening procedure of the epoxy has a significant impact on the residual free filling itself.

Finite Element Method (FEM) is an accurate numerical solution strategy; however, for viscous fluid flow, there exists numerical instabilities that hinders extensive use of the FEM. One possible solution is use different finite elements for velocity and pressure [3], which increases the computational cost significantly. Another method is to employ the same element type and add more conditions on the pressure change. For the latter, we follow [4] that is validated in [5] and add a level-set method for tracking the fluid surface. Therefore, an additional equation is solved alongside the balance equations. Such an addition of level-set method necessitates a robust implementation that is used herein. In this way, the hardening procedure is monitored by the degree of cure and the level of fluid is tracked by the level-set method. A possible optimization of such processes becomes possible with a digital twin of the whole system.

This talk explains the modeling of epoxy in general, starting with a kinetic model [6] for curing and discussing the response, while curing creates a solid from fluid. Such a transition is often modeled by a sharp state change; however, at least in the case of epoxy, there is a more gradual change that makes research needed for this coupled and nonlinear system.

References

[1] B. E. Abali, J. Vorel, and R. Wan-Wendner, "Thermo-mechano-chemical modeling and computation of thermosetting polymers used in post-installed fastening systems in concrete structures," *Continuum Mechanics and Thermodynamics*, vol. 35, pp. 971–989, 2023.

[2] B. E. Abali, M. Y. Yardımcı, M. Zecchini, G. Daissè, F. H. Marchesini, G. De Schutter, and R. Wan-Wendner, "Experimental investigation for modeling the hardening of thermosetting polymers during curing," *Polymer Testing*, vol. 102, p. 107 310, 2021.

[3] V. John, *Finite element methods for incompressible flow problems*. Springer, 2016, vol. 51.

[4] B. E. Abali, "An accurate finite element method for the numerical solution of isothermal and incompressible flow of viscous fluid," *Fluids*, vol. 4, no. 1, p. 5, 2019.

[5] B. E. Abali and Ö. Savaş, "Experimental validation of computational fluid dynamics for solving isothermal and incompressible viscous fluid flow," *SN Applied Sciences*, vol. 2, p. 1500, 2020.

[6] B. E. Abali, M. Zecchini, G. Daissè, I. Czabany, W. Gindl-Altmutter, and R. Wan-Wendner, "Cure kinetics and inverse analysis of epoxy-amine based adhesive used for fastening systems," *Materials*, vol. 14, no. 14, p. 3853, 2021.

Corresponding author: b.emek.abali@angstrom.uu.se

ON THE CONVERGENCE OF CYLINDRICAL SHOCK WAVE

S. Bhardwaj[1], N. Apazidis[1], M. Liverts[1]

[1]*Department of Engineering Mechanics, KTH Royal Institute of Technology, Stockholm, Sweden*

The technique of shock focusing is an efficient way of producing localized high-pressure and temperature conditions in the laboratory. This high energy density in mediums can be used in biomedicine, initiation of nuclear fusion reactions, fragmentation of kidney stones (shock wave lithotripsy), etc. The present study is an experimental and numerical investigation of the phenomenon of shock convergence. The experiments were performed in shock tube operated by a fast-opening valve. The test gas in the experiments was Argon. The study shall present high temporal data of cylindrical shock convergence. Along with experiments, numerical simulation of the flow is performed for comparison.

Figure 1 shows the shadowgraph images (taken at 2 million fps) of the convergence of the cylindrical shock up to its focus. The first image shows the shock when the cylindrical convergence of the shock starts, with shock Mach number (M_0) of 4.6. The last shadowgraph image is at the instant just after the reflection of the shock. The flash of light can be observed at the focus.

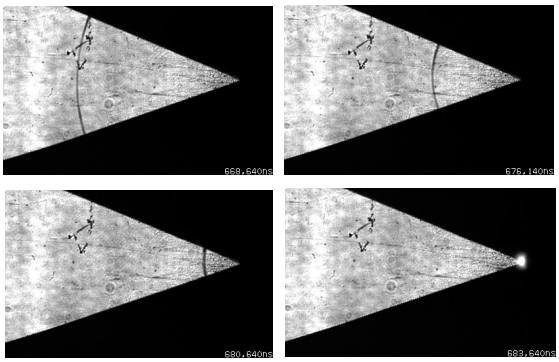

Figure 1: Shadowgraph images of convergence of cylindrical shock wave of Mach 4.6.

In the study, the shock location from the shadowgraph images is tracked and trajectory of the cylindrical shock is traced. In figure 2, the non-dimensional radius of the shock (normalized with initial radius (r_0) of 25.6 mm) is plotted with non-dimensional time (normalized by the time at the instant of shock focusing (t_0)). Along with the experimental data, numerical data, and self-similarity solution of Guderley[1] are plotted. The analytical relation by Guderley is given as:

$$\frac{r}{r_o} = \left(1 - \frac{t}{t_o}\right)^{\alpha}$$

where, r and t are instantaneous radius and time. The exponent α is the similarity exponent. For Argon and cylindrical shock convergence, it is 0.81562. Overall, a fairly good match of the data is obtained.

It is not expected that the experimental and computational data should match the analytical relation due to two main reasons. First, the Guderley solution assumes that the convergence of the shock is self-similar. Previous works in the literature[2] suggest that the Guderley solution is an 'intermediate asymptotic' solution and is applicable only very close to the focus of convergence. Second, the downstream disturbances of the flow travelling on C_+ characteristics influences the motion of the converging shock. These two phenomena shall be described in more detail to understand the mechanisms of shock convergence. Along with this, the data from experiments and computations performed for a range of Mach numbers shall be presented. An interesting trend in the exponent of convergence for different initial shock strength is observed which shall also be presented.

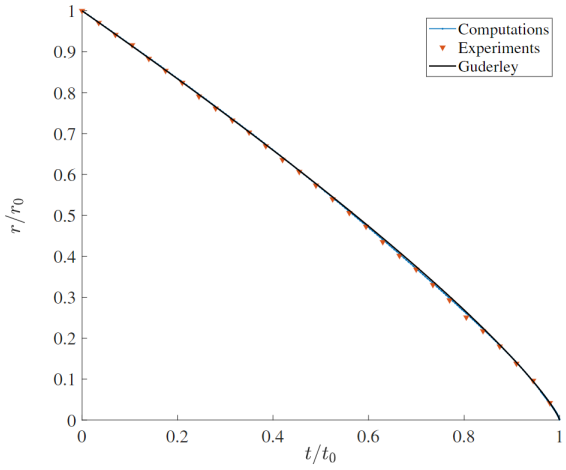

Figure 2: Comparison of the trajectory of cylindrical converging shock.

References

[1] G. Guderley, "Starke kugelige und zylindrische verdichtungsst oe in der n ahe des kugelmittelpunkter bzw. der zylinderachse." Luftfahrtforsch 19 (1942).

[2] Y. Nakamura, "Analysis of self-similar problems of imploding shock waves by the method of characteristics," Phys. Fluids 26, 1234 (1983).

Corresponding author email: sourabhb@kth.se

IMPROVING AN EXPLICIT ALGEBRAIC STRESS MODEL USING NEURAL NETWORK

L. Davidson[1]

[1]*Div. of Fluid Dynamics, Dept. of Mechanics and Maritime Sciences, Chalmers Univ. of Techn., Gothenburg, Sweden*

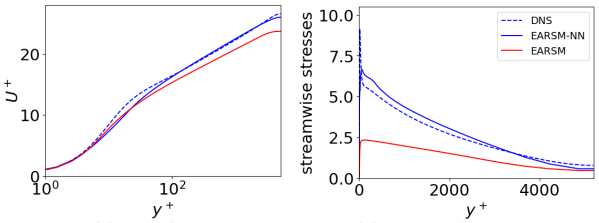

(a) Velocity. **(b)** Streamwise stress.

Figure 1: Channel flow at $Re_\tau = 5\,200$.

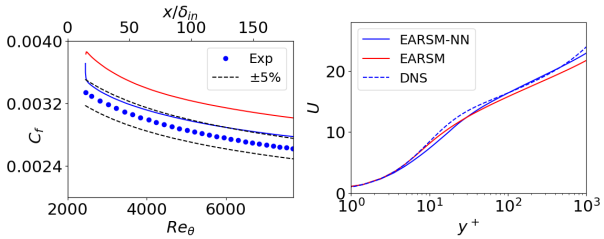

(a) Skin friction. **(b)** Velocity. $Re_\theta = 5\,500$.

Figure 2: Flat-plate boundary layer.

The EARSM

In 2D, the EARSM reads [1]

$$a_{ij} = \beta_1 \bar{s}^*_{ij} + \beta_2 \left(\bar{s}^*_{ik}\bar{s}^*_{kj} - \frac{1}{3}\bar{s}^*_{mn}\bar{s}^*_{nm}\delta_{ij} \right) + \beta_4(\bar{s}^*_{ik}\bar{\Omega}^*_{kj} - \bar{\Omega}^*_{ik}\bar{s}^*_{kj}) \quad (1)$$

where

$$\beta_1 = -\frac{A_1 N}{Q}, \quad \beta_2 = 2\frac{A_1 A_2}{Q}, \quad \beta_4 = -\frac{A_1}{Q}$$
$$Q = N^2 - 2II_\Omega - \frac{2}{3}A_2^2 II_S \quad (2)$$

N is given by a cubic equation, solved analytically.

Instead of computing β_1, β_2 and β_4 from Eqs. 2, I will in the present work make them functions of some input parameter(s) (to be determined) using Neural Network (NN). The process can be depicted as:

1. The production term, $P^{k,+}$ and y^+ are chosen as input parameters
2. The output (target) parameters are β_1, β_2, β_4
3. Train the NN model in fully-developed channel flow, $Re_\tau = 10\,000$.
4. Use the NN model to compute β_1, β_2, β_4 in the EARSM (k and ω predicted with the $k-\omega$ model) in the **pyCALC-RANS** CFD code
5. The new model is denoted EARSM-NN.

Figure 1 presents the predicted velocity and streamwise Reynolds stress using the EARSM (Eqs. 1 and 2) and the EARSM-NN model and the agreement for the EARSM-NN is much better.

Next, the flat-plate boundary layer is studied. A precursor $k-\omega$ simulation of a flat-plate boundary layer is carried out and U, V, k and ω are stored at $Re_\theta = 2\,500$ where θ denotes the boundary-layer momentum thickness. These stored data are used as inlet boundary condition in the subsequent flat-plate boundary-layer simulations using the two EARSM models. Figure 2 show the predicted skin friction. The EARSM-NN predicts C_f within 5% of experimental data whereas the EARSM over-predicts is by 14%. More results can be found in [2].

Conclusions

An Explicit Algebraic Reynolds Stress Model (together with Wilcox $k-\omega$ model) has been improved using Neural Network (NN). The NN model is trained in channel flow at $Re_\tau = 10\,000$. It is found that target data cannot be taken from DNS because the stress-strain relation and the turbulent kinetic energy are not the same in the DNS and the $k-\omega$ predictions. Hence the target data are taken both from DNS ($\overline{v_1'^2}$ and $\overline{v_2'^2}$) and a $k-\omega$ simulation ($\frac{\partial \bar{v}_1}{\partial x_2}$, $\overline{v_1'v_2'}$, k, $\varepsilon = C_\mu k\omega$). In this way the strain-stress relation and the turbulent kinetic energy are the same in the training process and the CFD-NN predictions. Since k in the training process is taken from the $k-\omega$ results it means that $k \neq 0.5(\overline{v_1'^2}_{DNS} + \overline{v_2'^2}_{DNS} + \overline{v_3'^2}_{DNS})$. In the NN model, the spanwise Reynolds stress adapts to satisfy $a_{ii} = 0$ which means that $\overline{v_3'^2}$ is not correctly predicted (it even goes negative in the near-wall region). Hence, the EARSM-NN model is applicable only to two-dimensional flow where $\overline{v_3'^2}$ is not used. One way to make the model applicable in three-dimensional flow is to develop a $k-\omega$ (or $k-\varepsilon$ model) which accurately predicts the turbulent kinetic energy.

References

[1] S. Wallin, A. V. Johansson, A new explicit algebraic Reynolds stress model for incompressible and compressible turbulent flows, JFM (2000)

[2] L. Davidson, Using Neural Network for Improving an Explicit Algebraic Stress Model in 2D Flow, CUSF, Murray Edwards College, Cambridge, UK (2024) (to appear)

LARGE-SCALE FLUID-STRUCTURE INTERACTION TOPOLOGY OPTIMIZATION OF A HYDRAULIC SYSTEM COMPONENT

H. Hederberg[1] and C.-J. Thore[1]

[1]*Department of Solid Mechanics, Linköping University, Linköping, Sweden*

Topology optimization (TO) is a versatile tool for engineers to obtain novel and interesting designs with optimized performance given a set of constraints. Topology optimization started with the work of Bendsøe and Kikuchi [1] and has since been applied to a vast variety of problems in, e.g. mechanics, photonics and fluid flow. In recent years fluid-structure interaction (FSI), where the fluid forces deform the structure, has gained increased interest [2]. The goal of the present work is to couple FSI with TO to optimize a component in a hydraulic system.

A design field $\rho = \rho(\boldsymbol{x})$, varying within the domain Ω, dictates in each point $\boldsymbol{x} \in \Omega$, whether we have solid or fluid. The fluid flow is governed by the stationary Navier-Stokes equations for an incompressible fluid

$$\begin{aligned} &\text{div}(\boldsymbol{\sigma}_f) - \alpha(\rho)\boldsymbol{v} = \varrho(\nabla \boldsymbol{v})\boldsymbol{v} \quad \text{in } \Omega \\ &\text{div}(\boldsymbol{v}) = 0 \quad \text{in } \Omega, \end{aligned} \tag{1}$$

where $\boldsymbol{\sigma}_f = -p\boldsymbol{I} + 2\mu\boldsymbol{\varepsilon}(\boldsymbol{v})$. To be able to do TO we have introduce a so-called Brinkman-term $-\alpha\boldsymbol{v}$ [3] in the fluid problem which makes the solid material act as a porous media with a very high resistance to fluid flow in parts with material and very low resistance in parts without material.

The displacement $\boldsymbol{u}$ is governed by

$$\begin{aligned} &\text{div}(\boldsymbol{\sigma}_s) = \boldsymbol{0} \quad \text{in } \Omega \\ &\boldsymbol{\sigma_s} = \boldsymbol{D}(\rho)\boldsymbol{\varepsilon}(\boldsymbol{u}) \quad \text{in } \Omega \\ &\boldsymbol{\sigma}_s\boldsymbol{n} = \boldsymbol{\sigma}_f\boldsymbol{n} \quad \text{on } \Gamma_{sf}(\rho). \end{aligned} \tag{2}$$

Here $\Gamma_{sf}(\rho)$ is the solid-fluid interface and the coupling term $\boldsymbol{\sigma}_s\boldsymbol{n} = \boldsymbol{\sigma}_f\boldsymbol{n}$ gives the loads on the structure.

The TO problem is formulated as minimizing some measure of flow resistance, $f(\rho, \boldsymbol{v})$, while having a constraint, $g(\rho, \boldsymbol{u}(\boldsymbol{v}, p))$, on the mechanical deformation of the structure, i.e.

$$\begin{aligned} &\min_{\rho:\Omega\to[0,1]} \quad f(\rho, \boldsymbol{v}, p) \\ &\text{s. t.} \quad g(\rho, \boldsymbol{u}(\boldsymbol{v}, p)) \leq 0, \end{aligned} \tag{3}$$

where $\boldsymbol{u}(\boldsymbol{v}, p)$ and $(\boldsymbol{v}, p)$ are the solutions to the state problems (1) and (2) for a given design.

An interesting part of the hydraulic system to optimize is one of the valves. To be able to get the needed details of the flow channels we want to do large-scale TO. This means that we use a large amount of finite elements to get high resolution of the finished design. Therefore, problem (3) is implemented using the PETSc-framework [4] for massively parallel computing.

Figure 1a) shows a cut-through of the valve with the guiding pin at the top and prescribed traction at the bottom and Fig. 1b) shows an optimized design of the valve. The figures also show the streamlines of the flow through the valve, red indicating high velocity and blue indicating low velocity.

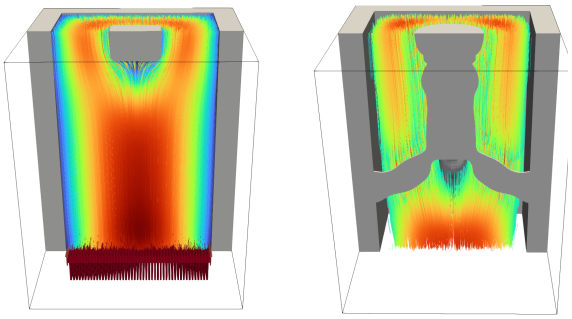

a) Initial design with prescribed traction for the fluid at the bottom and the guiding pin at the top.

b) An optimized valve.

Figure 1: Topology optimization of a hydraulic valve.

References

[1] Bendsøe, M. P., et al., Generating optimal topologies in structural design using a homogenization method. Computer methods in applied mechanics and engineering, 71(2), 197-224, (1988).

[2] Lundgaard, C., et al., Revisiting density-based topology optimization for fluid-structure-interaction problems. Structural and Multidisciplinary Optimization, 58, 969-995, (2018).

[3] Borrvall, T., et al., Topology optimization of fluids in Stokes flow. International journal for numerical methods in fluids, 41(1), 77-107, (2003).

[4] Curfman McInnes L., et al., PETSc, the Portable, Extensible Toolkit for Scientific computation. Argonne National Laboratory, 2(17), (1998).

Corresponding author: Hampus.Hederberg@liu.se

RAYLEIGH-BÉNARD CONVECTION AT HIGH RAYLEIGH NUMBER AND LOW ASPECT RATIO

E. Lindborg[1]

[1]*Department Engineering Mechanics, KTH, Osquars Backe 18, SE-100 44, Stockholm, Sweden*

The last two decades there has been a lively debate in the scientific community of whether there exist an 'ultimate state' of heat transfer in high Rayleigh number (Ra) convection in accordance with the (1962) theory of Kraichnan [**1**]. The theory predicts that the system enters into a state of very strong heat flux at high Ra, in which the Nusselt number scales as $Nu \sim Ra^{1/2}$. There have been repeated claims that the ultimate state theory has been experimentally confirmed [**2**, **3**] and numerically verified in two-dimensional direct numerical simulations (DNS) [**4**]. Last year, proponents of the theory also published a paper in Physics Today [**5**] repeating the arguments in support of the theory. As a scientist in the field of turbulence, I am utterly sceptical to the ultimate state theory. Last year, I published two papers on the problem, arguing against the existence of the ultimate state. In the first paper [**6**] I analysed 3-D Rayleigh-Bénard convection at high aspect ratio and in the second paper [**7**] I analysed the corresponding 2-D system. In both cases I found that the Nusselt number scales as $Nu \sim Ra^{1/3}$, sometimes called 'classical scaling', in accordance with the theory Malkus (1954) [**8**]. In the 2-D case I showed that the claims of a verifications of the theory based on DNS are unfounded.

In this presentation, I will extend the analysis to the low aspect ratio regime. A recent DNS study [**9**] in a cylindrical cell with aspect ratio $\Gamma = 1/10$, report $Nu \sim Ra^{0.331\pm0.002}$ at $Pr = 1$ and $Ra \in [10^{10}, 10^{15}]$. Using a straightforward similarity argument it is shown that the clean result is a realisation of classical scaling in the regime $Ra \gg 1, Ra^{-1/3} \ll \Gamma \ll 1$, and that the height, H, of the convection cell will vanish from scaling expressions of turbulent quantities in this regime. Using experimental and DNS data we show that the normalised root-mean-square of temperature does not depend on H. The scaling relation for this quantity is used to derive the scaling relation for the Reynolds number. The minimum Γ needed to reach the asymptotic regime for a given Ra is estimated and it is suggested that it can be reached in very low aspect ratio cells. It is further shown that the dissipative anomaly, $\epsilon \sim u^3/\mathcal{L}$, where ϵ is the mean kinetic energy dissipation, u is the turbulent velocity and $\mathcal{L}$ is the turbulent integral length scale, is not completely satisfied in the low aspect ratio regime. Nevertheless, Kolmogorov phenomenology is applicable at small scales, which is shown by deriving the four-fifth's law for the third order velocity structure function. Finally, it is discussed whether the same state as observed in the low aspect ratio limit will be observed n the high aspect ratio limit.

References

[1] KRAICHNAN, R. H. 1962 Turbulent thermal convection at arbitrary Prandtl number *Phys. Fluids*, **5**, 1374-1389

[2] HE, X., FUNFSCHILLING, D., NOBACH, H., BODENSCHATZ, E. & AHLERS, G. 2012 Transition to the Ultimate State of Turbulent Rayleigh-Bénard Convection *Phys. Rev. Lett.*, **108**, 024502

[3] AHLERS, G., BODENSCHATZ, E., HARTMANN, R., HE, X., LOHSE, D., REITER, P., STEVENS, R., VERZICCO, R., WEDI, M., WEISS, S., ZHANG. X., ZWIRNER, L. & SHISHKINA, O. 2022 Aspect Ratio Dependence of Heat Transfer in Cylindrical Rayleigh-Bénard Cell *Phys. Rev. Lett.*, **128**, 084501

[4] ZHU, X., MATHAI, V., STEVENS, R.J.A.M., VERZICCO, R. & LOHSE, D. 2018 Transition to the Ultimate Regime in Two-dimensional Rayleigh-Bénard convection *Phys. Rev. Lett.*, **120**, 144502

[5] LOHSE, D. & SHISHKINA, O. 2023 Ultimate turbulent convection *Phys. Today*, **76**, 26-32

[6] LINDBORG, E. 2023 Scaling in Rayleigh-Bénard convection, *J. Fluid Mech.*, **956** , A34

[7] LINDBORG, E. 2023 Reynolds-number scaling and convergence time scale in two-dimensional Rayleigh-Bénard convection, *J. Fluid Mech.*, **973** , A9

[8] MALKUS, W. V. R. 1954 The heat transport and spectrum of thermal turbulence *Proc. R. Soc.* Lond. **A225**, 196-212

[9] IYER, K.P., SCHEEL, J.D., SCHUMACHER, J. & SREENIVASAN, K.R. 2020 Classical 1/3 scaling of convection holds up to $Ra = 10^{15}$ *Proc. Nat. Acad. Sci.* USA **117**, 7594-7598

Corresponding author: erikl@mech.kth.se

SIMULATION OF VISCOELASTIC FLOWS APPLIED TO HEMMING

A. Mark[1], C. Cromvik[1], S. Ingelsten[2], M. Ottosson[2], F. Wandebäck[3], F. Edelvik[1]

[1]*Fraunhofer-Chalmers Research Centre, Gothenburg, Sweden.*
[2]*IPS IBOFlow AB, Gothenburg, Sweden*
[3]*RISE, Mölndal, Sweden*

Multi material combinations of complex products is becoming more and more common, to optimize product characteristics and reduce weight. Joining methods are then central and for hang on parts in the automotive industry a hemming process is often used. The focus of the VIVFAP project involving RISE, Fraunhofer-Chalmers Centre, Swedish automotive industry and suppliers, was to develop novel simulation tools for the hemming process. A complete simulation workflow must cover robot programming, adhesive extrusion, folding the edge of the outer part over the inner part, and finally curing of the adhesive, see Figure 1.

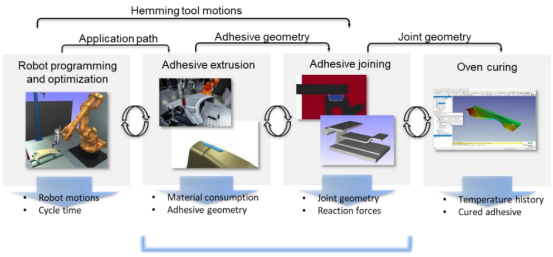

Figure 1: Simulation workflow of the hemming process.

The interaction between the sheet metal and the adhesive in the assembly process is a fluid-structure interaction problem that is highly challenging to simulate and requires robust methods that can handle fluid dynamics, structural mechanics, and their coupling [1].

The extrusion of the adhesive on the sheet metal is simulated to get the correct placement and shape. A new backwards-tracking Lagrangian-Eulerian method [2] has been developed to enable simulation of the two-phase flow of viscoelastic adhesive and surrounding air. To handle the sheet metal deformation, an anisotropic plasticity model for shell elements has been developed.

A hemming process involves a relatively long physical time, and the small distances between the sheets require a method with very fine spatial and temporal resolution, resulting in long simulation times. To improve performance, several methods have been developed. For the flow solver, a phase-dependent adaptive time-stepping has been introduced to optimize the adhesive's time step and thus reduce the total number of time steps. Furthermore, an adaptive method for volume mesh refinement has been developed to handle narrow gaps. For the structural solver a method to compute only on an active zone near the hemming tools has been developed. To validate the simulation results, SAM-scanned test bodies from hemming, both with and without adhesive, have been used. For simulations without adhesive, good predictions of roll-in and hem thickness have been obtained. To validate the results with adhesive, several sections of the test body have been measured in detail for different adhesive bead heights and distances from the hem edge, Figure 2. A visual comparison focusing on adhesive extrusion has been conducted, concluding that general trends are captured.

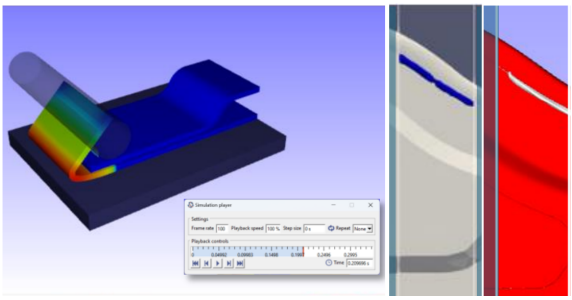

Figure 2: Left: Example hemming simulation. Right: Comparison of final squeezed out adhesive, blue simulation and white experiment.

This work has been supported in part by VINNOVA through the FFI Sustainable Production Technology program and the project "Virtual Verification of the Hemming Process (VIVFAP)", and in part by the Chalmers Area of Advance Production.

References

[1] Ingelsten, S., et al., Simulation of viscoelastic squeeze flows for adhesive joining applications, Journal of Non-Newtonian Fluid Mechanics 300, 104722, 2022

[2] Ingelsten, S., et al., A backwards-tracking Lagrangian-Eulerian method for viscoelastic two-fluid flows, Applied Sciences 11 (1), 439, 2021

Corresponding author: andreas.mark@fcc.chalmers.se

FLOW DISTURBING STRUCTURES FOR AIR-COOLED BATTERY THERMAL MANAGEMENT SYSTEMS

A. Moosavi, A.-L. Ljung, S. Lundström

Division of Fluid Mechanics, Department of Engineering Sciences and Mathematics, Luleå University of Technology, Luleå, Sweden

Despite the growing popularity and development of renewable energy technologies and electric vehicles, providing reliable energy storage systems remains a significant obstacle to this transition [1]. While lithium batteries are a mighty option to transform the energy storage domain, their temperature sensitivity issue makes them unreliable in extreme conditions, adversely affecting their performance, safety, and lifespan. There are different strategies to regulate the temperature within a lithium battery system known as battery thermal management system, which may be categorized as air-, liquid-, and PCM-based techniques based on the cooling medium. Although each method has pros and cons and might serve as a suitable choice for a certain application or working condition, air-based methods are more attractive for industrial applications, particularly electric vehicles, owing to their lightweight, simple design, no sealing requirement, no need for secondary cooling system, and low cost. However, air-based battery thermal management systems have limitations due to the poor thermal conductivity of air coolant flow, requiring multi-objective optimization and design modifications to fulfill the increasing cooling requirement for electric vehicles. Flow-disturbing structures, among other enhancing strategies, could be an advantageous technique due to their acceptable effectiveness and compatibility with compact designs. There are numerous types of flow-disturbing structures such as spoilers, baffles, vortex generators, fins, and so on; however, they can generally be divided into two types: attached and detached flow-disturbing structures. In detached flow-disturbing structures, increased turbulence intensity and better flow mixing are the main reasons for enhanced heat transfer. However, the expanded active heat transfer area also benefits attached flow-disturbing structures.

Motivated by the proven effectiveness of flow-disturbing structures in tube banks and the compatibility of their integration in compact battery thermal management systems, straight splitter plates as attached structures and customized-shape baffles as detached structures are incorporated in an air-cooled battery system to assess their functionality and effectiveness on the system's performance. The battery module under consideration consists of 87 cylindrical 26650 LFP cells placed in a staggered arrangement. The effect of flow-disturbing structures on the performance of the battery system is investigated using a hybrid modeling approach [2]. The approach breaks down the general model into three submodels, involving a CFD model for flow characterization, an analytical thermal model for the cells, and an empirical capacity fading model to determine how many cycles the battery runs before its end of life.

The results indicate that splitter plates compared to baffles are more effective in the enhancement of the thermal performance. This advantage is not only from the larger surface area available for heat transfer via splitter plates but also due to flow stream splitting by the baffle, thereby reducing the potential of the air coolant flow for heat dissipation. While splitter plates enhance the thermal performance of the system, they lead to greater flow resistance in compact systems, which is contrary to observations for wide-spaced tube banks [3]. This behavior may be attributed to the smaller wake bubble in compact systems, diminishing the effect of splitter plates on flow interaction in the wake region. Nonetheless, the results imply that splitter plates are a potential solution to reduce cyclical costs in air-cooled battery systems.

References

[1] M. Hannan, A. Q. Al-Shetwi, R. Begum, P. J. Ker, S. Rahman, M. Mansor, M. Mia, K. Muttaqi, Z. Dong, Impact assessment of battery energy storage systems towards achieving sustainable development goals, Journal of Energy Storage 42 (2021) 103040.

[2] A. Moosavi, A.-L. Ljung, T. S. Lundström, A study on the effect of cell spacing in large-scale air-cooled battery thermal management systems using a novel modeling approach, Journal of Energy Storage 72 (2023) 108418.

[3] C. K. Mangrulkar, A. S. Dhoble, J. D. Abraham, S. Chamoli, Experimental and numerical investigations for effect of longitudinal splitter plate configuration for thermal-hydraulic performance of staggered tube bank, International Journal of Heat and Mass Transfer 161 (2020) 819 120280.

Corresponding author: amin.moosavi@ltu.se

MULTIPHYSICS TOPOLOGY OPTIMIZATION FOR OPTIMAL INTERNAL COOLING

J. Lundgren[1], C.-J. Thore[2], H.N. Najafabadi[3], J.-E. Lundgren[4]

[1]*Structural Analysis, Aeronautics, Saab AB, Linköping, Sweden*
[2]*Division of Solid Mechanics, Linköping University, Linköping, Sweden*
[3]*Division of Applied Thermodynamics and Fluid Mechanics, Linköping University, Linköping, Sweden*
[4]*Siemens Energy, Finspång, Sweden*

Good cooling is important in many applications, ranging from computer chips to gas turbine parts. Design of cooling solutions is a challenging multi-physics problem involving mechanical, thermal and flow fields, each with their own design requirements. Computational optimal design tools such as topology optimization (TO) show promise as a way to achive optimal designs that balance multiple conflicting design criteria [1,2,3].

In this talk we consider TO for interior cooling of gas turbine guide vanes (Fig. 1). Such vanes are used inside

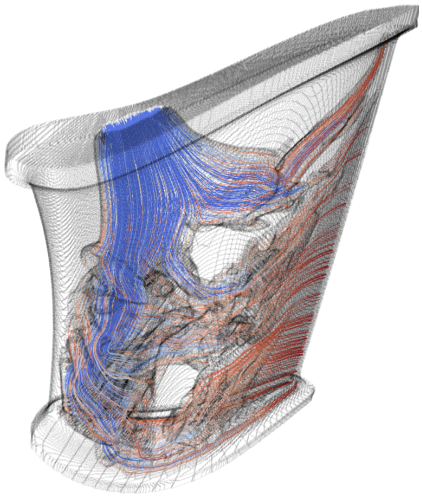

Figure 1: A (slightly transparent) guide vane with topology optimized interior. Streamlines, colored according to temperature, show cooling air flowing in through a hole at the inlet, through the vane and out at the trailing edge.

the turbine to guide the flow of hot gas onto the turbine blades. The distribution of material in the vane is described by a field γ indicating solid material ($\gamma = 1$) or void/fluid ($\gamma = 0$) in each point of the domain Ω. The velocity $\boldsymbol{v}$ and the hydrostatic pressure p of the cooling air inside the vane are governed by the stationary, incompressible Navier-Stokes equations. The temperature T in the domain is governed by a convection-diffussion equation, resulting in the coupled system

$$\rho(\boldsymbol{v}\cdot\nabla)\boldsymbol{v} = \mathrm{div}\boldsymbol{\sigma}(\boldsymbol{v},p) - \alpha(\gamma)\boldsymbol{v} \ \text{ in } \Omega$$
$$\mathrm{div}(\boldsymbol{v}) = 0 \ \text{ in } \Omega$$
$$c\boldsymbol{v}\cdot\nabla T - \mathrm{div}(\kappa(\gamma)\nabla T) = 0 \ \text{ in } \Omega$$

where ρ is the density of the coolant, and $\boldsymbol{\sigma}(\boldsymbol{v},p) = -p\boldsymbol{I} + 2\mu\boldsymbol{\varepsilon}(\boldsymbol{v})$, in which μ is the viscocity and $\boldsymbol{\varepsilon}(\boldsymbol{v})$ the symmetric velocity gradient. The design-dependent parameters $\alpha(\gamma)$ (impermeability) and $\kappa(\gamma)$ (conductivity) are obtained by interpolation between the values for solid and fluid material. The flow is driven by a pressure load applied at the inlet (top face in Fig. 1), and the main goal of the TO is to reduce the maximum temperature on the outer shell of the vane which is heated by convection from hot gas. A constraint on the mass flow of coolant is included to avoid spending too much compressed air on cooling.

The basic (exterior) geometry of guide vanes are complex, and therefore an automatic voxelization approach is proposed for computational mesh generation. This means that the geometry is embedded in a structured voxel mesh and the computational domain is the union of those voxels that intersect the geometry.

Pure fluid-thermal TO, which does not account for mechanics and manufacturability, can lead to unphysical features such as "islands" – solid regions ($\gamma \approx 1$) disconnected from the main structure or any mechanical supports. To suppress the formation of islands we formulate an optimization constraint based on the response from an artificial heat conduction problem.

The TO problem is implemented in C++ using the parallell numerical library PETSc to allow solution of large-scale instances of the optimization problems. In the talk we'll discuss the feasibility of the proposed TO approach for design in complex multi-physics problems as well as important remaining challenges.

References

[1] Lundgren J., Lundgren J.-E., Najafabadi H.N., Thore C.-J., Flow-heat topology optimization of internally cooled high temperature applications using a voxelization approach for domain initialization. Engineering Optimization, 2023

[2] Lundgren J., Internal Cooling Design Using Multiphysics Topology Optimization, PhD Thesis. Linköping University, 2024

[3] Alexandersen J., Andreasen C.S., A review of topology optimisation for fluid-based problems. Fluids, 5(1), 2020

Corresponding author: carl-johan.thore@liu.se

BLAST RESPONSE OF COMPOSITE PLATES IN BARREL EXPERIMENT

H. Delmotte[1], S. Clementz[2], S. Hallström[1]

[1]*Department of Engineering Mechanics, KTH Royal Institute of Technology, Stockholm, Sweden*
[2]*FOI- Swedish Defence Research Institute, Stockholm, Sweden*

Naval vessels are traditionally metallic structures for which blast and ballistic loads have been extensively studied. Composite structures are more and more integrated into vessel designs since they offer interesting stealth properties due to their low thermal and electromagnetic signatures, combined with lower weight. Sweden has been one of the pioneers in this respect, as demonstrated by the Visby corvette class vessel. There has been an effort to widen the understanding of the behavior of composite structures under blast loading, but general design rules are still lacking. High safety factors are often used in design resulting in heavy structures that limit the benefits from using lightweight composite materials [1]. In defense applications, blast resistance is typically a critical design requirement for structures. When the blast is due to an explosive threat, it is often combined with high-velocity fragments that impact and damage the structure before the arrival of the blast wave, thus reducing its structural integrity. Blast loads can be divided into different categories such as far-field and near-field explosions, underwater and air blasts. While the pressure profile of the far-field explosion can easily be modeled, these models can not be transposed to the near-field explosion where additional effects such as reflected waves can contribute to the deformation [2].

In this study, the blast response of fiber-reinforced polymers is investigated in a barrel experiment; a near-field air blast event in enclosed environment as illustrated in Figure 1. The study follows previous work by Clementz and Andersson who investigated the response of thin pre-perforated steel plates under blast loads in a barrel numerically and experimentally [3].

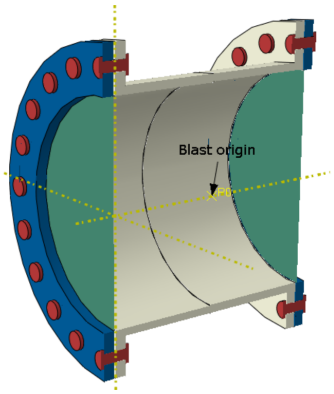

Figure 1: Barrel assembly - Barrel (white), Metal clamps (blue), Composite plates (green), Bolts (red).

A new experimental campaign with carbon and glass fiber reinforced composite plates with quasi-isotropic layup is designed alongside a simulation using ABAQUS. The goal is to compare the response of the composite plates with the steel plates and to investigate the effect of fiber type and areal weight on the blast resistance of the composite panels. Panels with drilled and shot holes are also tested to explore how initial delamination affect the structural integrity of the panel under blast. Preliminary tests have been conducted to adapt the previous experimental setup to the new tests as shown in Figure 2. They showed promising results, demonstrating that a carbon fiber laminate with the same areal weight as the steel plate could withstand similar explosive load without total failure of the panel. Consecutively, a test matrix has been established for the experimental campaign, combining tests on carbon fiber and glass fiber laminates with either the same thickness or same areal weight, undamaged or with pre-drilled or pre-shot holes in different patterns.

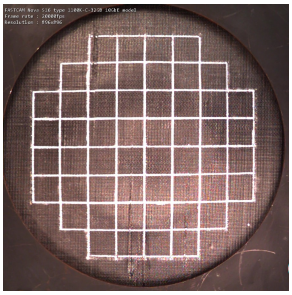

Figure 2: Preliminary experimental test - Front view.

References

[1] Mouritz, A. P., Gellert, E. Burchill, P., Challis, K., Review of advanced composite structures for naval ships and submarines, Compos. Struct., 53, 1, 21-42, (2001).

[2] Gargano, A., Das, R., Mouritz, A. P., Finite element modelling of the explosive blast response of carbon fibre-polymer laminates, Compos. Part B Eng., 177, 107412, (2019).

[3] Clementz, S., Andersson, O., The damaging effect of blasts on thin, pre-perforated plates, 33rd ISB, Bruges (2023).

Corresponding author: delmotte@kth.se

STUDY OF ELECTRIC AND FRICTION BRAKING AT LOW-SPEEDS

S. Deylaghian[1], M. Jonasson[1], P.T. Piiroinen[1]

[1]*Department of Mechanics and Maritime Sciences, Chalmers University of Technology, Gothenburg, Sweden*

Most daily driving involves non-critical conditions, where intense performance is not required. This observation highlights the importance of improving ride comfort and control in everyday scenarios such as braking in a hill. A key aspect of such improvement is to minimise jerk, ensuring smoother transitions and a more comfortable driving experience [1-3]. In this study, we develop a minimal vehicle model (Figure 1) to capture the main longitudinal comfort phenomena close to stand-still in order to conduct an analysis. The model simplifies a vehicle complexity by lumping all wheels into a single representative wheel that includes both friction and electric braking models. Similarly, the stiffness and damping characteristics from the tires and suspension are consolidated into one spring and damper. The model has two degrees of freedom, which are the sprung mass movement x_1 and the wheel's translational position x_2. The effects of motion resistance such as air drag, rolling, etc. are ignored. Further, T_p is propulsion torque and F_c is break clamp force. The wheel, with angular velocity ω rad/s and longitudinal velocity $\dot{x}_2$, assumes no tyre slip (so that $\dot{x}_2 = R_w\omega$). The parameters r and J denote wheel radius and inertia, respectively. Following this, the equations of motion are given by

$$\begin{aligned}\ddot{x}_1 =& \frac{1}{m_b}\Big(k(x_2 - x_1) + d(\dot{x}_2 - \dot{x}_1) + m_b g\sin(\varphi)\Big)\\ \ddot{x}_2 =& \frac{r}{J + r^2 m_s}\Big(- rk(x_2 - x_1) - rd(\dot{x}_2 - \dot{x}_1)\\ &+ T_p - rF_b + rm_s g\sin(\varphi)\Big),\end{aligned} \tag{1}$$

where $m_s = m_w + m_a$ combined mass and the friction force including Stribeck effect is defined as

$$F_b = \begin{cases}[-\mu_s F_c, \mu_s F_c], & \dot{x}_2 = 0,\\ -\mathrm{sgn}(\dot{x}_2)F_c f(\dot{x}_2), & \dot{x}_2 \neq 0.\end{cases} \tag{2}$$

By utilizing this simplified longitudinal model, we delve into the effects of electric and friction torques during low-speed maneuvers as well as the impact of gravity during hill driving. By gaining a deeper understanding of vehicle dynamics, we aim to explore how to reduce excessive jerk when starting and approaching stand still. An additional aim of this research is to understand the conceptual comfort difference between breaking using a shaft torque, for instance generated by an electric engine, and a friction brake (Figure 2). In summary, our research aims to enhance understanding and provide solutions for better ride comfort in everyday driving conditions.

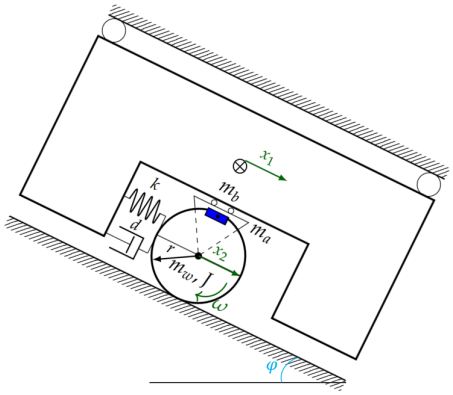

Figure 1: Quarter vehicle body and wheel model.

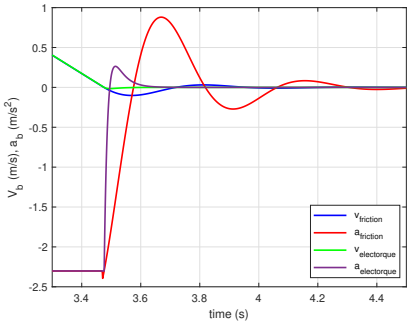

Figure 2: Vehicle body velocity and acceleration.

References

[1] Lee, J., Choi, S.: Braking control for improving ride comfort. In: MATEC Web of Conferences. vol. 166, p. 02002. EDP Sciences (2018)

[2] Shi, B., Xiong, L., Yu, Z.: A control method for improving ride comfort in braking. In: 2021 5th CAA International Conference on Vehicular Control and Intelligence (CVCI). pp. 1–6. IEEE(2021)

[3] Singh, A., Nishihara, O.: Modeling of autonomous emergency braking system with minimum jerk. In: 2022 22nd International Conference on Control, Automation and Systems (ICCAS). pp. 40–44. IEEE (2022)

Corresponding author: Samira.deylaghian@chalmers.se

PERFORMANCE ANALYSIS OF A HYDROGEN FUELLED COMPOSITE CYCLE AEROENGINE

A. Johansson[1], P. Miltén[1], A. Lundbladh[2], C. Xisto[1]

[1]*Department of Mechanics and Maritime Sciences, Chalmers University of Technology, Gothenburg, Swedenn*
[2]*GKN Aerospace, Trollhättan, Sweden*

To decrease the climate impact of aviation and become carbon neutral a transition away from kerosene is inevitable, where the two main contestants at the moment are hydrogen (H_2) and sustainable aviation fuel (SAF). Engines powered by either of the renewable fuels will have even higher requirements for fuel efficiency than today, since the supply of both energy carriers will be limited. One of the most promising concepts of achieving significant fuel burn improvements is the composite cycle engine (CCE) [1], a turbofan with the burner being replaced with a reciprocating engine. The CCE cycle has been investigated in numerous studies, but so far no analysis has been performed on a H_2 fuelled CCE. In this study a design point performance analysis of a H_2 CCE powerplant is presented and compared with a SAF fuelled CCE and a year 2035 state of the art conventional turbofan.

A thermodynamic model of a piston engine has been developed to asses the power output, mass flow, outflow temperature, maximum pressure and fuel consumption of the reciprocating engine core of the power plant. Publicly available simulation data from a model problem has been used to cross validate the developed piston engine model [2], where the validation result of the crank angle resolved cylinder gas pressure is shown in Figure 1. Since the simulation cost of the reciprocating engine is several orders of magnitude larger than the rest of the power plant, a surrogate model of said engine was trained. An hydrogen-air intercooler located prior to the high pressure compressor (HPC) is utilised for cooling the core flow and thus reducing the compression work of the HPC and allowing for higher overall pressure ratios. Lower temperatures increases the air density of the core flow, hence decreasing the size of the piston engine and increasing the specific work, ultimately yielding lighter and smaller engines [3]. Using the liquid hydrogen fuel as heat sink both increases the fuel enthalpy upon injection into the engine, leading to decreased fuel consumption, and allows for a lighter and compacter heat exchanger compared to an air to air heat exchanger. The heat produced from the piston engine is rejected into the bypass stream via an oil-to-air heat exchanger.

The cycle is evaluated for a year 2035 short-range aircraft at cruise. In Table 1 the conditions of the operating point are listed. Specific thrust is set to 80 m/s, corresponding to a propulsive efficiency of 83%, which is a typical value for the latest generation of ultra high bypass ratio engines. Comparison of the thrust specific fuel consumption is based on the lower heating value of the fuel, to adjust for the difference in energy content.

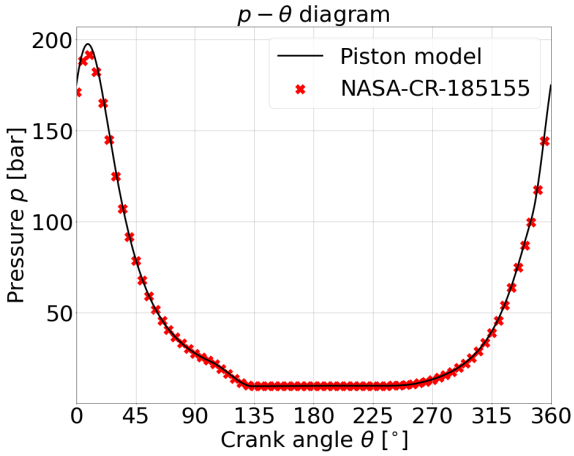

Figure 1: Cross validation of crank angle θ resolved cylinder pressure p against reference data [2].

Parameter	Unit	Value
Mach	-	0.70
Altitude	m	10058
Δ T ISA	K	0
Net thrust	N	19501

Table 1: Design point conditions for year 2035 short-range aircraft at cruise.

References

[1] Grönstedt, T., et al. Conceptual design of ultra-efficient cores for mid-century aircraft turbine engines. In Proceedings of the 24th ISABE Conference, Canberra, Australia, 201, 22-27, (2019)

[2] VanGerpen, J. H., A two-stroke diesel engine simulation program. Technical report, Engine Research Institute, Iowa State University, Ames, Iowa, Feb. 1990.

[3] Rolt, A., et al. Scale effects on conventional and intercooled turbofan engine performance. The Aeronautical Journal, 121(1242):1162–1185, 2017.

Corresponding author: adam.l.johansson@chalmers.se

Fault diagnosis of Single Rotor System Using Rigid-Flexible Hybrid Modelling

Yu-Hung Pai[1], Petri T. Piiroinen[1], Shivesh Kumar[1,2], Håkan Johansson[1]

[1]*Department of Mechanics and Maritime Sciences, Chalmers University of Technology, Gothenburg, Sweden*
[2]*Robotics Innovation Center, German Research Center for Artificial Intelligence, Bremen, Germany*

Data-driven fault diagnosis plays an important role in condition monitoring for rotating machinery to prevent system from catastrophic accidents [1]. However, the performance of data-driven methods highly relies on a large quantity of fault training data. Since rotating machinery operates normally for most of the time, collecting sufficient fault data from experiments takes a huge amount of time and expense, let alone from various operating conditions [2][3]. To overcome the fault data insufficiency, building a virtual testbed for generating fault data is a promising way in bridging the gap between data requirement and prediction accuracy [4][5].

In this research, a model-based fault diagnosis method is proposed to investigate the availability of simulation data. Firstly, a rigid-flexible hybrid model of a single shaft-bearing system is established using ADAMS® based on multi-body dynamics and finite element analysis as shown in Figure 1. We simulate different fault conditions including misalignment, unbalance, loose supports and defective bearing, and the vibration signals are also captured from the shaft and the bearing housing in the model as shown in Figure 2.

Afterwards, we perform feature extraction based on time and frequency domain analysis to select the fault-related features. In terms of time-domain waveform, the root-mean square, kurtosis and skewness of the vibration signal will be selected as features. In terms of frequency-domain waveform, wavelet packet decomposition will be used to extract the wavelet coefficient which represent the energy of every frequency band. Finally, the selected features will be assembled and then imported to machine learning classifiers for discriminating the fault categories [6]. This research lays a solid foundation for developing digital twin for fault diagnosis of rotor systems in the future.

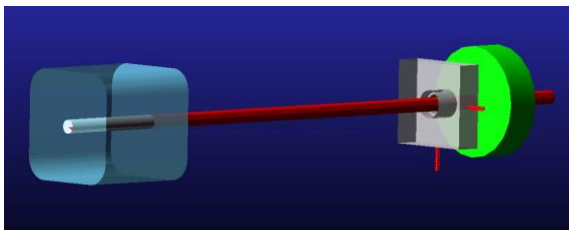

Figure 1: Single shaft-bearing model in ADAMS®.

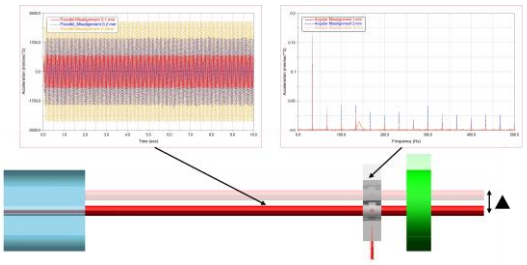

Figure 2 : Signal collection from the shaft and the housing with parallel misalignment.

References

[1] Lei, Yaguo, et al. "Applications of machine learning to machine fault diagnosis: A review and roadmap." *Mechanical Systems and Signal Processing*, 138, 106587, (2020)

[2] Hou, Wenbo, et al. "A new bearing fault diagnosis method via simulation data driving transfer learning without target fault data." *Measurement*, 215, 112879, (2023)

[3] Qian, Weiwei, et al. "A novel transfer learning method for robust fault diagnosis of rotating machines under variable working conditions." *Measurement*, 138, 514-525, (2019)

[4] Eisa, Abdelrahman IA, Li Shusen, and Wasim MK Helal. "Study on the lateral and torsional vibration of single rotor-system using an integrated multi-body dynamics and finite element analysis." *Advances in Mechanical Engineering*, 12.10, 1687814020968336, (2020)

[5] Xu, Kai, Yuqing Zhang, and Tingfeng Ming. "Research on vibration characteristics of propulsion shafting under unbalanced-misaligned coupling fault." *Journal of Physics: Conference Series*. Vol. 1802. No. 2. IOP Publishing, (2021)

[6] Umbrajkaar, A. M., A. Krishnamoorthy, and R. B. Dhumale. "Vibration analysis of shaft misalignment using machine learning approach under variable load conditions." *Shock and Vibration 2020*, 1-12, (2020)

Corresponding author email: paiy@chalmers.se

METHODOLOGY FOR EVALUATION OF LONG-TERM MECHANICAL PROPERTIES OF POLYMERS

R. Afshar[1], N. J. Ebi[2], B. E. Abali[1]

[1]*Department of Material Sciences and Engineering, Applied Mechanics Division, Uppsala University, Sweden*
[2]*Hitachi Energy, Lyviksvägen 3, Ludvika, Sweden*

Additive manufacturing (AM) techniques like fused deposition modeling (FDM) enable fabrication of complex geometries by depositing thermopolymer materials layer-by-layer. However, the anisotropic properties resulting from this layered structure can lead to uncertainties in predicting the long-term mechanical performance and viscoelastic characteristics of printed components. Comprehensive experimental characterization across extended timescales is challenging due to limitations in feasible testing durations.

The main objectives of this research were three-fold. Firstly, it aimed to investigate the applicability of Time-Temperature Superposition (TTS) for forecasting the viscoelastic properties of polymers fabricated through 3D printing. Secondly, it focused on developing a robust methodology to perform TTS analysis for viscoelastic materials using Python programming. Finally, it sought to apply this approach to conduct comprehensive stress relaxation testing on 3D printed polylactic acid (PLA) and construct a master curve capable of predicting PLA's mechanical behavior over extended times at a 26°C reference temperature.

A common approach utilized in finite element programs involves the implementation of the Williams–Landel–Ferry (WLF) equation, see Eq.1 ,which provides a means of determining the proportional relationship between time and temperature [**1**]. Example of the shift factor for a stress relaxation test at different temperatures is shown in Fig. 1.

$$\log\left(a_T\right) = \frac{-C_1\left(T - T_r\right)}{C_2 + \left(T - T_r\right)} \tag{1}$$

where C_1 and C_2 are material-specific constants determined from experimental data, T is the temperature at which we want to predict the relaxation time, T_r is the reference temperature at which the material's relaxation time is known and a_T is the shift factor at temperature T.

The key results are as following:

- Accelerated stress relaxation is observed at higher temperatures, indicating viscoelasticity of the material.
- By using inverse sigmoid fitting suitable WLF constants $c_1 = -1.37$ and $c_2 = 4.11$ are identified.
- The optimized master curve showed excellent agreement with the test data (PLA) at 26°C run in 5-days, as shown in Fig. 2.

Overall, this research underscores the potential to apply time-temperature superposition for polymeric materials produced by additive manufacturing. With comprehensive stress relaxation data across a wide temperature range, master curves can effectively predict long-term viscoelastic characteristics. This method allows accelerated determination of time-dependent properties, of significance for design and engineering applications. This methodology can be used for other polymeric materials too.

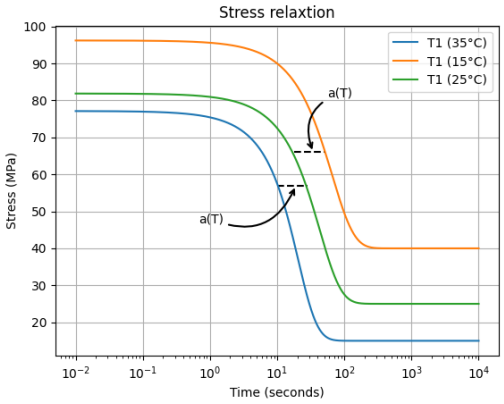

Figure 1: Example of the shift factor for a stress relaxation test at different temperatures, the x-axis is log-scaled.

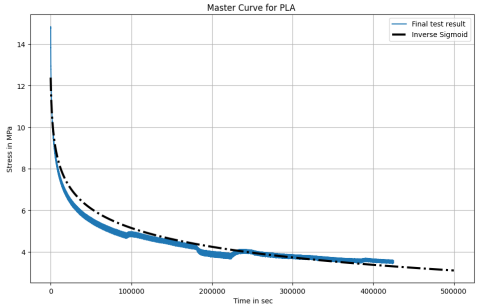

Figure 2: Validation of master curve with inverse sigmoid curve with actual data for 5 days.

References

[1] I. M. Ward and J. Sweeney, Mechanical properties of solid polymers. John Wiley & Sons, 2013.

Corresponding author: reza.afshar@angstrom.uu.se

SIMULATION-BASED ASSESSMENT OF RAILHEAD REPAIR WELDING PROCESS PARAMETERS

Björn Andersson[1], Erika Steyn[1], Magnus Ekh[1], B. Lennart Josefson[1]

[1]*Department Industrial and Materials Science, Chalmers University of Technology, Gothenburg, Sweden*

In modern railway networks, rail surface wear and damage are inevitable challenges due to increased traffic, higher speeds, and heavier axle loads. Rail maintenance is therefore essential to minimise disruption to rail operations. Repair welding is an important method for restoring rail surface quality in the event of local damage, providing a cost-effective and sustainable alternative to the replacement of entire rail sections. However, in terms of mechanical analysis, railhead repair welding has not been researched as extensively as welding techniques for joining rail, such as flash butt welding or aluminothermic (thermite) welding. This study presents a detailed investigation into the process parameters governing railhead repair welding to address this knowledge gap.

The study uses an FEM-based simulation methodology developed in previous works [1-3] for in-situ rail head repair welding to investigate the effect of welding process parameters on the quality of the repaired rail. The methodology includes material modelling that accounts for cyclic plasticity, phase transformations, transformation-induced plasticity, multiphase homogenisation and recovery of the virgin material state upon melting. The welding process is modelled using 3D heat transfer analysis and 2D mechanical analysis. The 3D heat transfer analysis is calibrated using measurements from a repair welding experiment. The 2D mechanical analysis uses a generalised plane strain model extended to include out-of-plane stiffnesses. In addition, rolling contact simulations are performed to evaluate the mechanical performance of the repaired rail and to estimate the risk of fatigue crack initiation.

Specifically, the process parameter study focuses on the effects of preheating and operating temperature conditions, as well as variations in repair geometry, for the Swedish stick weld railhead repair process shown in Figure 1a. The results show significant effects on the temperature distribution, spatial gradients and time history, which influence the overall material response and repair quality. In addition, the study highlights the inherent robustness of the process and identifies regions that are susceptible to parameter variations. The zig-zag pattern of the final weld layer provides effective resistance to variations in additional heating. The beginning and end sections of the repair weld are most susceptible to parameter variations. Chamfered and deeper cut-out repair geometries are found to be effective in mitigating adverse effects.

In agreement with field observations, the simulations identify the fusion zone of the base and filler material as the critical region of repair welded rail sections. This is attributed to the integrated effects of unfavourable microstructures, residual longitudinal tensile stresses from the repair weld and tensile stresses from operational traffic loads, as shown in Figures 1b and 1c.

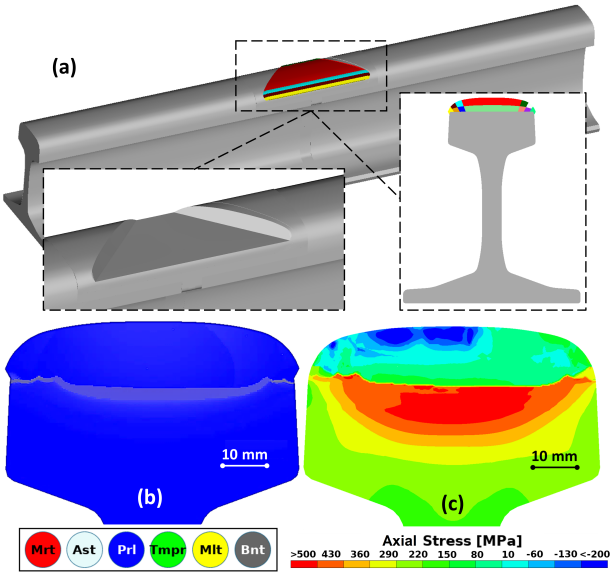

Figure 1: Figure 1. a) FE-model of the rail head with weld passes modelled. b) predicted material phases. c) calculated residual longitudinal residual stress after repair welding and over-rolling operation.

References

[1] Esmaeili A. et al., Modelling of cyclic plasticity and phase transformations during repeated local heating events in rail and wheel steels, International Journal of Fatigue, 151, (2021), 106361

[2] Andersson B. et al., Homogenization based macroscopic model of phase transformations and cyclic plasticity in pearlitic steel, Journal of Thermal Stresses, 45:6, 470-492, (2022)

[3] Andersson B. et al., Computationally efficient simulation methodology for railway repair welding: Cyclic plasticity, phase transformations and multi-phase homogenization, Journal of Thermal Stresses, 47:2, 164-188, (2023)

Corresponding author:abjorn@chalmers.se

Efficient Simulation of Evolving Plasticity in Rails using Reduced Order Modelling

C. Ansin[1], F. Larsson[1], R. Larsson[1]

[1]*Department Industrial and Materials Science, Chalmers University of Technology, Gothenburg, Sweden*

The contact between wheel and rail in railway operations results in high contact stresses, causing wear and plastic deformation to accumulate at the rail surface. Over time, with many wheel passages, this cumulative effect can result in alterations to the rail geometry and formation and propagations of cracks. Therefore, effective maintenance strategies are essential to prevent rail failure and extend the lifespan of the rail. Numerical computations offer a promising approach to cost-effectively predict rail damage under different operational conditions, which can optimize maintenance procedures.

Prior work [1] has proposed a methodology to compute long-term rail surface damage. It considers feedback loops that involve dynamic vehicle-track interaction, elastic-plastic wheel-rail contact, and accumulative rail damage attributed to plasticity and surface wear to update the rail profile. However, the framework limits the elastic-plastic computation to a 2D analysis, which does not fully capture the complexity of rail behaviour under contact.

We aim to address the limitations of two-dimensional analysis by transitioning to a more comprehensive 3D description of the elastic-plastic computation. While this approach offers a more accurate representation, it is computationally demanding since it demands numerous degrees of freedom to ensure an accurate 3D description of this nonlinear problem.

To enhance computational efficiency, we employ Reduced Order Modelling (ROM) using the Proper Generalized Decomposition (PGD) method. PGD utilizes separated functions to successively enrich the solution in each iteration, allowing for the introduction of many extra coordinates without affecting the model's solvability. Our approach involves solving a reduced-order problem for the displacement field of a 3D rail head with elastic-plastic material properties, considering various contact scenarios. The model is based on a PGD model explored in [2], which considered linear elastic material with a domain decomposition and parametric load framework.

In this work, the PGD model is extended to not only work for linear elasticity but also account for elastic-plastic rail material. The elastic-plastic rail material is addressed through two key features: 1) handling the moving load assuming a steady state, thereby employing a moving coordinate system along the rail to convert the problem into one with a stationary contact load, and 2) employing fixed-point iterations to solve displacements caused by a loading scenario and plastic strains as seen in Figure 1, as well as to solve plastic strains given by the displacement field. This approach facilitates an efficient speed-up of online simulations, particularly in evaluating the accumulated plastic deformation resulting from many over-rollings.

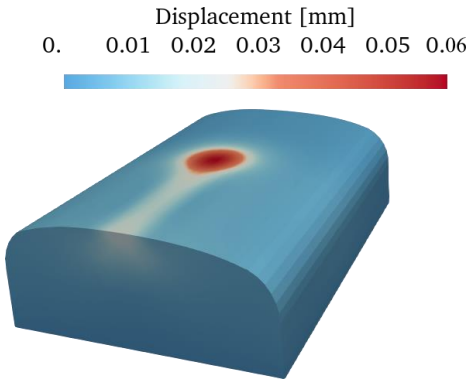

Figure 1: Displacement field in the entire rail segment given a loading scenario and the plastic strain.

References

[1] C. Ansin, B. A. Pålsson, M. Ekh, F. Larsson, and R. Larsson, “Simulation and field measurement of the long-term rail surface damage due to plasticity, wear and surface rolling contact fatigue cracks in a curve,” in *12th International Conference on Contact Mechanics and Wear of Rail/Wheel Systems*, Melbourne, Australia, Sep. 2022, p. 11.

[2] C. Ansin, F. Larsson, and R. Larsson, “Fast simulation of 3D elastic response for wheel–rail contact loading using Proper Generalized Decomposition,” *Comput. Methods Appl. Mech. Eng.*, vol. 417, Sep. 2023, doi: 10.1016/j.cma.2023.116466.

Corresponding author email: caroline.ansin@chalmers.se

STRESS-CONSTRAINED TOPOLOGY OPTIMIZATION WITH THE AUGMENTED LAGRANGIAN METHOD

G. A da Silva[1]

[1]*School of Science and Technology, Örebro University, Örebro, Sweden*

Handling stress constraints in topology optimization problems is not an easy task, mainly due to the large number of stress constraints that arise in the formulation. The direct application of standard optimization methods for topology optimization, such as the Method of Moving Asymptotes (MMA) [1], is impractical in this case, since it is necessary to perform sensitivity analysis for each stress constraint separately. Over the years, strategies have been proposed to handle stress constraints at the cost of one adjoint problem per iteration only, with P-norm/P-mean and KS aggregation techniques as the most popular ones [2].

The augmented Lagrangian (AL) method emerged, in the field, as an alternative to aggregation strategies, managing to deal with all stress constraints of the optimization problem also at the cost of a single adjoint analysis per iteration, but without having to resort to aggregation techniques [3]. Although not yet as widespread as aggregation strategies, the AL method has demonstrated great potential for use in industry. Da Silva et al. [4], for instance, have presented evidence that the local approaches based on the AL method are more efficient and have better performance than the conventional aggregation approaches, Figure 1. In another work, da Silva et al. [5] have applied the AL method to solve 3D problems with more than 100 million elements and 600 million stress constraints, in no more than 700 iterations.

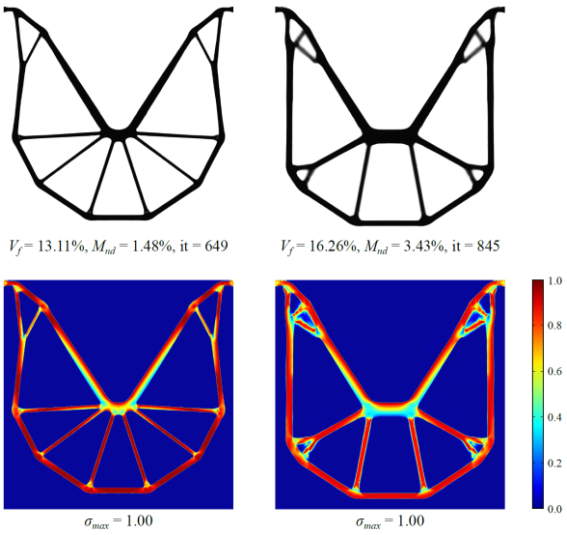

Figure 1: Crack problem. Optimized topologies and respective von Mises stress fields obtained with the AL method (left) and P-mean aggregation strategy (right). Source: da Silva et al. [4].

Despite promising results, however, the AL method is sometimes criticized for requiring a sequential approach to work properly, which may lead to many iterations to achieve convergence. We believe that the next step in the development of the AL method for topology optimization is to reduce the large number of iterations sometimes necessary to solve the problem, to allow its application in industry. To achieve this goal, it is necessary to put research effort into investigating new techniques for solving AL subproblems.

In density-based topology optimization formulations, the AL subproblems are usually solved with either the MMA or the steepest descent method with move limits [5]. The objective of this work is to study alternative approaches to the above.

Since AL subproblems are bound-constrained by nature, focus will be given to the most efficient methods for general bound-constrained optimization, like L-BFGS-B, GENCAN and ASA [6]. At the end of this study, it is expected to obtain a robust and efficient optimization strategy to solve general stress-constrained topology optimization problems.

References

[1] Svanberg K., The method of moving asymptotes - a new method for structural optimization. Int J Numer Methods Eng, 24(2), 359-373, (1987)

[2] Verbart A., Langelaar M., van Keulen F., A unified aggregation and relaxation approach for stress-constrained topology optimization. Struct Multidiscip Optim, 55, 663-679, (2017)

[3] Fancello E.A., Pereira J.T., Structural topology optimization considering material failure constraints and multiple load conditions. Latin Am J Solids Struct, 1(1), 3-24, (2003)

[4] da Silva G.A., Aage N., Beck A.T., Sigmund O., Local versus global stress constraint strategies in topology optimization: A comparative study. Int J Numer Methods Eng, 122(21), 6003-6036, (2021)

[5] da Silva G.A., Aage N., Beck A.T., Sigmund O., Three-dimensional manufacturing tolerant topology optimization with hundreds of millions of local stress constraints. Int J Numer Methods Eng, 122, 548-578, (2021)

[6] Hager W.W., Zhang H., A new active set algorithm for box constrained optimization. SIAM Journal on Optimization, 17(2), 523-557, (2006)

Corresponding author email:gustavo.assis-da-silva@oru.se

Predicting the stress response and failure of natural fibre composites with generative adversarial networks based on X-ray computed tomography three-dimensional images

Robert Auenhammer[1], Renaud Gutkin[2,1], Leif Asp[1]

[1]*Material and Computational Mechanics, Department of Industrial and Materials Science, Chalmers University of Technology, SE-41296 Göteborg, Sweden*
[2]*Safety Centre, Volvo Car Corporation, SE-40531 Göteborg, Sweden*

In recent years, natural fibre composites, comprising materials like kenaf, flax, jute, hemp, silk, cotton, or wood combined with a polypropylene matrix, have attracted attention for their potential applications in automotive, construction, aerospace, and renewable energy industries. These composites contribute to sustainability efforts in production and end-of-life processes, but harnessing their full potential requires a profound understanding of their mechanical characteristics, particularly their complex failure behaviour.

The failure process of natural fibre composites involves complex interactions, including fibre failure, matrix cracking, and debonding at the fibre-matrix interface. Numerical material models designed for composite failure analysis reflect the micro and macro-level behaviour of these composites. However, the non-uniform shape and distribution of natural fibres pose challenges in establishing reliable failure criteria, making it difficult to understand the onset and propagation of damage.

To address these challenges, image-based modelling using X-ray computed tomography scans [1] is employed. This approach allows detailed characterisation of the composite's microstructure, revealing fibre, matrix, and void distribution, as well as fibre orientation [2]. While X-ray computed tomography has been mainly applied to man-made fibres like glass [3] and carbon [4], its potential for extensive utilisation in random-oriented natural fibre composites at a coupon level presents promising opportunities. Subsequently, this approach holds the potential to be employed in developing material models at the structural level.

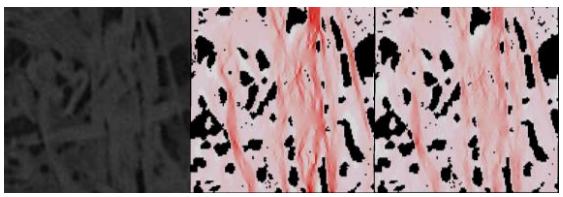

Figure 1: X-ray computed tomography scan (right), simulation result (middle), predicted with generative adversarial network (left).

The developed X-ray computed tomography aided engineering (XAE) process utilising a relatively large voxel-size of 8 µm, proves effective in achieving precise segmentation of all three phases (fibres, matrix, and void) within the scanned samples. By this the model can be effectively calibrated for elasticity, plasticity, and damage parameters. This calibration process is informed by tensile tests and integrated digital image correlation analysis. Once the material model is calibrated sub-models can be used to train a generative adversarial network. The trained model proves to provide accurate stress fields (Figure 1).

Modelling the failure mechanisms of natural fibre composites, particularly utilising X-ray computed tomography, presents significant challenges due to the non-uniformity in fibre shape and orientation. Despite the low contrast between fibres and matrix, we demonstrate the efficacy of X-ray computed tomography based modelling techniques. This enables the development of a generative adversarial network capable of swiftly providing highly accurate predictions of stress fields based on grayscale X-ray computed tomography images. This approach not only advances our understanding of natural fibre composites on the structural level but also facilitates their application by fostering sustainable utilisation of composite materials.

References

[1] R. M. Auenhammer, et al., Automated x-ray computer tomography segmentation method for finite element analysis of non-crimp fabric reinforced composites, Composite Structures, 256, 113136, 2020.
[2] R. M. Auenhammer, et al., Robust numerical analysis of fibrous composites from X-ray computed tomography image data enabling low resolutions, Composites Science and Technology, 224, 113136, 2022.
[3] R. M. Auenhammer, et al., Fibre orientation distribution function mapping for short fibre polymer composite components from low resolution/large volume X-ray computed tomography, Composites Part B: Engineering, 275, 111313, 2024.
[4] R. M. Auenhammer, et al., X-ray scattering tensor tomography based finite element modelling of heterogeneous materials, npj Computational Materials, 224, 113136, 2024.

Corresponding author email: robaue@chalmers.se

GRADIENT-ENHANCED PHASE-FIELD CRYSTAL PLASTICITY MODELING OF DUCTILE FAILURE IN POLYCRYSTALS

K.L. Auth[1], J. Brouzoulis[2], M. Ekh[1]

[1]*Department Industrial and Materials Science, Chalmers University of Technology, Gothenburg, Sweden*
[2]*Department Mechanics and Maritime Sciences, Chalmers University of Technology, Gothenburg, Swede*

Failure of engineering components made from metals is often preceded by the development of significant plastic strains. For the life span prediction of such components, it is important to understand the details of the fracture process. This particularly includes the interaction between the development of plastic deformation and damage on a microstructural level, leading to microscopic cracks which ultimately evolve into macroscopic cracks and then cause structural failure.

This study addresses ductile fracture of metals by modeling the nucleation and propagation of transgranular cracks in single- and polycrystals. We present a model that integrates gradient-enhanced hardening, phase-field modeling for fracture, and crystal plasticity, presented in a thermodynamic framework within large deformation kinematics. The phase-field model employs a micromorphic formulation [1] that is used for assuring irreversibility upon unloading.

We present ability of the model to predict the influence that grain boundaries and other obstacles have on transgranular crack growth. Therefore, we study the size effects introduced by the length-scale parameters in the gradient-enhanced hardening and phase-field models. Furthermore, it is demonstrated that the model is able to handle loading-unloading situations. Finally, we provide an example of how the presented model handles material inhomogeneities, such as inclusions arising during casting. Numerical examples are provided both in 2D and 3D.

References

[1] Bharali, R., Larsson, F. Jänicke, R. A micromorphic phase-field model for brittle and quasi-brittle fracture. Comput Mech 73, 579–598 (2024). https://doi.org/10.1007/s00466-023-02380-1

Corresponding author: kim.auth@chalmers.se

MODELING BENDING STIFFNESS OF SINGLE-FACE HONEYCOMB CORE SANDWICH SPECIMENS

M. O. Ayanoglu[1], L. A. Carlsson[1], and V. Saseendran[2]

[1]*Department of Ocean and Mechanical Engineering, Florida Atlantic University, Boca Raton, FL 33431, USA*
mayanoglu2012@fau.edu, carlsson@fau.edu
[2]*Department of Aerospace Engineering, The Pennsylvania State University, University Park, PA 16802, USA.*
vms5575@psu.edu

In this study, analysis of the bending behavior of single-face sandwich specimens with honeycomb core is presented. This is important from the perspective of End-Notch Flexure (ENF) and Mixed Mode Bending (MMB) testing, where a sandwich beam with a face/core debonds at one end of the specimen is loaded in flexure, see Figure 1. Analysis of bending of the single face specimen will utilize laminate beam theory and finite element analysis. The lower part of the specimen consists of a single face sheet bonded to the core. The situation for the MMB specimen is similar. The in-plane response of isolated honeycomb core and honeycomb core bonded to stiff face sheets is vastly different, as the attachment of the cell walls to face sheets prevents the cell walls from bending providing a strong stiffening effect. The influence of one-sided constraints due to bonding of the core to a single face sheet will be examined using a gradient model of the cores, and the result will be related to experiments on three and four-point testing of specimens consisting of a single face sheet bonded to a layer of honeycomb core.

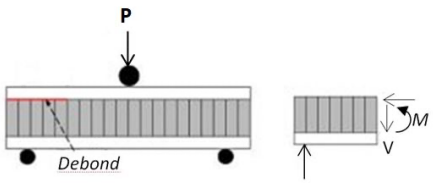

Figure 1: ENF test loading configuration with Free-body diagram of the debonded region.

Corresponding author email: Mustafa O. Ayanoglu
mayanoglu2012@fau.edu

AN ARC-LENGTH METHOD FOR PHASE-FIELD FRACTURE MODELS

R. Bharali[1], F. Larsson[1], R. Jänicke[2]

[1]*Department Industrial and Materials Science, Chalmers University of Technology, Gothenburg, Sweden*
[2]*Institute of Applied Mechanics, TU Braunschweig, Braunschweig, Germany*

Recently, the phase-field fracture models have grown in popularity owing to the ease of implementation into existing finite element software frameworks and their ability to simulate topologically complex fractures (branching, kinking and merging) in a straight-forward fashion. However, the model entails a non-convex energy functional. This results in a poor convergence of the Newton-Raphson method, resulting in solver break-down, even before a fracture starts propagating in the simulated material. The reason for this break-down is the ill-behaving indefinite stiffness matrix [1].

In this contribution, an arc-length method is proposed as a convergent monolithic solution techniques for the phase-field fracture model. To this end, an incremental fracture energy-based constraint equation is utilized, which assumes the form,

$$\int_{\Omega} \Delta g(\varphi)\, \Psi^{+}\, \mathrm{d}\Omega + \Delta s = 0, \tag{1}$$

where, $g(\varphi)$ is the phase-field degradation function, Ψ^{+} is the part of the strain energy that drives the fracture, and Δs is the arc-length. This constraint on the fracture energy dissipated at every step of the analysis allows us to trace the equilibrium path, including snap-backs.

A performance assessment of the proposed arc-length method is carried out on a single edge notched specimen under tension (see [2] for details). Table 1 presents a comparison of the arc-length method with the 'popular' BFGS method in terms of iterations required to achieve convergence and CPU time. The arc-length method outperforms the BFGS method in these performance measures.

Solution technique	tol	Steps	Total Iters.	Avg. Iters.	CPU time [s]
Arc-length	10^{-4}	265	1668	6.29	1357.0
	10^{-6}	265	1763	6.65	1719.0
	10^{-8}	312	2554	8.18	1637.0
BFGS	10^{-4}	251	5938	23.66	6701.0
	10^{-6}	251	13284	52.92	11740.0
	10^{-8}	251	30958	123.34	24720.0

Table 1: Table presents the total numbers of steps and iterations, average iterations and CPU time (in seconds) for the arc-length and BFGS methods.

The proposed arc-length method was also extended towards multiphysics applications, in particular, fluid-driven fractures in porous media (hydraulic fracture). Hydraulic fracturing problems are often driven by constant flux (external force). As such, conventional arc-length method which scales the external force cannot be used. To circumvent this issue, a novelty is introduced in the arc-length method, where the scalar unknown is the time step-size instead of the load parameter. The arc-length constraint remains the same as Equation (1).

The time step-size computing arc-length method is then adopted to solve a fluid injection problem, presented in Figure 1. The fluid is injected in the both initial fractures (see Figure 1a), and the relevant modeling parameters are adopted from [2]. Figures 1b and 1c present the distribution of the phase-field at later stages of the analysis, demonstrating propagation and merging of the two fractures.

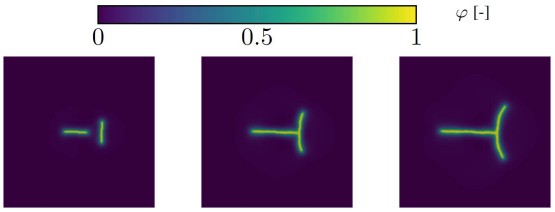

(a) t = 0.01 [s] **(b)** t = 0.026 [s] **(c)** t = 0.044 [s]

Figure 1: Figures (a-c) present the distribution of the phase-field for the rock specimen.

In order to demonstrate the robustness of the arc-length method, the residual-based tolerance was varied as $\{10^{-4}, 10^{-6}, 10^{-8}\}$ and convergence was achieved with $\{6.11, 7.70, 8.48\}$ average number of iterations, respectively. Based on these observations, we propose the arc-length method as a monolithic solution technique with superior convergence behaviour for phase-field fracture models.

References

[1] Heister, T., Wheeler, M.F., Wick, T., A primal-dual active set method and predictor-corrector mesh adaptivity for computing fracture propagation using a phase-field approach. Computer Methods in Applied Mechanics and Engineering, 290, 466-495, (2015)

[2] Bharali, R., Numerical methods and multi-scale modelling for phase-field fracture. PhD Thesis. Chalmers University of Technology (2024), `https://research.chalmers.se/en/publication/538910`

Corresponding author: ritukesh.bharali@chalmers.se

DELAMINATION OF PAPERBOARD EFFECTS OF IN-PLANE STRAINING

A.Biel[1] and U. Stigh[2]

[1]*Department of Engineering and Physics, Karlstad University, Karlstad, Sweden*
[2]*Kevenhüllers väg 7, Karlstad, Sweden*

Paperboard is creased before it is formed into boxes. Creasing provides a localised damage zone along which a precise corner of a box can be formed. During the creasing process, the paperboard is fixed. This may lead to substantial in-plane straining of the paperboard. Simple geometrical estimates indicates strain levels of the order of 10 %. At present, these strains are supposed not to influence the damaging process during creasing. In the present study, we show that in-plane straining decreases the out-of-plane strength of three different qualities of paperboard by about 6 % per % pre-straining in the plane of the paperboard.

The experimental study is conducted in two steps. During step 1, samples of paperboard are strained to fracture in tensile tests; during the second step, the pre-strained samples are tested for their delamination strength. By this method, effects of the pre-straining is evaluated.

Tensile tests are conducted similarly as in the standard ISO 1924-3 with two substantial differences: the width of the strips of paperboard is increased to 30 mm in order to supply the later tests with large enough test samples. By the same reason, the length of the test samples is maximised. This gives test specimens with the lengths 238 mm in MD and 151 mm in CD, where MD and CD indicates the Machine and Cross Directions, respectively.

Tests in the out-of-plane direction (ZD), are conducted using two different methods. With J-integral methods, the energy release rate J is measured directly and the traction separation relation is given by $\sigma_{\mathrm{n}} = \partial J/\partial w$ where w is the deformation of the paperboard at a tip of a crack-like object in the test-specimen. For a Double Cantilever Beam (DCB) specimen, $J = 2F\Theta$ where F and Θ are the applied force and the rotation of the loading point, respectively, cf. [1,2] and Fig. 1.

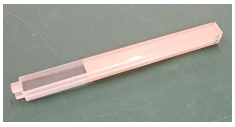

Figure 1: Double Cantilever Beam specimen with beams in plexiglas.

The second method for testing in ZD is according to the standard TAPPI T541. Here, a special fixture is used, cf. Fig. 2. A double coated pressure sensitive tape is used in both the DCB- and ZD-tests to fix the paperboard to the plexiglas beams (DCB) and steel fixture (ZD).

Figure 2: Fixture for ZD-tests.

Three qualities of paperboard are used in the study; two from Billerud designated B315 and B290, and one from Holmen Iggesund (H330) where the number is the nominal grammage of the paperboard.

Figure 3 shows the effect of pre-straining on the decrease in ZD-strength for the three different qualities of paperboard, each quality tested in three states: virgin, i.e. without pre-straining; with about 1 % pre-straining; and with about 4 % pre-straining.

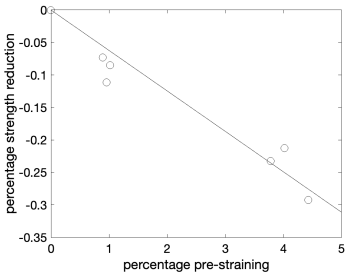

Figure 3: Percentage decrease in ZD-strength vs. percentage in-plane pre-straining.

References

[1] Andersson, T., Stigh, U., The stress–elongation relation for an adhesive layer loaded in peel using equilibrium of energetic forces. International Journal of Solids and Structures, 41, 413-434, (2004)

[2] Biel, A., et al., Experimental evaluation of normal and shear delamination in cellulose-based materials using a cohesive zone model. International Journal of Solids and Structures, 252, 111755, (2022)

Corresponding author: anders.biel@kau.se

EXPLORING GRAIN BOUNDARIES IN CRYSTALLINE MATERIALS THROUGH THE PHASE FIELD CRYSTAL METHOD

K. H. Blixt[1] and H. Hallberg[1]

[1]*Division of Solid Mechanics, Lund University, Lund, Sweden*

Crystalline materials represent one of the most important types of materials used today. However, we still lack a comprehensive understanding of their underlying physics, particularly concerning the impact of microstructural changes on material properties. Current experimental techniques often fall short in capturing atomistic interactions as they occur, leaving us with a snapshot of the initial and end states of the system. This limitation underscores the need for simulations to study the dynamics between these states. One such simulation tool is the Phase Field Crystal (PFC) method, first introduced in [1]. This method is capable of capturing atomistic rearrangements at both the atomic length scale and longer, diffusional, time scales – a combination seldom achieved by a single numerical method.

The PFC method is based on a free energy functional defined to minimize a continuous density field into crystalline order, as shown in Figure 1. The diamond cubic (DC) crystalline structure is clearly visible in Figure 1 from the stick-and-ball representation extracted from the density field. The use of a continuous density field enables efficient calculations based on spectral methods, making longer time scales possible.

PFCs have been used to study phenomena such as particle pinning [2], nanoscale deformations [3], and grain boundary multiplicities [4]. Furthermore, material properties such as grain boundary energy, stiffness, and strains are accessible through the PFC method [3, 5], making it attractive for studying static and dynamic processes.

Although the application of PFC modeling has proved to be a versatile and effective numerical tool for analyzing crystalline microstructures and their evolution, the predominant focus of many studies has been on bulk crystal behavior in 2D, with less exploration into 3D crystal defects such as grain boundaries (GBs), where [2-6] are notable exceptions. This gap is particularly noticeable in crystal structures beyond face- and body-centered cubic crystals, such as DC crystal structures. To overcome this limitation, three formulations of PFC free energies were studied in [6], where possibilities for studying DC were uncovered using a three-point correlation.

Further development of the PFC method and its applications might bring forth new insight into the relationship between microstructure and material properties, as well as the microstructure evolution of polycrystalline materials. This will facilitate improvements to materials through grain boundary engineering. This is targeted in ongoing research efforts in the characterization of grain boundary migration and how dynamic properties differ from static ones.

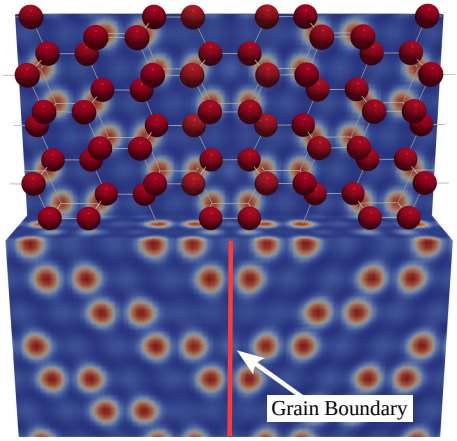

Figure 1: Grain boundary separating two crystals with diamond cubic structure. Shown both as the continues density field used in the phase field crystal method and as a representative stick-and-ball representation extracted from the density field.

References

[1] K.R. Elder, M. Katakowski, M. Haataja and M. Grant, Physical Review Letters, 88, 245701, (2002)

[2] K. H. Blixt and H. Hallberg, Materials & Design, 220, 110845, (2022)

[3] H. Hallberg and K. H. Blixt, Metals, 12, 1630, (2022)

[4] H. Hallberg and K. H. Blixt, Materials Today Communications, 38, 107724, (2024)

[5] K. H. Blixt and H. Hallberg, Modelling and Simulation in Materials Science and Engineering, 30, 014002, (2022)

[6] K. H. Blixt and H. Hallberg, Physical Review Materials, Accepted, (2024)

Corresponding author: kevin.blixt@solid.lth.se

REDUCED ORDER MULTISCALE MODELING OF PAPERBOARD

G. Boman[1], M. Ristinmaa[1], M. Wallin[1], E. Borgqvist[2]

[1]*Division of Solid Mechanics, Lund University, Sweden*
[2]*Tetra Pak Packaging Solutions, Lund, Sweden*

Paperboard is an important material for packaging food and beverages, with hundreds of billions of packages produced every year. The mechanical response of paperboard is dictated by its microstructure, i.e. fiber, fiber-fiber interface properties and fiber orientations. Material models that take the microstructure into account in the modeling framework can be used to design the paperboard structure and be used as a virtual test environment.

To gain insight into the mechanical behavior of paperboard and predict its response in complex load cases, virtual modeling is a powerful alternative to experiments. Macroscopic continuum based paperboard models have successfully been used to predict the macroscopic mechanical response during creasing and folding in industrial packaging applications [1]. For a deeper insight into the micromechanical response, and to further optimize the material designs, a micromechanical model is needed.

In this contribution, a multiscale framework is implemented, where the macroscopic response is determined entirely by a microscale representative volume element (RVE) (see Figure 1). To alleviate the inherent computational effort of multiscale analyses, an eigenstrain-based reduced order model (ROM) [2] is implemented. In this reduction, the RVE is divided into partitions, where plastic strain fields are assumed to be uniform for each partition.

The multiscale analysis successfully captures simple loading cases, such as uniaxial loading. This contribution provides a very promising framework upon which a more complex model will be developed.

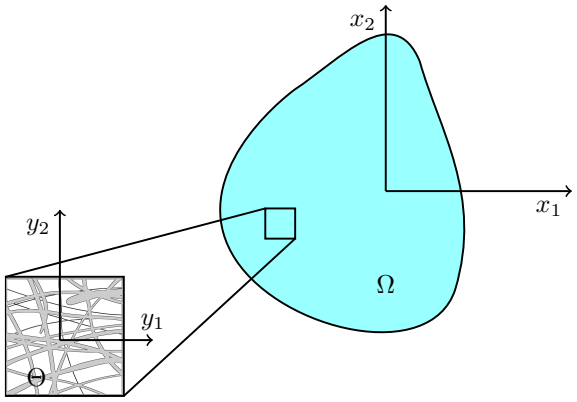

Figure 1: Multiscale spatial domains. The mechanical response at the macroscopic domain Ω is governed by the response of an X-ray based fibrous unit cell domain Θ.

References

[1] Robertsson, K., Jacobsson, E., Wallin, M., Borgqvist, E., Ristinmaa, M., Tryding, J. *A continuum damage model for creasing and folding of paperboard*, Packaging Technology and Science, Vol. 36, 2023.

[2] Fish. J., Filonova. V., Yuan. Z. *Hybrid impotent-incompatible eigenstrain based homogenization*, International Journal for Numerical Methods in Engineering, Vol. 95, 2013.

Corresponding author: gustav.boman@solid.lth.se

VARIATIONALLY CONSISTENT HOMOGENISATION OF PLATES

E. Börjesson[1], F. Larsson[1], K. Runesson[1], J.J.C. Remmers[2], M. Fagerström[1]

[1]*Department Industrial and Materials Science, Chalmers University of Technology, Gothenburg, Sweden*
[2]*Department Mechanical Engineering, Eindhoven University of Technology, Eindhoven, The Netherlands*

Multi-scale modelling is widely used to examine the effects of material heterogeneities at the sub-scale. This process involves the application of both prolongation and homogenisation techniques to establish connections between the macro-scale and the sub-scales (e.g micro-scale or meso-scale). Moreover, in a variety of industrial settings, the structural elements at the macro-scale are commonly represented by beams, plates, and shells, where they are important for many design considerations. Therefore, there is a need for multi-scale approaches that are specifically developed for structural elements. This work focuses on the development of multi-scale framework for plate elements.

In [**1**] we propose a computational homogenisation framework specifically aimed for plate elements, illustrated in Figure 1. The framework's general methodology is as follows: Kinematic quantities from the macro-scale, namely membrane strains $\bar{\boldsymbol{\varepsilon}}$, bending curvatures $\bar{\boldsymbol{\kappa}}$, and shear strains $\bar{\boldsymbol{\gamma}}$, are prolonged to the sub-scale. This sub-scale is characterised by a Representative Volume Element (RVE) of the target material, and the macro-scale kinematic quantities are imposed as boundary conditions on the lateral faces of the RVE. Subsequently, the sub-scale problem is solved, resulting in membrane forces $\bar{\boldsymbol{N}}$, bending moments $\bar{\boldsymbol{M}}$, and shear forces $\bar{\boldsymbol{V}}$ which are then homogenised back to the macro-scale.

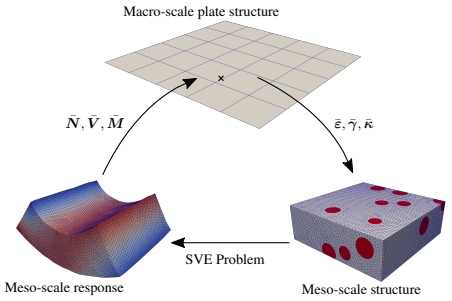

Figure 1: Illustration of computational homogenisation for plates.

The framework is developed within a variationally consistent framework, leading to the derivation of a set of prolongation and homogenisation conditions that maintain kinematic consistency. Interestingly, we show that a non-standard volumetric constraint emerges when enforcing a deformation-consistent homogenisation procedure. This volume-constraint is crucial for accurate prediction of the homogenised shear forces, especially for thin RVEs. An additional advantage with our approach lies in the fact that the macroscopic problem, that is, the complete plate theory, can be derived from an underlying kinematic description.

The efficency of the proposed homogenisation framework is validated through a series of numerical examples. We demonstrate that the predicted homogenised stiffness properties agree with known analytical theories, such as classic laminate theory. Furthermore, the framework's application to a realistic sub-scale structure of a 3D-woven composite showcases results that closely match those of a full-scale reference solution.

References

[1] Börjesson, E., Larsson, F., Runesson, K., Remmers J.J.C., Fagerström, M. Variationally consistent homogenisation of plates. Comput. Methods Appl. Mech. Engrg. 413 (2023)

Corresponding author: elias.borjesson@chalmers.se

NEUTRON IMAGING OF HYDROGEN EMBRITTLMENT AND SERENDIPITY DUE TO EXPERIMENTAL CONSTRAINTS

C.F.O. Dahlberg[1], A.E. Halilovic[1], D. Lindblom[1], R. Woracek[2], T. Chulapakorn[2], L. Helfen[3], A. Tengattini[3], J. Pan[4],

[1] *Department of Engineering Mechanics, KTH Royal Institute of Technology, Stockholm, Sweden*
[2] *ESS European Spallation Source, Lund, Sweden* · [3] *ILL Institute Laue-Langevin, Grenoble, France*
[4] *Department of Chemistry, KTH Royal Institute of Technology, Stockholm, Sweden*

Hydrogen embrittlement (HE) is one of the main challenges in modern high-strength engineering alloys. It is a complex and poorly understood materials phenomena where small amounts of H in the lattice cause embrittlement and subsequent pre-mature failure.

Here, we investigate HE in 3-point-bend fracture mechanics, and tensile, specimens. Both high strength martensitic steel and duplex stainless-steel is investigated. Two dedicated environmental cells have been developed for in-situ neutron imaging under mechanical load in HE conditions [1]. Neutron transmission images of crack propagation in a reference in-air sample is shown in Figure 1.

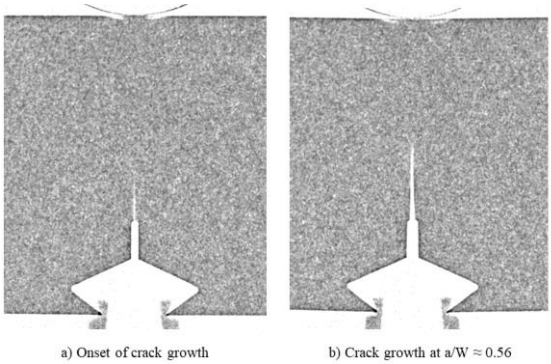

Figure 1: Neutron imaging of crack propagation [1].

Experimental protocols are derived from hydrogen fracture mechanics testing [2] and combine mechanical loading with electrochemical charging of H. Mechanical load is introduced by a mobile load frame that can be deployed at various neutron beamlines. H is introduced via partial submersion in H_2O + 3.5% NaCl while a cathodic polarization current is applied to promote H ingress. Water is effectively opaque to neutrons and must therefore not be present in, or near, the neutron image field of view. This imposes strict constraints on the experimental setup. Especially since H is light, mobile, and diffuse easily [3] thereby requiring a true in-situ investigation. These challenges and our proposed solutions will be discussed in some detail.

The methodology is utilized in two ongoing research projects: ISOTOPE and ReHEART. The final goal is to better understand and model HE on engineering relevant length and time scales. Particularly, we hope to be able to image a spatially and temporally resolved H concentration under in-situ HE conditions. While this challenging goal is not yet met, we have been able to directly image intermittent crack propagation under static load because of HE, so called delayed hydrogen cracking, see figure 2. Valuable information on H diffusion and crack growth resistance can be extracted from such data. This finding was, in part, due to a modified test protocol due to neutron imaging constraints. One could call it a *serendipitous complication* and this concept will also be discussed.

Finally, upper bounds on H distribution will be presented. Bounds are based on neutron transmission signal fidelity, fractography, stress-assisted H diffusion modelling, and classical fracture mechanics considerations.

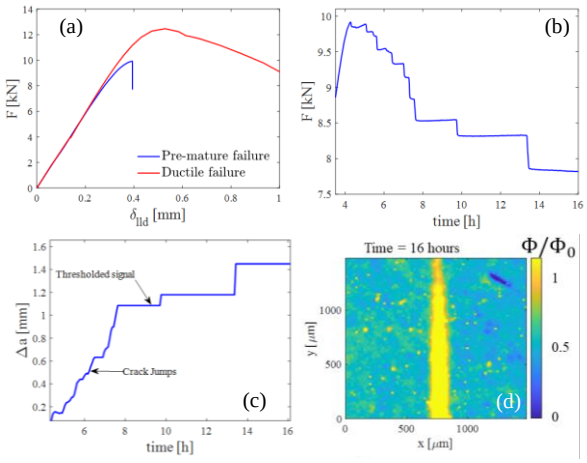

Figure 2: Force vs displacement (a), force (b) and crack propagation (c) vs time during delayed cracking and neutron transmission intensity after 16 hours (d) [1].

References

[1] Lindblom, D., et al., In-situ neutron imaging of delayed crack propagation of high strength martensitic steel under hydrogen embrittlement conditions, *Materials Science and Engineering: A*, 895, 146215, (2024)

[2] Halilovic, A.E., et al., An experimental-numerical screening method for assessing environmentally assisted degradation in high strength steels, *Engineering Fracture Mechanics*, 245, 107572, (2021)

[3] Cairney, J., Atoms on the move-finding the hydrogen, *Science*, 355, 1128-1129, (2017)

Corresponding author email: carldahl@kth.se

Modular Simulation Approach for Case Hardening of Steel

Clas Dahlin[1], Carl F.O. Dahlberg[1], Henrik Larsson[1]

[1]*Department of Engineering Mechanics, KTH Royal Institute of Technology, Stockholm, Sweden*

The microstructure and phase fractions in steel play a pivotal role in determining the material properties and performance of steel components. Especially in modern high-performance surface-treated bearing steel. To fully describe the case hardening process from virgin material to a case-hardened component, it requires knowledge of spatially resolved chemical composition from carbonitriding, subsequent phase transformation to predominantly martensite during quenching, and the stress and strain state during the whole process. These steps are coupled, notably the stress/strain state and the phase transformation.

In this project, we aim to simulate the entire case hardening process with all steps properly included. This is accomplished by linking together state-of-the-art models in a modular framework. Modularity is a key feature since it allows us to investigate model sensitivity on the final output by easily exchanging one model for another. The goals are to be able to evaluate the effect of process parameters and eventually be able to run the process backwards in an optimization loop.

The framework is designed with a central structure in which programs interface with a data stream to store all intermediate results. Simulations can then be run in loops and results compared automatically and input is adjusted before the next loop.

Key modules include,

- Diffusion (Thermo-Calc, DICTRA)
- Transformation estimation (Thermo-Calc, DICTRA)
- Transformation model fitting (Python)
- FEM modelling (COMSOL Multiphysics)
- Optimization loop (Python)

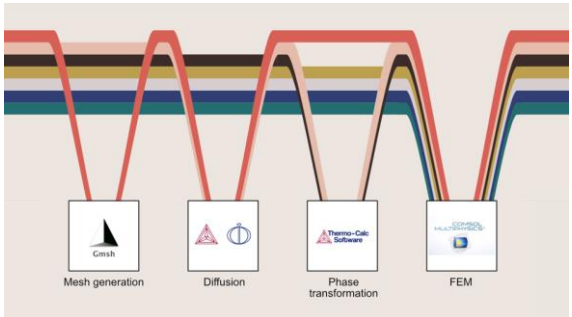

Figure 1: Schematic visualization of the framework.

The phase transformation models that are implemented is KJMA [1] for bainite and pearlite transformation,

$$f_i = 1 - \exp\left(-\left(\frac{t}{\tau}\right)^n\right) \qquad (1)$$

and Koistinen-Marburger [2] for martensite transformation,

$$f_i = 1 - \exp(-\beta(M_s - T)). \qquad (2)$$

Under these conditions, a material point may experience elastic, plastic, thermal, molar volume, and transformation strains.

$$\varepsilon = \varepsilon_{el} + \varepsilon_{pl} + \varepsilon_{th} + \varepsilon_{ph} + \varepsilon_{tr} \qquad (3)$$

All these contributions are possible to include in the proposed modelling framework. As a first approximation the material properties are calculated with a general rule of mixture between the phases.

The simulation results will be validated against a heat-treated grade 159G steel. This will involve characterization of virgin and heat-treated material, including, tensile, compression, and hardness testing. Experimental validation will also include the estimation of phase fractions and residual stress by conducting wavelength dispersive neutron imaging.

References

[1] Avrami, Melvin. "Kinetics of phase change. I: General theory." *The Journal of chemical physics* 7(12), 1103-1112, (1939)

[2] Koistinen, D. P., Marburger R. E. “A general equation prescribing the extent of the austenite-martensite transformation in pure iron-carbon alloys and plain carbon steels.”. *Acta Metallurgica* 7(1), 59-60, (1959)

Corresponding author email: clasd@kth.se

THE CONSTITUTIVE RESPONSE OF TEXTILE REINFORCED CONCRETE SHELLS FROM COMPUTATIONAL HOMOGENIZATION

Gabriel Edefors[1,2], Fredrik Larsson[1], Karin Lundgren[2]

[1]*Department of Industrial and Materials Science, Chalmers University of Technology, Gothenburg, Sweden*
[2]*Department of Architecture and Civil Engineering, Chalmers University of Technology, Gothenburg, Sweden*

Textile reinforced concrete (TRC) has been around for many decades, still its widespread adoption has been limited. Partly this can be attributed to a lack of adequate mechanical models, particularly in the serviceability state [1]. The complex behavior of TRC arises from various factors, including concrete cracking, partial concrete penetration, inter-filament slip and debonding of the yarns [2]. This research aims at developing a homogenization scheme that captures these effects, without having to calibrate the parameters for every new reinforcement configuration.

The sub-scale problem is solved using the FE-software COMSOL. The concrete is modeled as an isotropic continuum using the Mazars damage model to account for damage, both in tension and compression. Additionally, the stiffness and the tensile strength are reduced in proportion to the reduction of concrete volume loss due to the yarns. This induces strain localization at the transverse yarns. The yarns are modeled using linear-elastic truss elements. The interfilament-slip in the yarns and the delayed activation of the filaments are accounted for by using efficiency factors for stiffness and strength. These parameters have been calibrated along with the the bond-slip parameters in [3]. The up-scaling from the RVE to the plate is performed using Variationally Consistent Homogenization, see [4]. Three different boundary conditions have been studied.

- Neumann BC: Boundary tractions prescribed (lower bound)
- Dirichlet BC: Boundary displacements prescribed (upper bound)
- Periodic BC: Periodic fluctuation fields

A simulation, subjecting the RVE to increasing uniaxial curvature $\bar{\kappa}_{xx}$, has been conducted to demonstrate the up-scaling from the sub-scale stress field to effective bending moment, see Fig. 1. We see that the Dirichlet and Neumann conditions are in fact upper and lower bounds on the effective bending moment, with the strongly periodic being somewhere in-between. Further, it can be observed that the simulation using Neumann condition fails already for small curvatures. This occurs because the prescribed traction tends to rupture the edges, before fully activating the yarns.

The proposed homogenization technique could be employed in large-scale plate models, either by on-the-fly RVE simulations at each integration point, or by identification of a surrogate model based on virtual testing of the RVE model.

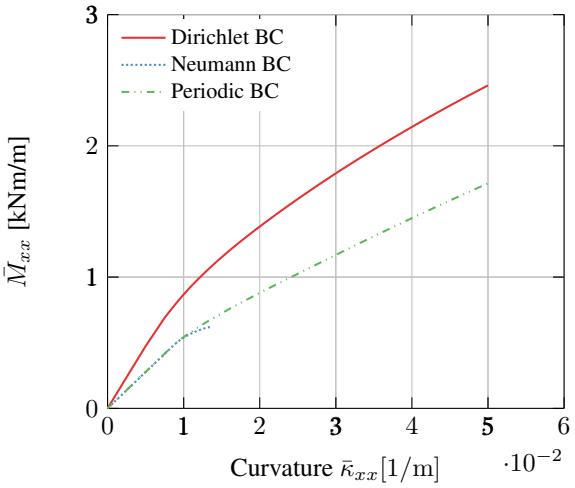

Figure 1: Large-scale curvature-moment response obtained using three different boundary conditions.

References

[1] Preinstorfer, P., Yanik, S., Kirnbauer, J., Lees, J.M., Robisson, A. Cracking behaviour of textile-reinforced concrete with varying concrete cover and textile surface finish. Composite Structures, 312, (2023).

[2] Chudoba, R., Sharei, E., Scholzen, A. A strain-hardening microplane damage model for thin-walled textile-reinforced concrete shells, calibration procedure, and experimental validation. Composite Structures, 152, 913-928, (2016)

[3] Sciegaj, A., Larsson, F., Lundgren, K.: Experiments and calibra- tion of a bond-slip relation and efficiency factors for textile reinforcement in concrete. Cement and Concrete Composites, 134, (2022).

[4] Sciegaj, A., Grassl, P., Larsson, F., Runesson, K., Lundgren, K. Upscaling of three-dimensional reinforced concrete representative volume elements to effective beam and plate models. International Journal of Solids and Structures, 202, 835-853 (2020).

Corresponding author: gabriel.edefors@chalmers.se

LARGE-SCALE ELASTO-PLASTIC TOPOLOGY OPTIMIZATION

G. Granlund[1] and M. Wallin[1]

[1]*Division of Solid Mechanics, Lund University, Box 118, SE-22100 Lund, Sweden*

Background

Solving 3D topology optimization (TO) problems is challenging as the required element resolution significantly increases the computational time of the optimization and incorporating elasto-plasticity into TO increases the computational complexity further.

For plasticity models where the plastic strain rate is coaxial to the stress, the plastic evolution laws can be reduced to a scalar equation. In this work we show that the adjoint computations also can utilize coaxiality to significantly reduce the computational cost for the sensitivity analysis which is used to provide an efficient framework for large-scale elasto-plastic TO.

Methods

Density-based optimization is employed wherein the design is defined by a piece-wise uniform field. To formulate a well-posed optimization problem, restriction by filtration is used via the partial differential equation (PDE) filter [1], so that a filtered design field is obtained. The Solid Isotropic Material with Penalization (SIMP) scheme [2] is used to interpolate the material properties.

The reduced equation used in the primary problem can be used in the path-dependent adjoint sensitivity scheme [3] to construct an efficient procedure to find the adjoints which is very similar to the elasto-plastic state update.

Results

The framework is used to design structures with energy absorption and tailored mechanical response. A cantilever beam, discretized using 2.1 million elements and 6.5 million degrees of freedom, is designed to be initially stiff until a break point is reached after which the structure becomes compliant, see Figure 1.

In the second problem we maximize the plastic work of a double clamped beam discretized using 16.8 million elements and 51 million degrees of freedom, see Figure 2.

Conclusions

Results show that the proposed sensitivity scheme is able to solve high resolution 3D elasto-plastic TO problems where structures with tailored mechanical response and energy absorption are designed.

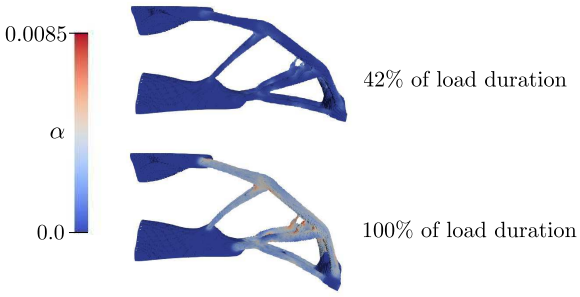

Figure 1: Equivalent plastic strain, after 42 % and 100 % of the maximum load is applied.

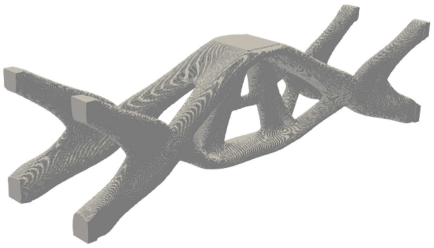

Figure 2: Design optimized for plastic work maximization.

References

[1] B. S. Lazarov, O. Sigmund, Filters in topology optimization based on helmholtz-type differential equations, International Journal for Numerical Methods in Engineering 86 (6) (2011) 765–781.

[2] M. P. Bendsøe, Optimal shape design as a material distribution problem, Structural optimization 1 (1989) 193–202.

[3] P. Michaleris, D. A. Tortorelli, C. A. Vidal, Tangent operators and design sensitivity formulations for transient non-linear coupled problems with applications to elastoplasticity, International Journal for Numerical Methods in Engineering 37 (1994) 2471–2499.

Corresponding author: gunnar.granlund@solid.lth.se

VOXEL-BASED MESOSTRUCTURE MODELLING OF TOW-BASED DISCONTINUOUS COMPOSITES FOR FINITE ELEMENT ANALYSIS

L. Gulfo[1], I. Katsivalis[1], L.E. Asp[1], M. Fagerström[1]

[1]*Department Industrial and Materials Science, Chalmers University of Technology, Gothenburg, Sweden*

Novel Tow-Based Discontinuous Composites (TBDCs) with ultra-thin spread tapes (~20 μm) have demonstrated a high performance in advanced structural applications in terms of stiffness, strength, and in-plane quasi-isotropic response [1]. By using chopped UD tapes in combination with random deposition and compression moulding, TBDCs are cost-effective and easy to manufacture compared with composite laminates. However, their mesostructure displays complex 3D features such as tape waviness, tape draping, resin pockets, local variations of plate thickness and fibre volume fractions, that have been shown to influence the mechanical properties [2]. Moreover, these characteristics largely vary depending on whether thick, thin, or ultra-thin tapes are used. Thus, new modelling techniques need to be developed and validated to capture the different mesostructures down to those of ultra-thin TBDs.

The present work proposes a new voxel-based mesostructure modelling approach based on a modified 3D Random Sequential Absorption (RSA) technique to generate virtual models of TBDCs for finite element analysis. The RSA consists of depositing each tape individually and sequentially in random positions to generate TBDC plates (Fig. 1) [3]. For this purpose, the proposed mesostructure generator integrates three tape deposition strategies, which are a bin-guided tape allocation, tape draping, and plate thickness control. The modelling parameters are driven by an experimental study of microscopic images and fibre volume fraction measurements of an ultra-thin TBDC. Realistic in-plane and out-of-plane angle distributions show the capabilities in capturing mesostructural features.

The developed modelling approach is then tested for three types of TBDCs, namely thick, thin, and ultra-thin TBDCs. Statistical Volume Elements (SVEs) are extracted from generated TBDC plates (Fig. 1), and a statistical study of several realisations is carried out to predict the elastic properties via computational homogenisation. The sizing of SVEs is assessed in terms of the convergence of both geometrical and mechanical properties of TBDCs, including the computational cost. Finally, the predicted elastic properties are compared with experimental data from the literature (Fig. 2), showing a good agreement despite sources of error and uncertainties linked to the input properties. A comparison with Equivalent Laminates (Els) is also presented, illustrating their limitations.

Future implications of the present work include studies on material optimisation and parametric analysis to characterise how manufacturing considerations and tow architectures influence mechanical properties, and strength prediction of TBDCs.

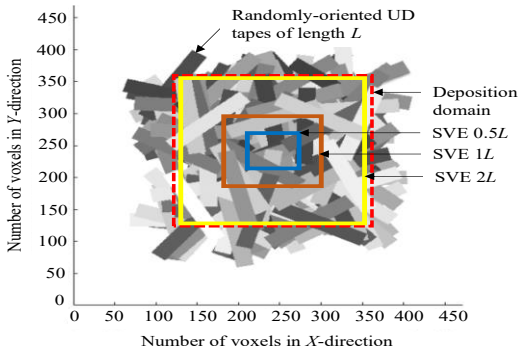

Figure 1: Voxel model of a TBDC plate and extraction of SVEs for prediction of elastic properties

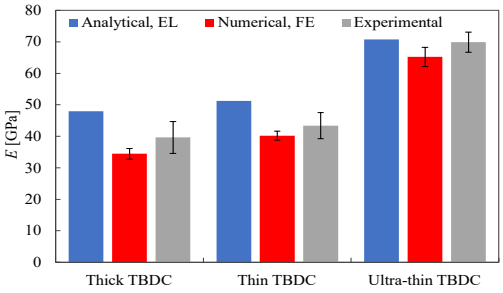

Figure 2: Comparison of predicted vs experimental *E* values for thick, thin, and ultra-thin TBDCs

References

[1] Katsivalis, I., Persson, M., Johansen, M., Moreau, F., Kullgren, E., Norrby, M., Zenkert, D., Pimenta, S., Asp, L.E. Strength analysis and failure prediction of thin tow-based discontinuous composites. *Composites Science and Technology*, 245, 110342, (2024)

[2] Alves, M., Pimenta, S. The influence of 3D microstructural features on the elastic behaviour of tow-based discontinuous composites. *Composite Structures*, 254, 112484, (2020)

[3] Ryatt, J., Ramulu, M. Prediction of tensile failure of stochastic tow-based discontinuous composites via mesoscale finite element analysis. *Composite Structures*, 279, 114769, (2022)

Corresponding author email: gulfo@chalmers.se

FATIGUE LIFE ESTIMATION OF PUNCHED AND TRIMMED SPECIMENS

D. Gustafsson[1], S. Parareda[2], R. Munier[3], E. Olsson[4]

[1]*Department of Engineering Sciences and Mathematics, Luleå University of Technology, Luleå, Sweden*
[2]*Unit of Metallic and Ceramic Materials, Eurecat, Centre Tecnològic de Catalunya, Manresa, Spain*
[3]*Global R&D, ArcelorMittal, Maizières-lès-Metz, France*

It is known that shear cutting processes could reduce the high cycle fatigue life of high strength metal components significantly. Fatigue data for the base material, such as *S-N* curves are sometimes available but cannot be relied upon in designs featuring trimmed edges or punched holes. In this work a methodology for quantification of this effect is presented, where the main sources for life reduction are assumed to be the residual stresses and notches on different scales. The approach is validated for three different complex phase steels, one aluminum alloy, two load ratios and two different specimen geometries, showing acceptable agreement for all cases. The residual stresses in the fracture zone of the cut edge are obtained using finite element simulations of the cutting process following the methodology presented in [1], and the surface roughness in the same area is measured experimentally. To account for cyclic stress relaxation of the residual stresses a simple criterion is utilized assuming that the local total stress after cyclic relaxation will never exceed the material yield stress. Required data for utilization of the methodology are a high cycle *S-N* relationship for the material in polished condition, uniaxial tensile properties, and the cut edge fracture surface residual stress and roughness. No parameter fitting is needed. An example of the fatigue life estimation, the specimen geometries, and residual stress distribution in different cut edges are presented in Figures 1, 2 and 3, respectively.

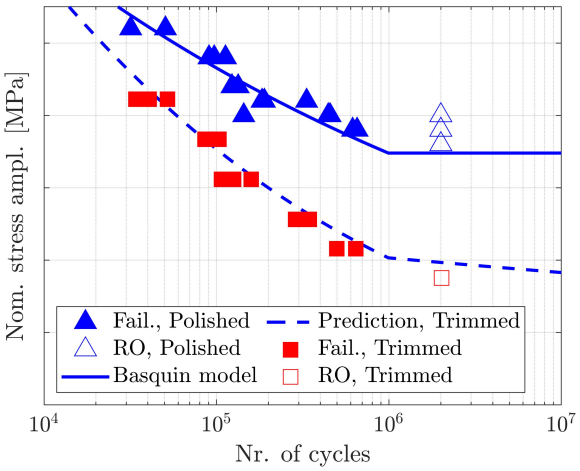

Figure 1: Estimation of fatigue life reduction of trimmed steel specimens tested at load ratio R = -1.

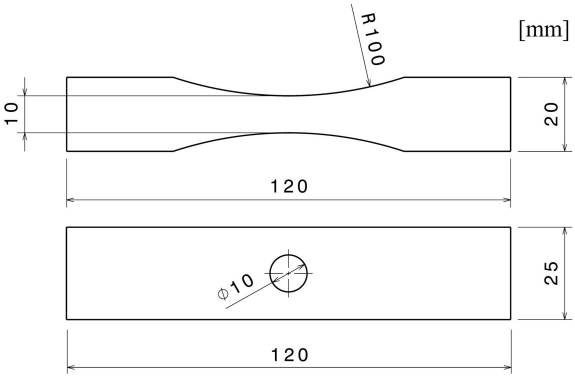

Figure 2: Geometries of punched and trimmed specimens.

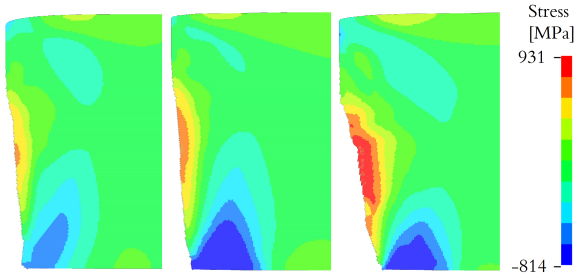

Figure 3: Residual out-of-plane stress distribution.

The main findings from the study are:

- Uniaxial tensile properties, base material fatigue performance, surface roughness and residual stresses in the fracture zone of the cut edge could be used to accurately estimate fatigue life reduction of shear cut specimens in the HCF regime.
- Neglecting cyclic stress relaxation has a detrimental effect on the prediction accuracy of the model.

References

[1] Gustafsson, D., Parareda, S., Ortiz-Membrado, L., Mateo, A., Jiménez-Piqué, E., Olsson, E., Simulation of metal punching and trimming using minimal experimental characterization. Journal of Materials Processing Technology, 321, (2023)

Corresponding author: david.gustafsson@ltu.se

Svenska Mekanikdagar
17–19 June, 2024 Gothenburg, Sweden

FRACTURE TOUGHNESS CHARACTERIZATION OF HIGH STRENGH MARTENSITIC STEELS SUBJECTED TO HYDROGEN

Armin E. Halilović*, Jonas Faleskog, and Pål Efsing

Solid Mechanics, Department of Engineering Mechanics, KTH Royal Institute of Technology, Teknikringen 8D, SE-100 44 Stockholm, Sweden.
** Presenting Author email: arminh@kth.se*

Abstract
High strength steels that are subjected to hydrogen may experience environmentally assisted degradation. These types of steels exhibit a loss of load bearing capacity. This paper presents a numerical-experimental method for screening materials' susceptibility subjected to hydrogen. In this work it is found that hydrogen needs time to diffuse into the material and time to cause degradation.

1. Introduction

Hydrogen Embrittlement (HE) is a phenomenon that reduces the mechanical properties of high strength steels. Although HE has been a known phenomenon for over 150 years as discovered by Johnsson (1875), it is still not evident what causes the degradation. One reason for this is that HE manifests itself in different ways for different high strength steels. Another reason for this misconception is that a standard testing procedure does not exist. A commonly used experimental method employed is *slow strain rate testing* (SSRT). In SSRT a tensile test is performed in a hydrogen rich environment. The testing can provide hydrogens influence on the maximum stress, yield stress, elongation to failure and ductility reduction. SSRT is a method that is easy to perform, it is inexpensive and gives a good indication of a material's susceptibility to HE. However, the results conducted from these experiments are difficult to reproduce and to utilize in a predictive manner. For this reason, a fracture mechanics approach is studied in this work. Here a single-edge notch bend specimen is utilized, which is subjected to a constant displacement rate and cathodic polarization. A fractography study is conducted to further assist in the interpretation of the results obtained from the experiments.

2. Results

The material investigated was a high-strength, low hardening martensitic steel with ultimate tensile stress of 1.5 GPa. The tests are subjected to hydrogen-charging in a 3.5% NaCl electrolyte with a platina mesh as the auxiliary electrode. Nitrogen purging is present throughout the whole experiment. All electrochemical experiments are performed in a simplified autoclave made of hard plastic with ceramic rolling supports to ensure no metal-metal contact in the environment. Several parameters were investigated that may influence the fracture mechanical properties. These include current density, pre-charging time and loading rate. A method based on FEM-solutions was developed to continuously evaluate the *J*-integral and crack length. It is found that the loading rate has a significant effect on the J-R curves, seen in Figure 1. It should also be mentioned that no significant effect on the fracture toughness is observed by reducing the loading rate in air. The results presented in Figure 1 include the key findings from this study, i.e., the effect of loading rate on the J-R curve for a martensitic steel subjected to a hydrogen rich electrolyte. Here a brief discussion of each individual curve is presented top-down. The loads are defined in terms of the rate of the initial stress intensity factor, $\dot{\chi} = K_I/\left[\mathrm{MPa}\sqrt{\mathrm{m}}\ \mathrm{s}^{-1}\right]$.

The fastest loading rate is performed in air and in accordance with ASTM E1820. From this experiment the fractography shows that dimple failure is the dominating mode of failure. The remaining curves are subject to hydrogen charging and different individual loading rates. By reducing the loading rate by a factor of 100, from $\dot{\chi} = 3.3$ to $\dot{\chi} = 3.3 \cdot 10^{-2}$, it is seen that the onset of crack growth is reduced from 110 kN/m to 60 kN/m. A fractography examination of this test reveals that failure is still dominated by dimple rupture. However, in these experiments, secondary cracks are also present. The secondary cracks are growing in the middle of the specimen in a direction perpendicular to macroscopic crack front.

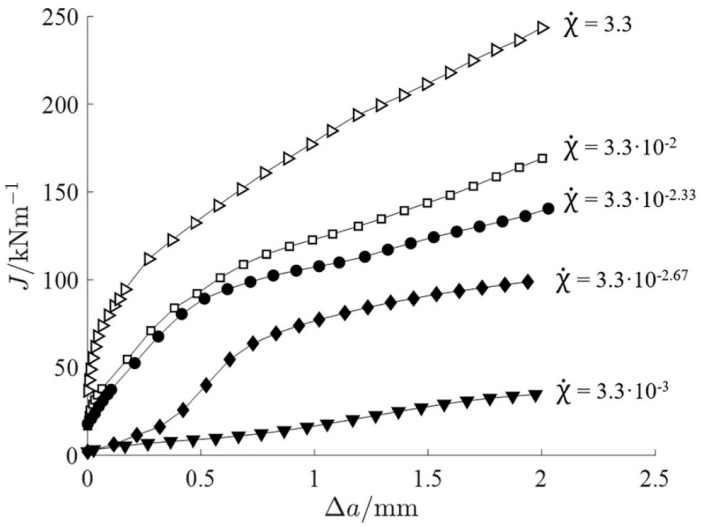

Figure 1: Resistance curves subjected to different loading rates and hydrogen charging.

By further reducing the loading rate to $\dot{\chi} = 3.3\cdot10^{-2.33}$, no significant change in the fracture mechanical properties is observed. The fourth curve from the top pertain to $\dot{\chi} = 3.3\cdot10^{-2.66}$, and here, the J-R curve is initially low and increases rapidly after approximately 0.3mm of crack growth to a plateau at around 60 kN/m. To the author's knowledge, this shape of the J-R curve has not previously been observed in high strength steels. The outcome of this test is interpreted as follows; during charging hydrogen accumulate ahead of the crack tip, and as the loading rate is slow enough, the hydrogen has sufficient time to cause substantial degradation of the material prior to crack initiation. However, as soon as the crack starts to propagate, hydrogen does not have sufficient time to cause degradation of the material in the uncracked ligament. This is further supported by the fractography which shows a region ahead of the crack tip where a mixture of dimple failure and intergranular failure is present in the middle of the specimen, close to the pre-fatigue crack tip. Outside of this region, the intergranular failure is not as intuitively observed. Rather a combination of dimples, secondary cracks and intergranular failure is observed. At the slowest loading rate, $\dot{\chi} = 3.3\cdot10^{-3}$, a rather flat J-R curve with a slightly increasing tearing modulus ($\mathrm{d}J/\mathrm{d}\Delta a$). Here the fracture toughness is reduced by 90% compared to the experiment in air. The dominating mode of failure is intergranular. However, it should be emphasized that although failure is dominated by intergranular fracture, large regions of dimple rupture is still observed.

3. Conclusions

It is seen in this work that experimental fracture mechanics combined with cathodic polarization is an excellent choice to obtain reproducible results as well as a screening method of materials sensitivity to hydrogen embrittlement. An environmentally driven transition from high to low toughness was observed in a rather narrow range of loading rates. In this range, it was also observed that the hydrogen degradation may be mitigated by crack growth leaving less time for the degradation process to occur and a rise in toughness.

Acknowledgements

The work was carried out within the Strategic Innovation Program Metallic materials and STRIM, a collective venture by Vinnova, Formas and the Swedish Energy Agency. The material used is provided by SSAB Special Steels.

OPTIMIZING SCANNING STRATEGIES FOR ADDITIVE MANUFACTURING PROCESSES

G.A. Haveroth[1], C-J. Thore[2], R.F. Ausas[3], S. Jakobsson[4], M.R. Correa[1], J.A. Cuminato[3]

[1]*Departamento de Matemática Aplicada, Universidade Estadual de Campinas, Campinas, Brazil*
[2]*Department of Management and Engineering, Linköping University, Linköping, Sweden*
[3]*Department of Applied Mathematics and Statistics, University of São Paulo, São Carlos, Brazil*
[4]*GE Additive, Arcam EBM Center of Excellence, Mölnlycke, Sweden*

Metal Additive Manufacturing (AM), particularly the Electron-Beam Powder Bed Fusion (EB-PBF) process, is an increasingly adopted technique for constructing metallic components layer-by-layer. This study aims to investigate the influence of various scanning strategies, determined here by the heat source path, on the quality of the final built structure [1]. Metrics such as heat and residual stresses are employed to identify the optimal scanning strategy.

To define the problem, let us consider a domain $\Omega \subset \mathbb{R}^3$ with boundary Γ, and an AM process taking place within Ω over the time interval $[0, T]$. Additionally, Γ is partitioned into $\Gamma = \Gamma_{\text{dn}} \cup \Gamma_{\text{up}} \cup \Gamma_{\text{rg}}$ boundary parts, as depicted in Fig. 1. In the AM-PBF process, the heat source moves across the upper surface Γ_{up}, selectively transforming powder into bulk solid material.

To perform the proposed analysis, we employ a thermo-mechanical one-way coupled methodology, accounting for elastoplastic behavior and temperature-dependent parameters. The heat transfer problem is described by:

$$\begin{aligned} \rho\, \partial_t \left(c_p \theta + L f_l\right) &= \operatorname{div}\left(\kappa \nabla \theta\right) && \text{in } \Omega \times (0, T] \\ \theta &= \theta_{\text{ph}} && \text{in } \Omega \times \{0\} \\ \theta &= \theta_{\text{ph}} && \text{on } \Gamma_{\text{dn}} \times [0, T] \\ -\kappa \nabla \theta \cdot \boldsymbol{n} &= 0 && \text{on } \Gamma_{\text{rg}} \times [0, T] \\ -\kappa \nabla \theta \cdot \boldsymbol{n} &= q H_{\text{beam}} - q_{\text{rad}} && \text{on } \Gamma_{\text{up}} \times [0, T] \end{aligned} \tag{1}$$

where ρ, c_p, L, f_l, and κ represent the material density, specific heat capacity, latent heat of fusion, liquid fraction, and thermal conductivity, respectively. Furthermore, θ_{ph} denotes the pre-heating temperature, H_{beam} is a Heaviside function to localize the beam on Γ_{up}, while q and q_{rad} correspond to the heat fluxes related to the electron beam and radiation, respectively. On the other hand, the mechanical problem is given by:

$$\begin{aligned} \operatorname{div}\left(\boldsymbol{\sigma}\left(\boldsymbol{u}\right)\right) &= \boldsymbol{0} && \text{in } \Omega \\ \boldsymbol{\sigma} \cdot \boldsymbol{n} &= \boldsymbol{0} && \text{on } \Gamma \setminus \Gamma_{\text{dn}} \\ \boldsymbol{u} &= \boldsymbol{0} && \text{on } \Gamma_{\text{dn}} \end{aligned} \tag{2}$$

where $\boldsymbol{u}$ is the displacement vector field, and $\boldsymbol{\sigma}$ is the stress tensor. The constitutive relation is described by the linear Duhamel–Neumann thermoelastic law. Additionally, for the plasticity model, we adopt the von Mises yield function and the Prandtl–Reuss flow rule.

Our primary focus is on determining the heat source path, which involves moving the beam over discrete positions in space. To achieve this, we propose an Optimization Problem (OP) involving the exploration of the set P, encompassing all permutations of the positions, to identify the most suitable heating sequence for the AM-PBF process. The OP is formulated as finding $\boldsymbol{p} \in \mathrm{P}$ such that:

$$\begin{aligned} \min_{\boldsymbol{p} \in \mathrm{P}} \quad & f\left(\theta\left(\boldsymbol{p}\right), \boldsymbol{u}\left(\theta\left(\boldsymbol{p}\right)\right)\right) \\ \text{s.t} \quad & \text{state problems} \end{aligned} \tag{3}$$

with the objective function f representing some metric of the heat and residual stresses. The proposed methodology is applied for print simulation and optimization with the Ti6A14V material.

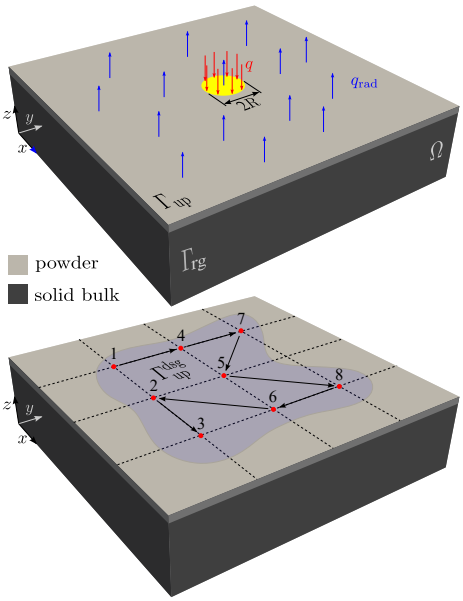

Figure 1: Domain, boundary conditions, and initial bulk/powder material distribution. Example of heating path.

References

[1] D. Ramos, F. Belblidia, J. Sienz: New scanning strategy to reduce warpage in additive manufacturing. Additive Manufacturing 28, 554–564 (2019)

Corresponding author: geovane.haveroth@liu.se

EXPLICIT AND IMPLICIT SIMULATION OF UD-FIBRE COMPOSITES LOADED IN COMPRESSION

Krisztián Hertelendy[1], Ragnar Larsson[1], Renaud Gutkin[1,2]

[1]*Department of Industrial and Materials Science, Chalmers University of Technology, Gothenburg, Sweden*
[2]*Volvo Car Corporation, Gothenburg, Sweden*

The main failure mode of carbon fibre reinforced plastics (CFRP) in longitudinal compression is fibre kinking. It occurs when the loading direction does not align perfectly with the local orientation of the reinforcing fibres, which in turn results in an additional shear component in the stress tensor in the coordinate system aligned with the fibres. Initial misalignment can arise from manufacturing or loading imperfections or local fibre bending introduced by entangling fibres.

Although the causes for the formation of kink-bands are still an area of research, many believe that the main driving force is the local matrix failure [1]. Shearing of the matrix material degrades the support of the fibres, allowing for even larger fibre bending of the already misaligned fibres locally. This self-reinforcing process continues until the fibres snap in a band-like fashion, leading to the failure of the ply. An example of such a kink-band is shown in Figure 1.

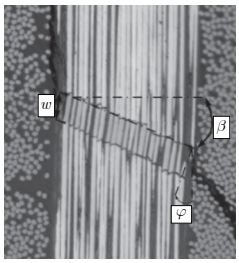

Figure 1: A typical kink-band [1].

The usual observed kink-band width (denoted as w in Figure 1) is of the order $10 \ldots 30$ fibre diameters. Today, carbon fibres have a diameter of $5 \ldots 10$ μm. This corresponds to a kink-band width not greater than a few hundred microns. This scale is computationally impossible to resolve in a structural simulation, where the element size is at least one order of magnitude larger.

To be able to account for the effects of the kink-band in a larger-scale simulation, a multiscale material model is introduced, in which the macro-level response is obtained from the micro-level one through homogenisation of the stress response. The model was first introduced in [2], and a representative volume element is shown in Figure 2.

Locally, a transverse elastic response is assumed outside of the kink-band, while it is enhanced with elastic continuum damage inside the kink-band, as indicated in Figure 1. Therefore, energy dissipation is concentrated in the kink-band that constitutes part $k \,/\, l$ of the RVE.

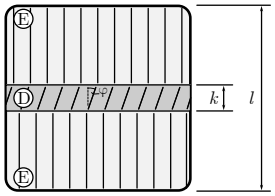

Figure 2: Representative Volume Element (RVE) of the material model.

The model parameters have been calibrated based on stress-strain responses in uniaxial compression and shear, and validated for different off-axis loading cases with *explicit* solution schemes. A large part of the mechanical experiments for material characterisation are done with small strain rates to exclude dynamic effects in the response. These quasi-static conditions can be better approximated with an *implicit* solution scheme, in which static force balance is ensured at every time step. However, in a simulation where dynamic effects cannot be disregarded, the use of an explicit solver is usually more beneficial. If material characterisation is carried out in a quasi-static manner, while the application is in the dynamic range, there are competing interests for the two solvers, and therefore it is essential to be aware of the capabilities and limitations of the two approaches.

In this presentation, we investigate how the two solution procedures perform in terms of stability, sensitivity of the results to the material parameters, and predictive capability. The results are discussed for both the parameter calibration process and the application in finite element simulations for a range of strain rates.

References

[1] R. Gutkin, S. T. Pinho, P. Robinson, and P. Curtis, "On the transition from shear-driven fibre compressive failure to fibre kinking in notched CFRP laminates under longitudinal compression," Composites Science and Technology, vol. 70, no. 8, pp. 1223–1231, 2010.

[2] R. Larsson, G. Brambati, and R. Gutkin, "Compressive failure and kink-band formation modeling," European Journal of Mechanics - a/Solids, vol. 99, p. 104909, 2023.

Corresponding author: krisztian.hertelendy@chalmers.se

MULTI-MATERIAL TOPOLOGY OPTIMIZATION OF EAP AND ELECTRODES

D. Hård[1], M. Wallin[1], M. Ristinmaa[1]

[1]*Division of Solid Mechanics, Lund University, Lund, Sweden*

Electroactive polymers (EAPs) [1] is a class of material with a nonlinear electro-mechanical coupling, meaning that they mechanically deform when subject to an electric field. Research in this field has seen much attention in recent years and has shown great potential for use as actuators or artificial muscles.

Topology optimization is a common method to optimize the material distribution in a structure to, e.g., maximize displacements while fulfilling a volume constraint. However, the research into using topology optimization to increase EAPs performance has been limited [2]. In this work, a multi-material topology optimization method has been formulated for optimizing EAPs and electrodes.

The goal is to optimize distribution of EAP and electrode materials for maximizing the output displacements. Of special consideration is accurately accounting for the electric field that surrounds the structure. This can be solved using a large, extended domain modelled as void material.

Figure 1 shows the design domain and an optimized compliant EAP mechanism, where the output displacement on the right side has been maximized for the applied potential difference. Gray indicates electrode material, red EAP material and blue void. Note that the electrodes creates a connection between the electric sources and the EAP material, causing the electric field to be concentrated within the EAP material.

The electric potential in the large surrounding space can be seen in Figure 2, where the design domain is highlighted as a black square.

The methodology developed in this work is shown to be able to generate designs with a combination of EAPs and electrode materials. This shows great potential for designing EAP structures.

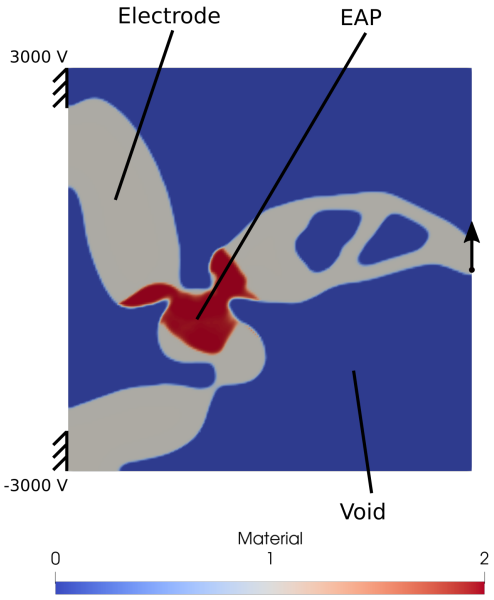

Figure 1: Design domain with two distinct material phases and void phase

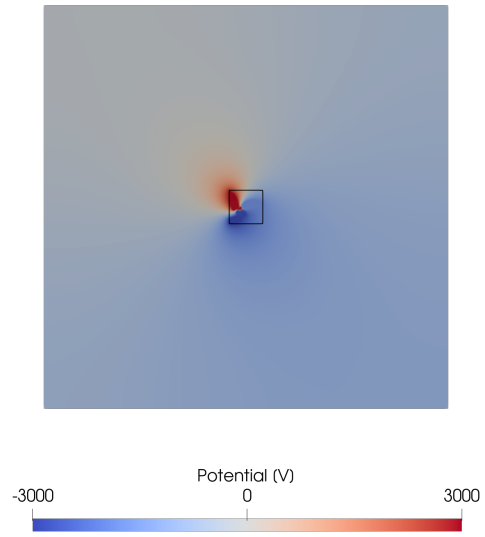

Figure 2: Electric potential in the design domain, the black square, as well as in the surrounding space

References

[1] Ask, A., Menzel, A., Ristinmaa, M., Electrostriction in electro-viscoelastic polymers. Mechanics of Materials, 50, 9-21, (2012)

[2] Hård, D., Wallin, M., Ristinmaa, M., Connectivity constraints ensuring continuous electrodes in topology optimization of EAP. Journal of Mechanical Design, (2024)

Corresponding author: daniel.hard@solid.lth.se

A LEVEL SET APPROACH TO MODELLING DIFFUSIONAL PHASE TRANSFORMATIONS UNDER FINITE STRAINS: AN APPLICATION TO Cu_6Sn_5 FORMATION

E. Jacobsson[1], H. Hallberg[1], J. Hektor[2], S. Iyengar[3], M. Ristinmaa[1]

[1]*Division of Solid Mechanics, Lund University, Lund, Sweden*
[2]*Department of Materials Science and Applied Mathematics, Malmö University, Malmö, Sweden*
[3]*Division of Materials Engineering, Lund University, Lund, Sweden*

Diffusion is the primary reason for the formation and growth of intermetallic compounds, common in many soldering and electroplating applications. For multi-phase systems governed by diffusion, the interfaces separating the different phases and grains can often be assumed to be in local equilibrium. This assumption is based on the premise that diffusion of atoms across the interfaces is as easy as diffusion of atoms in the bulk [1]. Moreover, local equilibrium implies a continuous chemical potential across the interface.

A variety of methods for modelling diffusional phase transformation exist. One popular method is the phase field method, in which a continuous chemical potential across the interface is generally not guaranteed. This aspect is accepted in the phase field community, as the diffuse interfacial region is not regarded as a physical quantity [2]. When studying diffusion-driven phase transformations, however, such non-equilibrium effects violate the physical nature of the phase transformation process.

Another approach to simulate microstructure evolution is to adopt the level set method. This method, which was introduced in 1979 and generalized by [3], is a general technique for tracing the evolution of moving interfaces. In contrast to the phase field method, the level set method provides a more accurate description of the interface, since the exact location of the interface is always known. This allows for boundary conditions to be applied directly at the interface. Finally, the level set method enables a computational efficiency that can be expected to be higher than what can be achieved in conventional phase field methods.

In our work, we present a sharp interface formulation for modelling diffusional phase transformations. Grain boundary motion is, in accordance with diffusional phase transformation kinetics, determined by the amount of flux toward the interface and is formulated in a level set framework. Compatibility of the interfaces is achieved through an interface reconstruction process, in which the locations of the triple junction points are also determined. To ensure local equilibrium and a continuous chemical potential across the interface, the chemical composition is prescribed at the phase interfaces. The presented model is used to study the growth of the intermetallic compound (IMC) Cu_6Sn_5 for a system with Sn plated on Cu. To investigate the effect of the large volume expansion resulting from the IMC formation, a finite strain formulation is incorporated into the model. In this formulation, the Cu and Sn phases are allowed to deform plastically. The numerical simulations show that the obtained IMC growth rate is in agreement with experimental measurements. Moreover, the IMC microstructure evolves into a scallop-like morphology, consistent with experimental observations. Finally, the numerical simulations indicate that the volume-averaged biaxial stress in the Sn layer saturates at a compressive value of approximately -7 to -8 MPa.

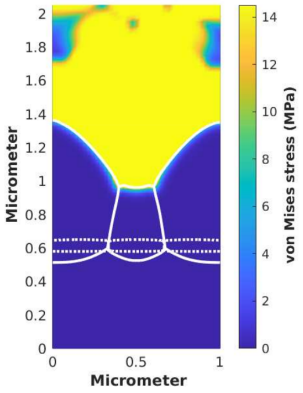

Figure 1: The von Mises stress distribution within the Sn layer after 600 h.

References

[1] D. A. Porter and K. E. Easterling. *Phase Transformations in Metals and Alloys*. CRC Press, 2nd edition, 1981.

[2] Inge Bellemans, Nele Moelans, and Kim Verbeken. Phase-field modelling in extractive metallurgy. *Critical Reviews in Solid State and Materials Sciences*, 43(5):417–454, 2018.

[3] Stanley Osher and James A Sethian. Fronts propagating with curvature-dependent speed: Algorithms based on Hamilton-Jacobi formulations. *Journal of Computational Physics*, 79(1):12–49, 1988.

Corresponding author: erik.jacobsson@solid.lth.se

STUDYING THE RATE EFFECTS ON PLANE STRESS FRACTURE TOUGHNESS IN PRESS HARDENING STEEL SHEETS

S. Jonsson[1], D. Frómeta[2], F. Larsson[1], J. Kajberg[1]

[1]*Division of Solid Mechanics, Luleå University of Technology, 971 87 Luleå, Sweden*
[2]*Eurecat, Centre Tecnològic de Catalunya, Plaça de la Ciència, 2, Manresa 08243, Spain*

Since the vehicle fleet is getting progressively heavier due to powertrain electrification and customer demands, lightweighting and crash safety are hot topics in the automotive industry. Press hardening steel (PHS) sheets allow automotive makers to manufacture complex high-strength safety parts with low or no springback, with different PHS grades being suitable for either energy absorbing or anti-intrusion applications depending. High strength steel grades are generally more prone to cracking, especially in crash situations involving failure modes involving local ductility such as tight-radius bending. Cracking or tearing of the material in a component can drastically change its intended behaviour, which is undesirable in a crash situation where safety zones are generally carefully engineered. These local failures cannot be rationalised with traditional global formability mechanical properties such as total elongation or forming limit curves. Instead fracture resistance has to be considered when selecting high strength steel materials for crash applications. Plane stress fracture toughness obtained with the essential work of fracture (EWF) has emerged as a viable material property to rationalise the local ductility failure of high-strength steel sheets [**1**]. A previous study investigated the effect of loading rate on this property for advanced high strength steel (AHSS) grades and concluded that a clear increase in fracture toughness could be seen for higher strain rates [**2**]. However, the published data on the loading rate effect of fracture toughness for PHS grades are still limited, and the cause of this effect is still largely unknown. High strain rates lead to adiabatic heating which can introduce softening behaviour of the material such as necking and formation of shear bands. This heating effect can also have a detrimental effect on the metastable austenite in certain TRIP steels. Thus, finding a method to measure this self-heating of the ligament in dynamic EWF testing is interesting to determine the thermal environment of this zone. This can open up for further studies of the temperature effect on fracture toughness of the investigated materials in more controlled quasi-static conditions or in finite element simulations to try to isolate the effect from fracture work and plastic work, respectively. In this study, the rate effect of two PHS grades with 1000 MPa and 2000 MPa ultimate tensile strength (UTS), respectively, are tested to investigate the rate dependency of this fracture mechanical property for PHS grades. The former is a more ductile grade for energy absorption applications while the latter is an ultra high strength grade for anti-intrusion safety structures. To identify crack initiation and to track the propagation at these loading rates, a high speed Phantom® camera operating at 62500 to 125000 frames per second (FPS). Furthermore, an attempt to observe the adiabatic heating in the fracture process zone at these rates was made using a FLIR SC4000 HS-MWIR thermal camera with a sampling rate of 700 FPS. The results will give information about the loading rate dependency of two different PHS grades and some information about the adiabatic heating in the ligament zone for EWF at high loading rates.

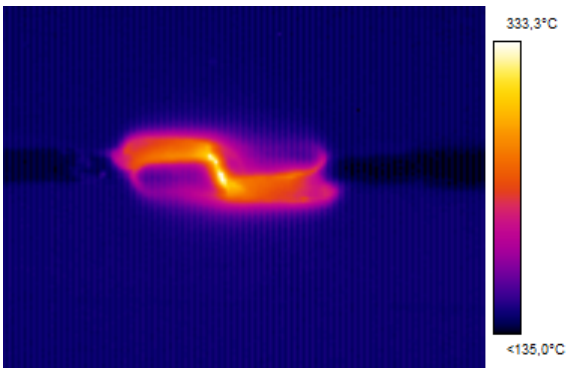

Figure 1: Post-fracture thermal image of a DENT specimen for the PHS 1000 material showing a clear adiabatic heating effect.

Corresponding author: simon.jonsson@ltu.se

References

[1] Frómeta, D., Lara, A., Casas, B., Casellas, D., Fracture toughness measurements to understand local ductility of advanced high strength steels, IOP Conference Series: Materials Science and Engineering, vol. 651, 2019.

[2] Golling, S., Frómeta, D., Casellas, D., Jonsén, P., Investigation on the influence of loading-rate on fracture toughness of AHSS grades, Materials Science & Engineering A, vol. 726, pp. 332-341, 2018

COMPRESSIVE PROPERTIES OF TOW-BASED DISCONTINUOUS COMPOSITES

I. Katsivalis[1], X. Wu[2], A. Tongloet[2], D. Zenkert[3], S. Pimenta[4] M. Wisnom[2] L.E. Asp[1]

[1]*Department of Industrial and Materials Science, Chalmers University of Technology, Gothenburg, Sweden*
[2]*Bristol Composites Institute, Queen's Building, University of Bristol, Bristol, UK*
[3]*Department of Engineering Mechanics, KTH, Sweden*
[4]*Department of Mechanical Engineering, Imperial College London, UK*

Inspired from nacre, or the mother of pearl, Tow-Based Discontinuous Composites (TBDCs) combine stiff and strong Carbon Fibre (CF) tapes with a soft matrix. The resulting composite material can achieve mechanical properties as high as continuous composites while also minimising the scrap and waste and allowing the forming and manufacturing of complex geometries with high curvatures [1]. Therefore, the design space is significantly expanded. However, the mechanical characterisation under complex loading conditions, can be challenging due to the complicated micro-architecture of TBDCs.

Compressive strength is typically a key design criterion for composite structures. However, measuring the compressive strength of composite materials is challenging and a high degree of variability has been reported in the literature. The main limitation during uniaxial compressive testing is related to premature failures due to stress concentrations in the gripping areas and instabilities which promote buckling in the specimen.

In this work, two different test methods were used to evaluate the compressive properties of TBDC materials. The first one was a uniaxial compressive test based on ASTM D3410. The specimen was 140 x 10 x 1.2 mm, and the loading rate was 0.6 mm/min. The load-displacement curve was recorded, and Digital Image Correlation (DIC) was also used to resolve the full-field strain. A non-linear stress/strain relationship was obtained which is an indication of buckling. This was also validated by post-mortem visual inspection as shown in Figure 1.

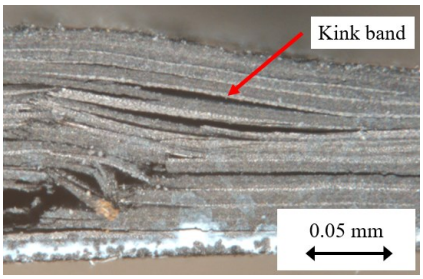

Figure 1: Formation of kink bands leading to buckling during uniaxial compressive testing

The second method was based on a 4-point bending Sandwich Beam (SB) specimen, as shown in Figure 2, which was recently developed [2]. The dimensions of the specimen were 300 x 25 x 20 mm, the thickness of the top and bottom skin was 1 mm while the thickness of the PMMA core was 18 mm. The load-displacement curve was recorded while the strain in the top skin was also measured with strain gauges allowing to extract the ultimate compressive strain.

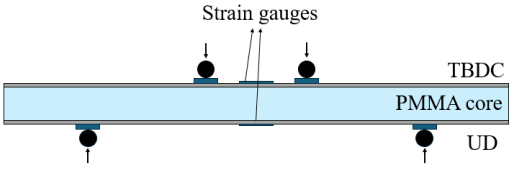

Figure 2: 4-point bending SB specimen

A comparison between the tensile and compressive properties obtained from uniaxial testing (Table 1) revealed a 10% lower compressive strain-to-failure. The lower strain is a result of the premature failure taking place during the compressive uniaxial test and is expected to be resolved utilising the SB specimen.

Preliminary analysis on the SB geometry predicted a maximum compressive strain of about 1.2%. This corresponds to a 36% increase compared to the compressive strain measured during uniaxial testing. Therefore, the SB geometry is expected to enable the measurement of the full compressive properties of the TBDC specimens and explore the full potential of these materials.

Testing	Strain-to-failure (%)
Tension	0.96 ± 0.10
Uniaxial compression	0.88 ± 0.09
SB compression	1.2

Table 1: Preliminary results

References

1. Katsivalis, I., et al., *Strength analysis and failure prediction of thin tow-based discontinuous composites.* Composites Science and Technology, 2024. **245**: p. 110342.
2. Wu, X. and M.R. Wisnom, *Compressive failure strain of unidirectional carbon fibre composites from bending tests.* Composite Structures, 2023. **304**: p. 116467.

Corresponding author email: ioannisk@chalmers.se

EFFECTS OF TOUGHNESS VARIATIONS IN RINGHALS 4 PRESSURIZER WELD ON BRITTLE FRACTURE TOUGHNESS

D. V. Klein[1], J. Faleskog[1]

[1]*Department of Engineering Mechanics, KTH Royal Institute of Technology, Stockholm, Sweden*

Failure in brittle materials typically initiates from brittle inclusions or embrittled grain boundaries. Due to the large gradients of the mechanical fields, i.e., stress and strain, in front of a crack tip in combination with the distribution of the initiators within the material, the fracture toughness is widely scattered. These problems are commonly addressed by weakest-link modelling, where the cumulative failure probability is expressed as

$$P_f = 1 - \exp\left(-\int_V h\left(\sigma_{ij}, \varepsilon_e^p\right) \mathrm{d}V\right) \qquad (1)$$

where h is a hazard function representing a field of cumulative failure probability per unit volume. In the case of a heterogeneous material, the volume integral in Eq. (1) is separated

$$P_f = 1 - \exp\left(-\int_{V_A} h_A \,\mathrm{d}V - \int_{V_B} h_B \,\mathrm{d}V\right) \qquad (2)$$

where the hazard functions h_A and h_B are active in the sub-volumes V_A and V_B, respectively. A length D, relating to the spatial variations between the phases, then defines the general behaviour of the resulting curve in Eq. (2). In the limiting case, when $D \to 0$, i.e., small-scale heterogeneity (SSH), the failure probability can be expressed as

$$P_f^{\mathrm{SSH}} = 1 - \exp\left[-\int_V \left(v_A h_A + v_B h_B\right) \mathrm{d}V\right] \qquad (3)$$

where v_A and v_B are the volume ratios of the phases. When $D \to \infty$, i.e., large-scale heterogeneity (LSH), the failure probability becomes

$$P_f^{\mathrm{LSH}} = 1 - w_A \exp\left(-\int_V h_A \,\mathrm{d}V\right) - w_B \exp\left(-\int_V h_B \,\mathrm{d}V\right) \qquad (4)$$

where w_A and w_B represent the number of specimens in which the fracture process zone is fully covered by phase A and B, respectively. A common assumption in weakest-link modelling is that an infinite number of specimens, which are randomly and uniformly placed in the material, are tested. Under LSH conditions this assumption leads to $w_A = v_A$ and $w_B = v_B$.

A Monte-Carlo study [1], where 20000 different crack-tip positions at different values of D were generated, showed that under SSH conditions Eq. (3) is valid. Under LSH conditions, only for a large number of specimens and a random and uniform distribution of crack-tip positions, Eq. (4) approximates the average failure probability curve well. If the crack-tip positions are not randomly placed in the material Eq. (4) cannot be applied anymore. Another conclusion from [1] is that cases in between SSH and LSH should rather be treated like LSH.

In this study, material from the pressurizer multipass welds of the Ringhals 4 powerplant is investigated for heterogeneity effects. When weld beads are placed on top of each other, the dendritic microstructure is reheated and forms new equiaxed grains, as can be seen in Figure 1. Therefore, a repetitive unit is created that contains the dendritic "as-welded" (aw) zone and the equiaxed "reheated" (rh) zone. Due to the welding procedure, those zones contain different brittle initiators. Another contributing factor may be ageing effects due to phosphorous segregation, which embrittles the grain boundaries.

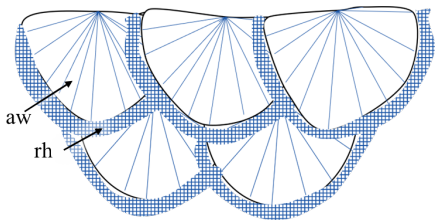

Figure 1: Weld beads in multipass weld

The fracture surfaces from experiments from a prior study [2] and a series of new experiments using Single-Edge-Notch-Bend specimens with various sizes and crack lengths, were examined. Preliminary results indicate that if the crack tip is placed in the aw zone and the crack surface is parallel to the dendrites the fracture toughness is significantly less than any other crack tip positions.

References

[1] Klein, D.V., Faleskog, J., Influence of heterogeneity due to toughness variations on weakest-link modeling for brittle failure. *Engineering Fracture Mechanics*, 292, 109643. Received April 11, 2023, https://www.sciencedirect.com/science/article/pii/S001379442300601X.

[2] Boåsen, M., Dahlberg C.F.O., Efsing, P., Faleskog, J., A weakest link model for multiple mechanism brittle fracture — Model development and application, 147, Received July 2, 2020, https://www.sciencedirect.com/science/article/pii/S0022509620304403

Corresponding author email: dklein@kth.se

MODELLING AND CALIBRATION OF STRUCTURAL BATTERY FULL CELLS

Carl Larsson, Fredrik Larsson, Johanna Xu, Kenneth Runesson, Leif E. Asp

Department Industrial and Materials Science, Chalmers University of Technology, Gothenburg, Sweden

Structural battery composites belong to the category of multifunctional materials with the ability to store electrochemical energy and carry mechanical load simultaneously. A conventional lithium-ion battery comprises a positive electrode, separator, and a negative electrode. The constituents are soaked in a liquid electrolyte, allowing lithium-ion exchange between the electrodes while electrons travel through an external circuit. In structural batteries, the negative electrode is replaced by multifunctional carbon fibres, enabling the additional function as mechanical reinforcement. The liquid electrolyte is replaced by a porous two-phase matrix material, in which the solid polymer phase transfers mechanical loads between carbon fibres, and the lithium ions travel in the liquid phase of the matrix as shown schematically in Figure (1). The lithium ions react on the carbon-fibre / electrolyte interface, forming neutral lithium that diffuses inside the carbon fibres. The process is accompanied by extensive carbon fibre expansion and change in elastic moduli, causing internal stresses [1, 2]. Conversely, applying a mechanical load to lithiated carbon induces a response in electric potential.

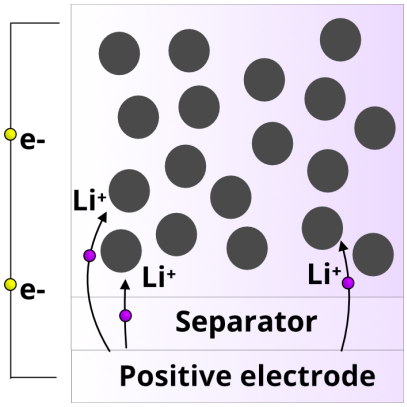

Figure 1: Illustration of a full cell structural battery, using carbon fibres as negative electrode.

To evaluate the behaviour and performance of the carbon fibre electrode against a known reference potential, the positive electrode can be replaced with lithium metal, known as a half-cell representation. The modelling of half-cell structural batteries has been addressed by Carlstedt et al., where a fully coupled electro-chemo-mechanical framework is introduced [3]. The presented model considers linear elastic materials and uses linearized reaction kinetics on the carbon-fibre electrode / electrolyte interface.

In this work, we model a full cell structural battery by considering a design where the positive electrode consists of coated, load carrying, fibres. To understand the details of chemical reactions in the battery, we adopt non-linear reaction kinetics on the electrode / electrolyte interfaces using the Butler-Volmer relation. In particular, we discuss the electro-chemo-mechanical modelling of the positive electrode, and the pertinent calibration towards experimental findings.

References

[1] Carlstedt, D., Runesson, K., Larsson, F., Xu, J., Asp, L. E. (2020). Electro-chemo-mechanically coupled computational modelling of structural batteries. Multifunctional Materials, 3(4).

[2] C. C. Foo, K. Guo, B. M. Srinivasan, N. Sridhar, K. Joshi, Z. Su, G. Zhang, D. W. H. Fam, Multiphysics modelling of structural battery composites, Composites Science and Technology 242 (9 2023).

[3] Carlstedt, D., Runesson, K., Larsson, F., Xu, J., Asp, L. E. Electro-chemo-mechanically coupled computational modelling of structural batteries. Multifunctional Materials, 3(4), 2020.

Corresponding author: calar@chalmers.se

Mechanical testing of a novel thick UHSS intended for warm forming

F.Larsson[1], S. Hammarberg[1], J. Kajberg[1]

[1] *Department of Engineering Sciences and Mathematics, Luleå University of Technology, Luleå, Sweden*

This work describes the mechanical material characterisation of a novel 7 mm thick Ultra High Strength Steel grade, WARMLIGHT-980 (UTS 980 MPa), intended for warm forming processes in the temperature range of 430 to 580°C. The aim is to produce lighter parts with high stiffness and good fatigue properties targeted for the Heavy-Duty Vehicle sector. The elastoplastic properties as well as the ductile failure properties were therefore determined at the enhanced temperatures for future use in numerical simulations of e.g. warm forming operations.

Studies to obtain mechanical properties have been performed by, e.g. Bao and Wierzbicki [1] who investigated 2024-T351 aluminium alloy and conducted numeral tests representing a wide range of triaxialities and they were able to recreate the tests with numerical simulation. Jonsson and Kajberg [2] characterized 1.4 mm and 1.55 mm steel sheets at room temperature using DIC and utilized a plane-stress fracture criterion to describe the failure of the material. Sjöberg et al. [3] characterized 1.6 mm thick Alloy 718 for different stress triaxialities at elevated temperatures. This was done utilizing Digital Image Correlation (DIC) to evaluate the strain at fracture. These successfully proven characterization methods will be utilized to support CAE of a warm forming process assuming a plane-stress condition. The elastoplastic properties as well as failure behaviour of a novel UHSS intended for warm forming are in this study investigated at three different temperatures, 430 °C, 505 °C and 580 °C using specimens with reduced thicknesses.

The failure strains at various stress triaxialities were extracted from digital image correlation of different specimen geometries. Due to the thickness (7 mm), impractically large specimens would be needed, therefore downsized 1.2 mm specimens were produced. The use of smaller and thinner specimens has been confirmed by comparing the work hardening up to necking obtained in uniaxial tensile tests (1.2- and 7-mm thickness). Elastic properties in the form of Young's modulus were determined by cycling tensile specimen in the elastic regime and The enhanced temperatures were obtained by inductive heating and the homogeneous temperature distribution was validated by thermal photography.

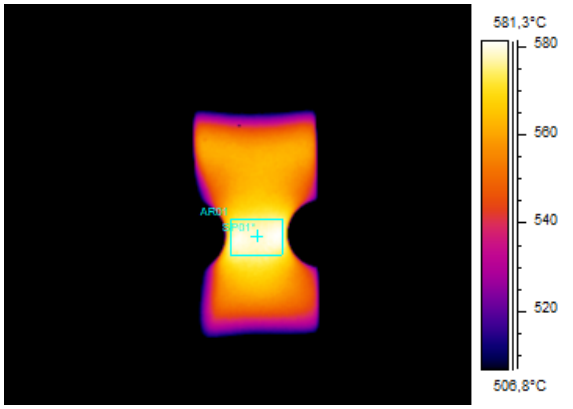

Figure 1: Representative heat map a tensile test of the WL980 material at 580 °C.

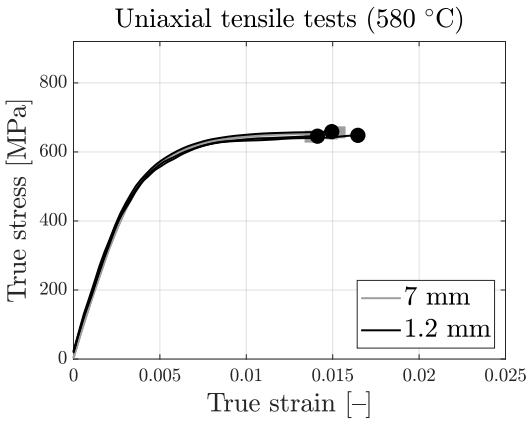

Figure 2: Representative stress vs strain behaviour comparison of as received and reduced thickness.

References

[1] Bao, Y., Wierzbicki, T., On fracture locus in the equivalent strain and stress triaxiality space, *Int J Mech Sci*, vol. 46, 1, 81–98, (2004)

[2] Jonsson, S., Kajberg, J., Evaluation of Crashworthiness Using High-Speed Imaging, 3D Digital Image Correlation, and Finite Element Analysis, *Metals (Basel)*, 13, (2023)

[3] Sjöberg, T., Kajberg, J., Oldenburg, M., Fracture behaviour of Alloy 718 at high strain rates, elevated temperatures, and various stress triaxialities, *Eng Fract Mech*, 178, 231–242, (2017)

Corresponding author email: fredrik.larsson@ltu.se

INFLUENCE OF TEMPERATURE GRADIENTS AND MICROSTRUCTURE ON HOT-ROLLED SHEET AND STRIP

J. Larsson[1], J. Edberg[1], E. Olsson[1]

[1]*Department of Engineering Sciences and Mathematics, Division of Solid Mechanics, Luleå University of Technology, Luleå, Sweden*

It is estimated that around 7% of the world's total emissions of greenhouse gases comes from traditional steel making. However, times are changing. Steel companies in Sweden are at the forefront of the transition into a sustainable and fossil free steel production. The most noticeable change might be the electronic arc furnace which replaces the blast furnace, but changes are also being made to other parts of the manufacturing process such as the hot rolling. In the new rolling mills, the steel will be rolled without intermediate cooling and reheating. This introduces some new microstructural phenomena, which further emphasizes the need for accurate and reliable simulation models in order to guarantee that the mechanical properties of the manufactured steel remains the same.

The challenges when modelling hot rolling are related to describing the material behaviour in an accurate way. The material's constantly fluctuating strain rates and temperatures trigger both work hardening and softening mechanisms, such as recovery and recrystallization [1]. The microstructure present at the end of rolling also has a direct impact on the final mechanical properties, and it is therefore important to consider both macro- and micro-parameters as well as their impact on each other when defining the constitutive equations. Edberg [2] proposed using the physically-based model originally developed by Bergström [3] where the athermal long range term of the flow stress is expressed as a function of the dislocation density ρ

$$\sigma = \alpha M G b \sqrt{\rho}, \tag{1}$$

where G is the temperature dependent shear modulus, b is Burger's vector, α is a material constant and M is the Taylor factor. Similar models have been used by for example Lissel and Engberg [4] or Lindgren et al [5]. It is also possible to combine physically based constitutive models with some model for recrystallization, which is an important softening mechanism to consider both during rolling and between passes.

This work seeks to investigate the possibility of combining a traditional thermomechanical finite element model, such as the example in Fig.1, with some physically-based model that considers the microstructural evolution during hot rolling. The ambition is for the simulations to provide insight into how the switch to direct rolling along with potential changes to for example the slab dimensions or the roughing mill design will affect the properties of the manufactured steel.

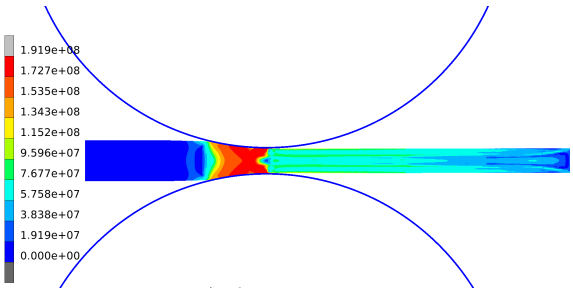

Figure 1: A typical FEM-model simulating hot rolling.

References

[1] Sellars, C.M., Whiteman, J.A., Recrystallization and grain growth in hot rolling, Metal Science, 3-4, 187-194, (1979)

[2] Edberg, J,. Computational Modeling of Hot Rolling, Doctoral dissertation, Luleå University of Technology, (1996)

[3] Bergström, Y., The plastic deformation of metals - A dislocation model and its applicability, Reviews on Powder Metallurgy and Physical Ceramics, 2, 79-265, (1983)

[4] L. Lissel,. G. Engberg, Prediction of the microstructural evolution during hot strip rolling of Nb microalloyed steels, Materials Science Forum, 558-559, 1127-1132, (2007)

[5] L.E. Lindgren., K. Domkin., and S. Hansson., Dislocations, vacancies and solute diffusion in physical based plasticity model for AISI 316L, Mechanics of materials, 40, 123-145, (2008)

Corresponding author: john.larsson@ltu.se

SUBSCALE MODELLING OF METAL CUTTING

A. S. Erturk[1] and R. Larsson[1]

[1]*Department Industrial and Materials Science, Chalmers University of Technology, Gothenburg, Sweden*

Simulation of metal cutting processes are commonly performed to find the optimum cutting condition. This is especially challenging considering the many different combinations of conditions and tool-workpiece pairs. Thus, it is crucial to establish accurate and cost-efficient models / simulations to predict suitable cutting conditions. In this regard, finite element chip formation simulations are widely used in the literature [1]. However, convergence issues exist in chip-forming simulations because of the largely deformed elements. This problem is generally overcome by using remeshing algorithms, which in turn increases the computational time of the simulations.

To establish a more cost-efficient model for metal cutting simulation, a subscale model is developed. In this model, the primary and secondary shear zones (see Figure 1) are specially considered. Information about these zones is obtained from a semi-analytical distributed primary shear zone deformation model [2] as a priori knowledge. Additionally, the velocity field in the subscale model has a long-range fluctuation velocity field, which is calculated from the semi-analytical model, and a subscale velocity field, which is derived from Navier-Stokes equations. In doing so, material flow during cutting in the specified region is represented as a Eulerian approach, which does not require costly remeshing algorithms.

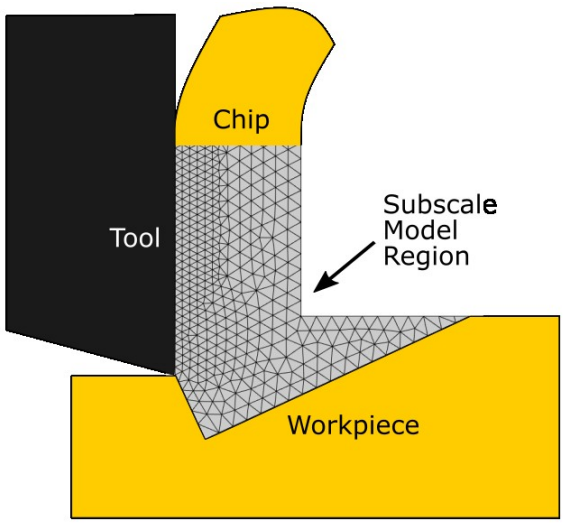

Figure 1: A representation of subscale model region.

In the model, the viscoplastic properties of the workpiece material are represented by the Johnson-Cook model [3]:

$$\sigma = (A + B\epsilon^n)(1 + C\ln\dot{\epsilon}^*)(1 - T^{*m}) \qquad (1)$$

where A, B, C, n and m are the model parameters, ϵ, $\dot{\epsilon}$ and T are strain, strain-rate and temperature, respectively. The interaction between material flow and tool is represented by a mechanical interface (see Figure 2), where stick-slip-separation conditions are applied in terms of material flow.

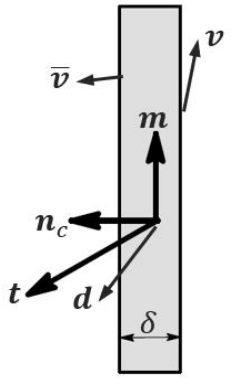

Figure 2: A representation of mechanical interface in terms of the traction t and interface velocity $d = \bar{v} - v$.

References

[1] Erturk, A.S., Malakizadi, A., Larsson, R. A thermomechanically motivated approach for identification of flow stress properties in metal cutting. International Journal of Advanced Manufacturing Technology, 111, 1055–1068, (2021).

[2] Shi, B., Attia, H., Tounsi, N. Identification of Material Constitutive Laws for Machining—Part I: An Analytical Model Describing the Stress, Strain, Strain Rate, and Temperature Fields in the Primary Shear Zone in Orthogonal Metal Cutting. Journal of Manufacturing Science and Engineering, 132, 051008, (2010).

[3] Johnson, G.R., Cook, W.H. A constitutive model and data for metals subjected to large strains, high strain rates and high temperatures. Proceedings 7th International Symposium on Ballistics, (1983).

Corresponding author: erturk@chalmers.se

PARTICLE SWARM OPTIMIZATION OF A TRIPOD SHAPED SUPPORT STRUCTURE FOR PRELIMINARY DESIGN OF FLOATING OFFSHORE WIND TURBINES

Jaseung Lee, Håkan Johansson, Wengang Mao, Jonas W. Ringsberg, Petri T. Piiroinen

Department Mechanics and Maritime Sciences, Chalmers University of Technology, Gothenburg, Sweden

The trend of upscaling floating offshore wind turbines highlights the need for weight and cost-efficient designs of support structures and floaters. Traditional support structure (single tower-based) inevitably needs to endure higher bending moment at the tower base in this trend [1 - 2]. To circumvent this problem, multiple masts-based support structures have been developed by companies such as X1 Wind and T-Omega Wind [2 - 3] (See Figure 1).

This study presents a methodology for pre-dimensioning multiple masts-based support structures with structural optimization. This work focuses on estimating cross section properties of masts in the tripod shaped support structure by using multi-objective particle swarm optimization. To assess serviceability and safety of structure, the optimization mainly considers the natural frequency of structures, yielding/buckling strength and stress distribution under extreme loading. SubDyn, time domain structural-dynamics module for multi-member substructure developed by NREL (National Renewable Energy Laboratory, US), is used to calculate frequency response modes and member internal reaction loads of the support structure. For case study, NREL 5MW and IEA (International Energy Agency) 15MW reference wind turbines with X1 Wind & PivotBuoy concept semi-submersible floater are used. The methodology presented in this work can be useful in pre-FEED (Front-End Engineering Design) studies for floating offshore wind turbines.

(a) (b)

Figure 1: Floating offshore wind turbines from (a) X1 Wind and (b) T-Omega Wind [4 - 5]

References

[1] Sizova, Sofya, et al. ”Influence of the Semi-Submersible Platform Flexibility on the Dynamic Response of the Wind Turbine.” International Conference on Offshore Mechanics and Arctic Engineering. Vol. 85932. American Society of Mechanical Engineers, 2022.

[2] Cahay, Marc, and Lucy Milde. ”NextFloat: structural benefit of innovative downwind floating wind concept.” (2023): 195-204.

[3] Wang, Lu, et al. ”OpenFAST Modeling of the T-Omega Wind Floating Offshore Wind Turbine System.” International Conference on Offshore Mechanics and Arctic Engineering. Vol. 87578. American Society of Mechanical Engineers, 2023.

[4] “Disrupting Offshore Wind.” X1 Wind, 13 June 2023, www.x1wind.com/.

[5] “The Solution - T-Omega WindTM.” T-Omega Wind, t-omegawind.com/solution. Accessed 12 Mar. 2024.

Corresponding author: jaseung.lee@chalmers.se

MESOSTRUCTURAL CHARACTERISATION AND MODELLING OF CLOSED-CELL FOAMS: IMPACTS OF CELL ANISOTROPY AND CELL WALL THICKNESS PROFILE

L. Liu[1], F. Liu[1], D. Zenkert[2], M. Åkermo[2], M.P.F.H.L. van Maris[3], J.P.M. Hoefnagels[3], M. Fagerström[1]

[1]*Department Industrial and Materials Science, Chalmers University of Technology, Gothenburg, Sweden*
[2]*Department of Engineering Mechanics, KTH Royal Institute of Technology, Stockholm, Sweden*
[3]*Department of Mechanical Engineering, Eindhoven University of Technology, Eindhoven, The Netherlands*

Foam materials consisting of a large number of closed cells, are being widely adopted in modern engineering applications, e.g. aviation, automotive, infrastructure, sports and packaging [1]. The exploitation of closed-cell foams has triggered intense efforts to understand the underlying deformation mechanisms and the structure-property relationships, where the compressive behaviour is of the most common interest.

tures (Fig. 1(b)) are generated using Laguerre tessellation incorporated with the measured distributions of cell aspect ratio and cell equivalent diameter. These SVE models are discretised using shell elements with the measured distribution of cell wall thickness profile accounted for. Base material behaviour is described using an isotropic elastoplastic model. Numerical simulations of single cell wall, single cell and SVE mod-

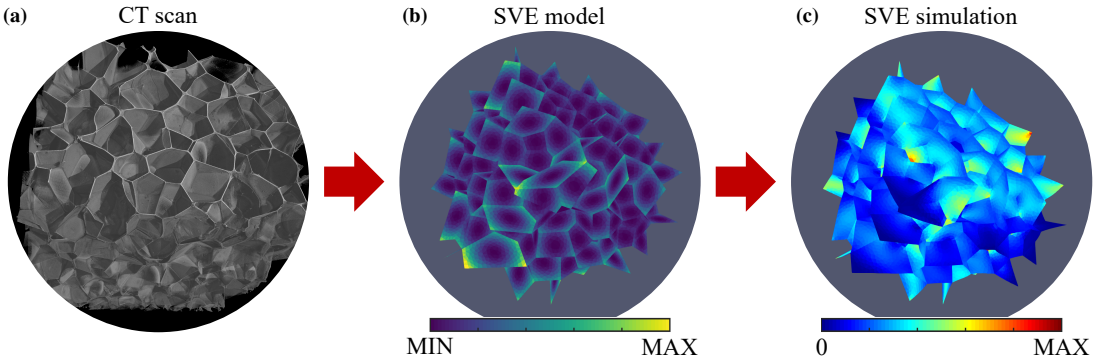

Figure 1: Schematic overview of the methodology: (a) CT scan of the PVC foam mesostructure, (b) SVE model consistent with the mesostructural characterisation, and (c) SVE simulation under compressive loading condition. The colormaps in (b) and (c) indicate the cell wall thickness and equivalent membrane strain, respectively.

Extensive studies to date have concluded two deformation mechanisms: cell wall buckling and bending [2]. The activation of these mesoscopic mechanisms, and the resulting macroscopic mechanical properties, are found to be strongly influenced by many mesostructural features, e.g. cell size and cell wall thickness as well as their variations [3-5]. Moreover, anisotropic cell shape and varying thickness over the cell wall are observed, inherently linked to the foaming process [6]. The impacts of cell anisotropy and especially cell wall thickness profile are often overlooked in the literature and thus systematically examined in this contribution.

Polyvinyl Chloride (PVC) foam grade H100 is focused on as one representative. Computed tomography (CT) scan is conducted on foam samples to obtain three-dimensional (3D) mesostructural characteristics (Fig. 1(a)), which are further post-processed to determine the aspect ratio and equivalent diameter of each cell, and the thickness profile of each cell wall. Statistical volume elements (SVE) of foam mesostructels under compressive loading condition are performed (Fig. 1(c)), and the results are compared with those considering isotropic cell shape and uniform thickness over the cell wall. It is shown that cell anisotropy and cell wall thickness profile play critical roles in governing the mesostructural deformation patterns and macroscopic structural properties of closed-cell foams.

References

[1] F. Rahimidehgolan et al. Compos. B Eng., 253:110513, 2023.
[2] P. Li et al. Int. J. Impact Eng., 127:154-168, 2019.
[3] Y. Zhou et al. Polym. Test., 117:107846, 2023.
[4] M.A. Kader et al. Mater. Des., 118:11-21, 2017.
[5] Y. Chen et al. Int. J. Solids Struct., 52:150-164, 2015.
[6] Y. Tang et al. Compos. B Eng., 238:109885, 2022.

Corresponding author: lei.liu@chalmers.se

MODELING MORTAR AS A REACTIVE POROUS MEDIUM AND CALIBRATION VIA IN-SITU XRCT EXPERIMENTS

K. A. Meyer[1] and R. Jänicke[1]

[1] *Institute of Applied Mechanics, TU Braunschweig, Braunschweig, Germany*

High initial strength is not sufficient for durable reinforced concrete structures. The ability to remain strong when subjected to the environment over time is equally important. For example, many concrete constructions are subjected to chloride via seawater or salt-based deicing. The rebar corrodes in such environments unless protective or corrective methods prevent chloride intrusion. However, developing such methods requires physically motivated and well-calibrated models.

Concrete structures are partially saturated with water, and ionic transport occurs via diffusion and convection. In the first part of this contribution, we study the water seepage driven by the capillary suction. In contrast to passive porous media, concrete and water react, changing the pore structure [1]. We have developed a methodology to calculate the water saturation distribution during in-situ X-Ray Computed Tomography (XRCT) experiments. The results in Figure 1 show this distribution at three different time instances.

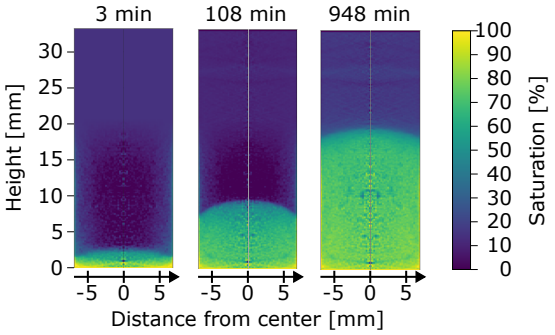

Figure 1: XRCT-measured saturation distributions during a capillary water suction experiment.

In the most basic setup, we model only the transport of water by considering the following conservation equation for liquid mass.

$$\dot{\Phi}_\mathrm{l} + [\rho_\mathrm{l}\bar{\boldsymbol{v}}_\mathrm{l}] \cdot \boldsymbol{\nabla} + \hat{e}_\mathrm{l} = 0 \qquad (1)$$

Here, Φ_l is the saturation and pressure-dependent storage of liquid (mass per volume), ρ_l the liquid density, $\bar{\boldsymbol{v}}_\mathrm{l} = -k\boldsymbol{\nabla}p_\mathrm{l}$ the Darcy velocity, p_l the liquid pressure and k the permeability. $\hat{e}_\mathrm{l}$ is the loss of liquid water binding to the solid structure. To model the anomalous suction, we propose a model where both the amount of bound water and the saturation degree affect the permeability, k. With this modeling concept, we accurately capture the average suction height during the experiment, as shown in Figure 2. We further evaluate the predictive abilities of the model by considering its ability to describe the spatial distribution of saturation.

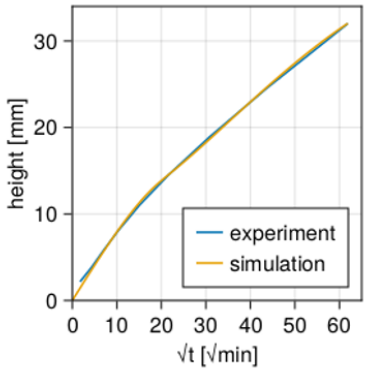

Figure 2: Comparison between model and experimental average water front heights during capillary suction.

Using the calibrated model, we extend the finite element methodology to contain partially saturated distinct pores. Specifically, we model each pore as a reservoir with volume V_p, liquid density ρ_p, and saturation S_p, subjected to the mass balance

$$\frac{\mathrm{d}}{\mathrm{d}t}\left[\rho_\mathrm{p} S_\mathrm{p} V_\mathrm{p}\right] = \int_{\Gamma_\mathrm{p}} \rho_\mathrm{l}\bar{\boldsymbol{v}}_\mathrm{l} \cdot \boldsymbol{n}_\Gamma \mathrm{d}\Gamma = \int_{\Gamma_\mathrm{p}} q_\mathrm{n} \mathrm{d}\Gamma \qquad (2)$$

The flux q_n, across the pore wall Γ_p, is then a nonlinear function of the pressure difference, $p_\mathrm{l} - p_\mathrm{p}$ and the pore saturation S_p. This results in a nonlinear Robin-like boundary condition.

The proposed constitutive and finite element models provide efficient seepage simulations in the mortar mesostructure. An extended partially saturated reactive porous media theory accounts for the behavior in nano-sized pores, and larger pores are explicitly resolved.

References

[1] P. J. McDonald et al. “Sorption, anomalous water transport and dynamic porosity in cement paste: A spatially localised 1H NMR relaxation study and a proposed mechanism”. In: *Cement and Concrete Research* 133 (2020), p. 106045.

Corresponding author: k.a.meyer@tu-braunschweig.de

CRACK PROPAGATION ANALYSIS IN ELECTROACTIVE POLYMERS USING A PHASE FIELD FRACTURE MODEL

A. Möglich[1], R. Denzer[1], M. Ristinmaa[1], A. Menzel[2,1]

[1]*Division of Solid Mechanics, Lund University, Sweden*
[2]*Institute of Mechanics, TU Dortmund University, Germany*

Electroactive polymers, a subgroup of smart materials, change their shape in response to an electric field. They are used in robotics, artificial muscles and sensors. Ensuring reliable performance is essential for such applications. Damage and fracture strongly influencing material performance. To address this problem, our work combines a material model for electroactive polymers with a phase field fracture model.

The behavior of electroactive polymers is described as a quasi-static large strain electromechanical model. This potential-derived model includes a Neo-Hookean mechanical component and an electromechanical coupling part, which is modeled using the relative permittivity. The selected material parameters ensure that the model reflects the properties of a soft electroactive polymer. A phase field fracture model is used to model crack propagation. This approach describes crack propagation using an additional scalar field, the phase field. This field varies between zero and one, that is between an undamaged material and a complete damaged material with a crack at the specific location. Adjustments to the model are made to account for the large strains inherent in soft polymer materials. A monolithic scheme is used to solve the electromechanically coupled problem, while the phase field fracture problem is solved by a staggered algorithm. The behavior of crack propagation show differences between purely mechanical cases and those with electromechanical coupling.

The proposed model is implemented within a nonlinear finite element framework. Representative numerical examples, for example as shown in figure 1, are discussed to demonstrate applicability of the model.

Corresponding author: annika.moglich@solid.lth.se

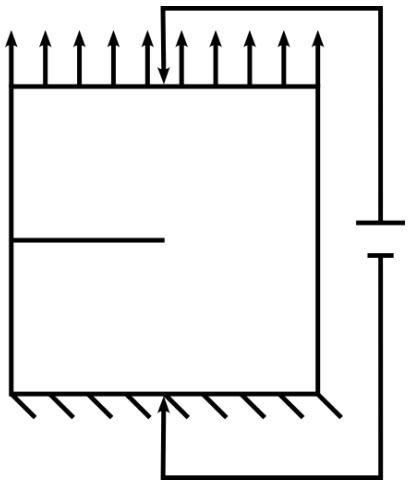

Figure 1: Electrical and mechanical loaded notched plate.

IS IT DAMAGE, PLASTICITY, RATE DEPENDENCE OR ALL OF THE ABOVE? CHARACTERISING AND MODELLING THE NON-LINEAR BEHAVIOURS OF 3D-FABRIC REINFORCED COMPOSITES

C. Oddy[1,3], F. Panteri[3], A. Kullerstedt[2], S. Saseendran[2]

[1]*Department Industrial and Materials Science, Chalmers University of Technology, Gothenburg, Sweden*
[2]Department of Aeronautical and Vehicle Engineering*, KTH Royal Institute of Technology, Stockholm, Sweden*
[3]Department of Composite Technology and Inspection, *GKN Aerospace, Trollhättan, Sweden*

As their name suggests, 3D-fabric reinforced composites, are manufactured by intertangling yarns together in three-dimensional space to create a near-net-shape dry fabric preform. After infusing this preform with a resin matrix system, a light-weight component is created which demonstrates both high in- and out-of-plane stiffness and strength. The through-thickness reinforcements present in this class of material, prevent delamination and allow for stable and progressive damage growth in a quasi-ductile manner.

Composites with 3D-fabric reinforcement present several advantages, both in terms of their manufacturing and mechanical performance. However, the complex yarn structure creates a material with several interesting behaviours and features which need to be accounted for when developing a model to predict how the material will deform and eventually fail. To begin with, these materials are highly anisotropic and show varying levels of non-linearity depending on loading mode. This non-linearity can be due to a variety of subscale behaviours: microcracking in the matrix or fibre-bundles, yarns straightening and fibres breaking as well as viscous effects from the polymer matrix.

One of the big questions when working with this class of materials is then; what is causing the non-linear behaviours and how can they be modelled in physically meaningful way. For this reason, a testing campaign initially proposed by Zscheyge [1] for laminated composites is carried out in this work. It involves cyclically loading and unloading test samples with creep and relaxation periods in between. From a single test, it is then possible to determine how permanent strains, stiffness degradation and rate dependence develop as the deformation increases. Further, by testing samples at different material orientations, it is possible to understand how these phenomena develop anisotropically with respect to loading mode.

Using the knowledge gained from the experimental testing campaign, a phenomenologically based macroscale model is developed and presented. It considers the material as a homogenous and anisotropic solid. The experimental tests results are used to formulate and calibrate an anisotropic viscoplastic-damage model for 3D-fabric reinforced composites.

References

[1] Zscheyge, M., Rate dependent non-linear mechanical behaviour of continuous fibre-reinforced thermoplastic composites – Experimental characterisation and viscoelastic-plastic damage modelling. *Materials and Design*, 193, 108827, (2020).

FATIGUE STRENGTH ASSESSMENT OF PRESS HARDENED CHASSIS MEMBERS

Erik Olsson[1], Gustaf Gustafsson[2]

[1]*Department of Engineering Sciences and Mathematics, Division of Solid Mechanics, Luleå University of Technology, Luleå, Sweden*

[2]*Gestamp HardTech AB, Research Digital & Testing, Technology and Innovation Office, Luleå, Sweden*

Press hardening is a forming technique for steel components where the steel blank is heated up above its austenization temperature, thereafter formed to its desired shape, and finally cooling to a martensitic microstructure. This results in a component that can have a complex shape while maintaining excellent static strength. There is a growing interest to use this technique for heavy-duty vehicles for weight-saving, and in that application, fatigue is an important dimensioning case.

Manufacturing prototypes for press-hardening is costly as new pressing tools needs to be designed for each new geometry. Hence, a fatigue life prediction model based on fatigue specimen test data is needed and outlined in the present work. Previous research has shown that press-hardened steels are very defect sensitive as expected for a material with such high strength and low ductility [1-2]. This possesses a major challenge when transferring fatigue life data from specimen scale to component scale as the effect of loaded volume becomes significant.

In the present work a cross member, pictured in Figure 1, is considered. The cross member is fatigue tested in bending in different directions. Planar fatigue specimens are also manufactured to obtain material data.

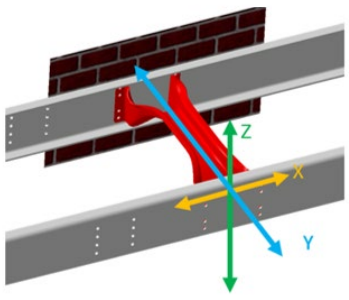

Figure 1: Picture of the studied component, a cross member used in truck chassis with the two bending directions *x* and *z* indicated in the figure.

The stress state in the loaded cross member is predicted using finite element simulations. Two types of fatigue assessment methods are explored. Firstly, the maximum stress occurring in the FE model is directly compared to the results from the fatigue specimen testing. Secondly, a weakest-link model for the probability of failure at a given load and cycles to failure are used which takes loaded volume into account in predicting the probability of failure of the component [3].

The comparison of the experimental fatigue results from the cross member and the predicted is presented in Figure 2 (a) and (b) for bending in the *x* and *z* directions respectively. It is clear that accounting for loaded volume is important for the prediction accuracy, and that the weakest-link model compares favourable compared to just utilizing the maximum stress occurring in the FE model.

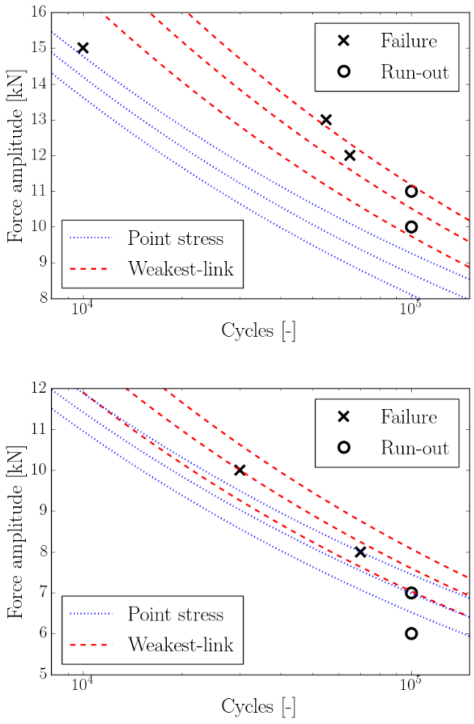

Figure 2: Comparison between experimental and predicted fatigue life using a point stress and a weakest link model for bending in (a) *x*-direction and (b) *z*-direction.

References

[1] Parareda S. et al., Fatigue resistance of press hardened 22MnB5 steels. Int J Fatigue (2020)

[2] Lara A. et. al., Effect of the cutting process on the fatigue behaviour of press hardened and high strength dual phase steels. J Mater Process Technol (2013)

[3] Olsson E. et. al, Fatigue of gears in the finite life regime - Experiments and probabilistic modelling. Eng Fail Anal (2016)

Corresponding author email: erik.1.olsson@ltu.se

NOISY BOUNDARIES AND STOCHASTIC SALTATION MATRICES

Petri T. Piiroinen[1] and Eoghan Staunton[2]

[1]*Department Mechanics and Maritime Sciences, Chalmers University of Technology, Gothenburg, Sweden*
[2]*School of Mathematics, Statistsics and Applied Mathematics, University of Galway, Galway, Ireland*

The equations of motion for a rigid-body system normally consist of a set of second-order ordinary differential equations (ODEs), which for analysis purposes are often rewritten as a system of first-order ODEs, also referred to as a dynamical system. For a smooth dynamical system of the form

$$\dot{x}(t) = F(x, t, \mu), \quad x(0) = x_0, \tag{1}$$

where $x \in \mathbb{R}^n$ is the state, $t \in \mathbb{R}$ is the time, $\mu \in \mathbb{R}^m$ are system parameters, and $F \in \mathbb{R}^n$ is the vector field, the local stability of a given trajectory can be determined by examining the linearized system about the trajectory. This is done by calculating the *fundamental solution matrix* $\Phi(x, T)$ by solving the *variational equations*

$$\begin{aligned} \dot{\Phi}(x, t) &= F_x(x, t, \mu)\Phi(x, t), \quad F_x, \Phi \in \mathbb{R}^{n\times n}, \\ \Phi(x, 0) &= I, \end{aligned} \tag{2}$$

for a time T. However, many dynamical systems that originates from rigid-body systems are nonsmooth or piecewise-smooth (PWS) in their nature due to interactions with the environment through impacts, friction or control. Therefore, for PWS systems we additionally introduce boundaries

$$\Sigma_{ij} = \{x \in \mathbb{R}^n \mid h_{ij}(x) = 0\} \tag{3}$$

for some scalar functions h_{ij} that locally divide the phase space into subspaces $S_i \in \mathbb{R}^n$ and $S_j \in \mathbb{R}^n$. Locally, this gives us two vector fields such that

$$F(x, t, \mu) = F_k(x, t, \mu), \quad x \in S_k \in \mathbb{R}^n \tag{4}$$

with $k = i, j$. For stability analysis of a trajectory of a PWS smooth system it is essential take into account what happens to both the trajectory and the vector fields locally when a boundary is crossed (from S_i to S_j). To do this, it is common to introduce the concept of a *saltation matrix*, which is given by

$$S(x) = G_x(x) + \frac{F(G(x)) - G_x(x)F(x)}{h_x F(x)} h_x(x), \tag{5}$$

that allows for linearisation of the trajectory when the system undergoes a discrete jump or has a discontinuous vector field through the piecewise construction

$$\Phi(x_0, T) = \Phi_j(G(x(t_e)), T - t_e)S(x(t_e))\Phi_i(x_0, t_e). \tag{6}$$

To introduce noise to the boundaries we define the stochastic processes $\chi(\mathbf{x})$ and $P(t)$ that describe stochastic ruggedness and oscillations of a boundary, respectively (see Figure 1). We require that the stochastic processes

Figure 1: Oscillating (left) and rugged (right) boundary.

- are at least once differentiable,
- are of small amplitude,
- are mean reverting,
- have mean 0.

Following this, we further broaden the earlier scope with stochastic boundaries by introducing the concept of a *stochastic saltation matrix* (SSM), which allows for the linearization of trajectories in PWS systems with stochastically oscillating boundaries or boundaries with stochastic surface profiles. We can now use SSMs to estimate local effects of a noisy boundaries as well as long-term invariant limit distributions [1,2], which will be shown through a few examples (see Figure 2).

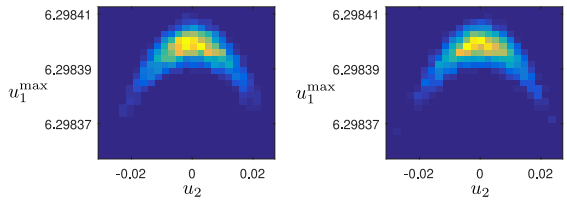

Figure 2: The distribution of the height of a bouncing ball and its corresponding horizontal position after one bounce on the rugged surface given by (left) simulation and (right) linear approximation.

References

[1] Staunton, E. and Piiroinen, P.T., *Discontinuity Mappings for Stochastic Nonsmooth Systems*, Physica D: Nonlinear Phenomena 406, Article no. 132405, (May 2020). (DOI: 10.1016/j.physd.2020.132405)

[2] Staunton, E. and Piiroinen, P.T., *Estimating the Dynamics of Systems with Noisy Boundaries*, Nonlinear Analysis: Hybrid Systems 36, Article no. 100863, (May 2020). (DOI: 10.1016/j.nahs.2020.100863)

Corresponding author: petri.piiroinen@chalmers.se

LATERAL VARIATIONS IN ZD-PROPERTIES OF LIQUID PACKAGING PAPERBOARD

C. Rydefalk[1,2], A. Hagman[2], S. Thorman[2], A. Kulachenko[1]

[1]*Department of Engineering Mechanics, KTH Royal Institute of Technology, Stockholm, Sweden*
[2]*RISE Research Institutes of Sweden, Packaging materials, Stockholm, Sweden*

Packaging paperboard is a thin, multi-layered, fiber-based, orthotropic material. The mechanical properties of a paperboard differs significantly between the different directions in the material. The directions of a paperboard are the in-plane directions, Machine Direction (MD) and Cross-machine Direction (CD), and the out-of-plane, or thickness direction, ZD. A micrograph of the ZD-structure of the paperboard in the present study is shown in **Figure 1**. The compression curve in ZD is non-linear as can be seen in **Figure 2**. The initial part of a ZD-compression curve is highly influenced by the surface structure and glued samples in compression show a continuous curve at 0-stress transition[1] There also appear large lateral variations due to flocks and anti-flocks, general unevenness in the plies or coating etc. In the process of converting the paperboard sheet into a packaging the ZD-properties and their variations become important during e.g. creasing and (contact) printing.

To gain insight into the compressive behaviour of paperboard previous studies by the authors have utilized a measuring device called The Rapid ZD-tester[2], [3]. The machine drops a weighted probe onto the substrate, thereby achieving a short pulse of 1-2 ms. The diameter of the probe is 5 mm, which is comparable to the length of a flexographic print nip. The maximum stress is slightly less than 1 MPa. The probe in the Rapid ZD-tester as it rests on a paperboard can be seen in **Figure 3**. While investigating the effect of slow versus rapid ZD-compression it was shown that the tangential stiffness after the initial non-linearity was comparable between quasi-static and dynamic measurements[3]. However, the comparison between slow and rapid compression did not fall out as hypothesised. Since the local stiffness and local thickness does not correlate, the present work attempts to further elucidate on the effect of local density on the compressive behaviour of the paperboard.

The lateral variations in structural, material and mechanical properties are investigated by marking the paperboard with 5x5 mm squares using a laser. The local thickness and stiffness are measured with the Rapid ZD-tester. Image analysis on high resolution scans provides the area of each square. By cutting the paperboard the mass of each square can be measured. Additionally, micrographs gives further information about the paperboard.

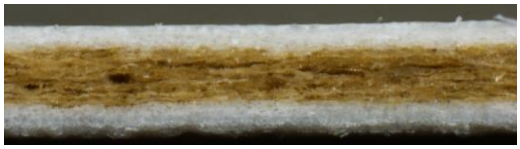

Figure 1 Micrograph of the ZD-structure of a liquid packaging paperboard

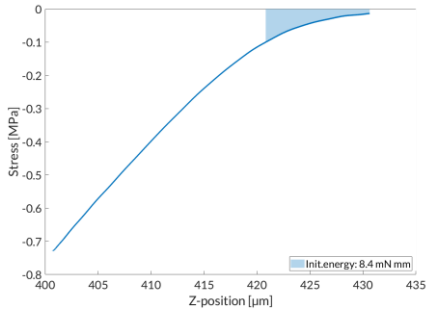

Figure 2 Compression curve from one point on the paperboard.

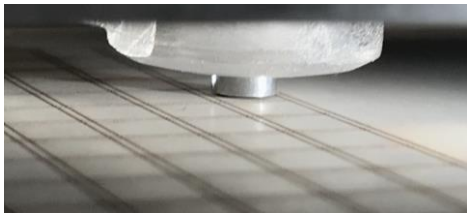

Figure 3 The Rapid ZD-tester measuring on a laser-marked paperboard

References

[1] A. Hagman and C. Rydefalk, "Z-Directional Testing of Paperboard in Combined Tensile and Compression Loading," *Tappi J.*, vol. Forthcoming, 2024.

[2] S. Thorman, C. Rydefalk, A. Hagman, and L. Granlöf, "Dynamic, Out-Of-Plane Compression of Paperboard," *TAPPI J.*, vol. 23, no. 2, pp. 113–122, 2024.

[3] C. Rydefalk, A. Hagman, L. Yang, and A. Kulachenko, "Mechanical response of paperboard in rapid compression – the ZD-tester, a measurement technique," in *Transactions of the 17th Fundamental Research Symposium*, D. W. Coffin and W. J. Batchelor, Eds., Cambridge, UK: Pulp & Paper Fundamental Research Society, 2022, pp. 311–331.

Corresponding author email: cecilia.rydefalk@ri.se

NOTCHED PERFORMANCE OF TOW-BASED DISCONTINUOUS COMPOSITES

V. Safranoglou[1,2], I. Katsivalis[1], L.E. Asp[1]

[1]*Department of Industrial and Materials Science, Chalmers University of Technology, Gothenburg, Sweden*
[2]*Department of Materials Science and Engineering, University of Ioannina, Ioannina, Greece*

Tow-Based Discontinuous Composites (TBDCs) are a growing class of high-performance materials, composed of chopped carbon-fibre tows randomly oriented and distributed in a polymeric matrix. These materials combine in-plane isotropy, high strength, and stiffness and, due to their ability to be compression-moulded, enhanced manufacturability. The combination of manufacturability and good mechanical properties makes TBDCs appealing for high-volume production of structural components. However, due to their complicated micro-architecture, characterising the performance of these materials and predicting their response can be challenging. [1]

The notch sensitivity is of particular importance for composite materials especially relating to high-performance applications which require the use of rivets and bolts. Conventional composites are particularly sensitive to material discontinuities which lead to stress concentrations and can trigger failure [2]. It is speculated that the micro-architecture of TBDCs would increase the damage tolerance and provide better performance in such loading conditions due to the random tape orientation. However, such studies on the notched response of TBDCs are currently lacking.

The OHT specimen was used to evaluate the notched performance of TBDCs under tension. The testing protocol was based on ASTM D3039. 300 x 300 mm plates were manufactured, and water jet cutting was used to extract the OHT specimens. The OHT specimens (Figure 1a) had dimensions of 300 x 36 mm while different sizes of notches (diameter of 6, 9, 12 mm) were evaluated. In addition, the response of the specimens was compared to continuous Quasi-Isotropic (QI) laminates.

The testing was performed on a 100 kN universal loading machine while the loading rate was set at 1 mm/min. The load-displacement curve was recorded while Digital Image Correlation (DIC) was also used to resolve the full-field strains. Finally, optical microscopy and Scanning Electron Microscopy (SEM) were used to identify and characterise the damage on the specimens.

Figure 1b shows the longitudinal strain distribution and evolution in a characteristic specimen. It is worth noting that stress concentrations exist around the notch which drive the failure. In addition, local tape orientations in the areas of stress concentrations govern the crack propagation.

Table 1 shows results of preliminary testing on one notch size (6 mm). The gross (maximum load over original cross-section) and net strength (maximum load over reduced cross-section) have both reduced significantly when compared to the un-notched value. Additional data points are currently being extracted and will allow for a more thorough investigation in the notch sensitivity of TBDCs.

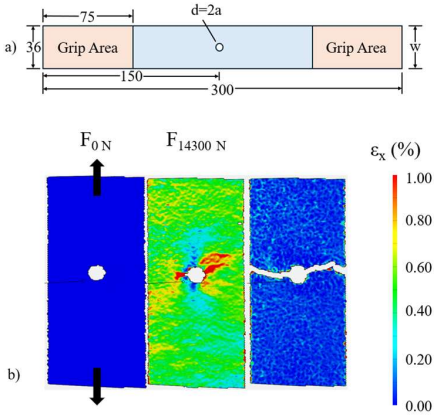

Figure 1: a) OHT specimen geometry (all dimensions in mm) and b) full-field strain evolution and fracture of a characteristic OHT specimen

Notch size (d/w)	Gross strength (MPa)	Net strength (MPa)	Damage mechanism
0	674 ± 49	674 ± 49	Tape pull-out
0.16	371 ± 53	445 ± 63	Tape pull-out

Table 1: Preliminary results.

References

1. Katsivalis, I., et al., *Strength analysis and failure prediction of thin tow-based discontinuous composites.* Composites Science and Technology, 2024. **245**: p. 110342.
2. Feraboli, P., et al., *Notched behavior of prepreg-based discontinuous carbon fiber/epoxy systems.* Composites Part A: Applied Science and Manufacturing, 2009. **40**(3): p. 289-299.

Corresponding author email: vassaf@chalmers.se

USING THE PARTICLE FINITE ELEMENT METHOD FOR PREDICTING OPTIMUM SHEAR CUTTING CLEARANCE

O. Sandin[1], P. Larour[2], JM. Rodríguez[1,3], S. Hammarberg[1], J. Kajberg[1], D. Casellas[1,4]

[1]*Department of Engineering Sciences and Mathematics, Division of Solid Mechanics, Luleå University of Technology, Luleå, Sweden*

[2]*voestalpine Stahl GmbH, Linz, Austria*

[3]*School of Applied Sciences and Engineering, EAFIT University, Medellin, Colombia*

[3]*Unit of Metallic and Ceramic Materials, Eurecat, Centre Tecnològic de Catalunya, Manresa, Spain*

Advanced High Strength Steel (AHSS) grades allows for light-weighting of sheet steel products through gauge reduction, while remaining the structural integrity. However, the increased strength of the AHSS grades negatively influences the formability of the sheet steel in conventional forming processes and makes the AHSS grades more susceptible to manufacturing defects. A common manufacturing defect is edge-cracking, arising from the damage imposed by the shear cutting process which generally precedes the sheet steel forming procedure [1]. Conventional forming limit analyses are unable to predict the influence of the sheared edge damage, thus new predictive tools are required.

This work presents numerical modelling of the shear cutting process of AHSS sheets using the Particle Finite Element Method (PFEM), with the aim to aid the understanding of the sheared edge damage and its relation to cut edge stretch-flangeability. PFEM is a numerical method proven to handle the numerical implications of shear cutting simulations by efficient management of mesh distortion and internal variable transfer in the remeshing steps, thus preserving the residual stress- and strain data along the cut edge [2]. Preservation of the cut edge residual data is important for subsequent analysis of the cut edge formability or fatigue properties.

By utilising PFEM for shear cutting modelling, numerical cut edges were obtained over a wide range of cutting clearances. The predictive capability of the PFEM model in terms of cut edge parameters (roll-over, burnish, fracture, burr) was stated through validation against experimental hole punching results.

The numerical- and experimental cut edge were then subjected to hole extrusion according to the ISO 16630 Hole Expansion Test (HET), where the Hole Expansion Ratio (HER) displayed the effect of varying cutting clearances to the cut edge formability. The experimental results showed that the presence of large notches, such as burr and secondary burnish, drastically reduced HER as the edge cracks were formed at these notches. In accordance, the numerical HET modelling showed similar fracture patterns and effect on numerical HER. An example is displayed in Figure 1, showing the fracture patterns in experimental- and numerical hole expansion tests, where the cracks originated from the interface between secondary burnish formation and the upper fracture surface. Therefore, it was shown that the numerically predicted cut edge morphology could generate the cut edge notches and residual states that gives the clearance-dependent cut edge stretch-flangeability.

Concludingly, the presented modelling procedure and experimental validation shows that the numerical shear cutting model can be used to define the optimum cutting clearance. Furthermore, the predicted clearance-dependent cut edge shapes also show the effect on local cut edge segments when using non-coaxial tools. By virtual assessment of the cut edge morphology from varying cutting clearances, a range of clearances without large notches may be determined, thus avoiding premature edge cracking during edge forming. Additionally, the numerical tool may be used for process optimisation, such as determining adequate tool sharpness or shape for remaining good quality cut edges.

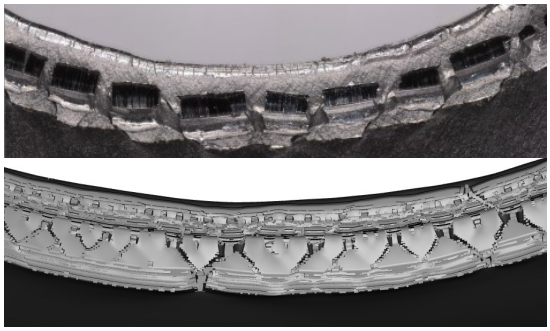

Figure 1: Fracture pattern of experimental- and numerical HET using 5.3% cutting clearance.

References

[1] Konieczny, A. Henderson, T., On formability limitations in stamping involving sheared edge stretching. SAE Technical Papers, (2007)

[2] Sandin, O. Rodríguez, JM. Larour, P. Parareda, S. Frómeta, D. Hammarberg, S. Kajberg, J. Casellas, D., A particle finite element method approach to model shear cutting of high-strength steel sheets. Computational Particle Mechanics, (2024)

Corresponding author: olle.sandin@ltu.se

A TWO-PLAYERS GAME FOR MULTI-SCALE TOPOLOGY OPTIMIZATION OF STATIC AND DYNAMIC COMPLIANCES OF TPMS-BASED LATTICE STRUCTURES

N. Strömberg[1]

[1]*Department of Mechanical Engineering, Örebro University, Örebro, Sweden*

In this work, a non-cooperative two-players game of minimizing static (player 1) and dynamic (player 2) compliances is set up by using a multi-scale topology optimization framework for triply periodic minimal surface (TPMS)-based lattice structures published recently in [1]. Player 1 will find the optimal macro-layout by minimizing the static compliance for a given micro-layout delivered from player 2, and player 2 will find the optimal micro-layout (grading of the TPMS-based lattice structure) by minimizing the dynamic compliance for a given macro-layout from player 1. The two multi-scale topology optimization formulations are obtained by using two density variables (ρ_e, γ_e) in each finite element e. The first one collected in $\boldsymbol{\rho}$ is the standard density variable, which defines if the finite element should be treated as a void ($\rho_e = \epsilon$) or contain the graded lattice structure ($\rho_e = 1$) . This variable is governed by the rational approximation of material properties (RAMP) model. The second density variable collected in $\boldsymbol{\gamma}$ is the local relative density of TMPS-based lattice structure, and it sets the effective orthotropic elastic properties of the finite element. The multi-scale game is solved by using a Gauss-Seidel algorithm with sequential linear programming (SLP), which is implemented for three-dimensional problems, and the numerical results are presented as implicit surface-based geometries. It is demonstrated that the proposed multi-scale game generates equilibrium designs that have good performance for both the static and harmonic load cases, and efficiently avoid resonance at frequencies of the harmonic loads.

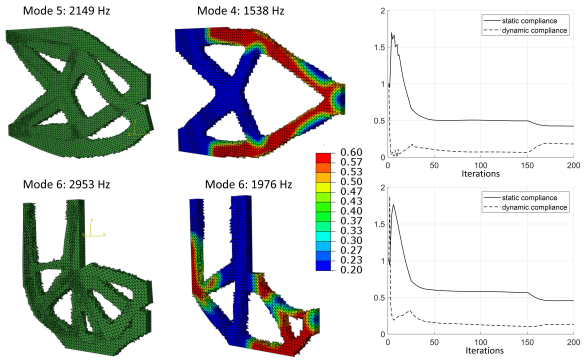

Figure 1: *Eigenmodes and eigenfrequencies for the optimal designs for $\Omega = 0$. The new optimal designs when Ω is set equal to the eigenfrequencies are presented in the middle column. Convergence in the compliances toward equilibrium points are presented to the right.*

The two players' strategies, P_1 and P_2, are defined by the following multi-scale topology optimization problems:

$$P_1 \begin{cases} \text{Given } \boldsymbol{\gamma}^*\text{:} \\ \min\limits_{(\boldsymbol{\rho},\,\mathbf{d})} c_s = \mathbf{F}^T\mathbf{d} \\ \text{s.t.} \begin{cases} \mathbf{K}(\boldsymbol{\rho},\boldsymbol{\gamma}^*)\mathbf{d} = \mathbf{F}, \\ V^{\text{macro}}(\boldsymbol{\rho}) \le \hat{V}^{\text{macro}}, \\ \epsilon\mathbf{1} \le \boldsymbol{\rho} \le \mathbf{1}, \end{cases} \end{cases} \tag{1}$$

$$P_2 \begin{cases} \text{Given } \boldsymbol{\rho}^*\text{:} \\ \min\limits_{(\boldsymbol{\gamma},\,\mathbf{u})} c_d = \dfrac{1}{2}\left(\mathbf{F}^T\mathbf{u}\right)^2 \\ \text{s.t.} \begin{cases} \left(-\Omega^2\mathbf{M}(\boldsymbol{\rho}^*,\boldsymbol{\gamma}) + \mathbf{K}(\boldsymbol{\rho}^*,\boldsymbol{\gamma})\right)\mathbf{u} = \mathbf{F}, \\ V^{\text{lattice}}(\boldsymbol{\gamma}) \le \hat{V}^{\text{lattice}}, \\ l_b\mathbf{1} \le \boldsymbol{\gamma} \le u_b\mathbf{1}, \end{cases} \end{cases} \tag{2}$$

where $\mathbf{d}$ is the static displacement vector, $\mathbf{u}$ contains the magnitudes of the dynamic response, $\mathbf{F}$ contains the external force amplitudes, $\mathbf{Kd} = \mathbf{F}$ is the static equilibrium equation ($\Omega = 0$), $(-\Omega^2\mathbf{M} + \mathbf{K})\mathbf{u} = \mathbf{F}$ is the dynamic equilibrium equation, where Ω is the angular frequency of the time dependent harmonic load $\mathbf{F}\cos(\Omega t)$, and $\hat{V}^{\text{macro}}$ and $\hat{V}^{\text{lattice}}$ are the upper limits on the macro-layout volume and the lattice volume, respectively. l_b and u_b are lower and upper limits on the relative density γ_e of the TPMS-based lattice structure.

Thus, the non-cooperative multi-scale two-players game is to find an equilibrium point $(\boldsymbol{\rho}^*, \boldsymbol{\gamma}^*)$ that is optimal simultaneously for players P_1 and P_2 in (1) and (2). In this work, we try to find such equilibrium points by applying a sequential Gauss-Seidel algorithm with SLP. In Figure 1 it is demonstrated how eigenfrequencies close to the harmonic excitation frequency can be avoided by solving the proposed game using this Gauss-Seidel strategy.

Reference

[1] Strömberg, N., A New Multi-Scale Topology Optimization Framework for Optimal Combinations of Macro-Layouts and Local Gradings of TMPS-based Lattice Structures. Mechanics Based Design of Structures and Machines, 52, 257–274, (2024)

Corresponding author: niclas.stromberg@oru.se

SIMULATION OF BRITTLE FRACTURE: AN APPLICATION FOR COMMINUTION

L.Suarez[1], V. Tojaga[2], J. Quist[2], E. Olsson[1]

[1]*Division of Solid Mechanics, Luleå University of Technology, Luleå, Sweden*
[2]*Department of Computational Engineering and Design, Fraunhofer-Chalmers Centre of Industrial Mathematics, Gothenburg, Sweden*

Due to the great dependence of societies on the extraction and processing of mineral and metals for the production of steels and batteries, optimization processes are needed to reduce the footprint of the mining sector. The increase in the efficiency of comminution processes can be performed from the point of view of either the dynamics of the machines or the material to be treated. This study presents a computational framework for simulating the fracture of brittle materials on different scales aiming to enable AI-based optimization of comminution processes. The numerical framework consists of a high-order Finite Element Method (FEM) to accurately predict the fracture of single real-shaped 3D geometries and an explicit Discrete Element Method (DEM) for scaling up the simulations to an industrial level where millions of particles are comminuted.

Explicit high-order FEM meso-scale simulations were implemented in ABAQUS. The KST-DFH constitutive model for fracture and damage of rock material was used as it provides a good description of the behavior of mineral material under different confining and strain rate conditions. The KST part of the model describes the deviatoric and volumetric behaviour by defining a yield surface as a function of the hydrostatic pressure (see Eq. 1).

$$\sigma_{eq} = \sqrt{a_0 k^2 + a_1 k P + a_2 P^2} \tag{1}$$

Fragmentation processes and damage to the material are addressed in the DFH part of the model. It describes the probabilistic behaviour of fracture accounting for crack initiation at the weakest defect by a Poisson process and probability of failure via a Weibull model (see Eq. 2).

$$P_f = 1 - \exp\left[-V_{eff}\lambda_t(\sigma_F)\right] \tag{2}$$

Calibration and validation schemes were developed based on the experimental background of Brazilian disc experiments and single particle breakage (SPB) of 3D scanned mineral material, respectively. Parametric analyses of the brittle fracture were performed to determine the probability of failure and the effect of statistical parameters on the mechanical response of the material under complex stress states. Breakage of individual particles was studied in detail obtaining a good correlation of the predicted failure load and fracture pattern (see Fig. 1).

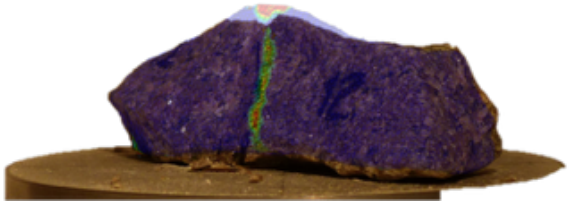

Figure 1: Correlated fractured pattern from a single particle breakage specimen of mineral material

In general, the framework presented here unlocks the possibility to accurately predict fragmentation processes of critical materials and optimize the overall system through AI algorithms within comminution processes.

References

[1] Forquin, P., & Hild, F. . A probabilistic damage model of the dynamic fragmentation process in brittle materials. Advances in Applied Mechanics, Vol. 44, 1–72 (2010). DOI: https://doi.org/10.1016/S0065-2156(10)44001-6.

[2] Olsson, E., Jelagin, D., Forquin, P.A.: Computational framework for analysis of contact-induced damage in brittle rocks. International Journal of Solids and Structures 167, 24–35 (2019). DOI: https://doi.org/10.1016/j.ijsolstr.2019.03.001

Corresponding author: laura.suarez@ltu.se

CORROSION FATIGUE OF HOLLOW CYLINDRICAL SPECIMENS IN SIMULATED LWR ENVIRONMENT

M. Subasic[1], B. Alfredsson[1], C. F. O. Dahlberg[1], M. Bjurman[1,3], J. Smith[2], M. Thuvander[4], P. Efsing[1,5]

[1]*Department of Engineering Mechanics, KTH Royal Institute of Technology, Stockholm, Sweden*
[2]*Electric Power Research Institute, Palo Alto, CA, USA*
[3]*Studsvik Nuclear AB, Nyköping, Sweden*
[4]*Department of Physics, Chalmers University of Technology, Gothenburg, Sweden*
[5]*Ringhals AB, Väröbacka, Sweden*

The objective of this research is an improved risk and life prediction method of corrosion fatigue in piping systems in light water reactor (LWR) nuclear power plants where the primary environment introduces an increased environmental risk for fatigue initiation. An experimental setup for performing corrosion fatigue tests with simulated PWR and BWR water environments in a testing machine has been constructed and manufactured. The tests have been conducted at the Studsvik laboratory on hollow cylindrical specimens. Direct current potential drop (DCPD) is utilized to measure crack initiation and propagation. The material is type 304L stainless steel and has its origin from the manufacturing of the now decommissioned nuclear power plant Barsebäck in Sweden. The specimen is subjected to an alternating mechanical load and water flowing through the interior, simultaneously. The temperature of the water is 300 °C and pressurized to 12 MPa.

Material characterization including uniaxial tensile tests, cyclic tests, fatigue tests and crack propagation tests with standardized specimens of the austenitic stainless steel has been carried out at both room temperature and 300 °C. Material modelling has been performed on the experimental tests to obtain material parameters. S-N curves for the fatigue life of the solid specimens have been obtained for comparison with the corrosion fatigue test results with the hollow specimens. The cyclic plasticity of the material has been modelled with a radial return mapping algorithm to determine isotropic and kinematic hardening parameters fitted to the cyclic stress-strain curves obtained from the experiments.

The experimental setup for the corrosion fatigue tests, see Figure 1, is electrically isolated in order to employ the DCPD method. Verification tests for the hollow cylindrical specimens have been conducted at both temperatures for enabling the comparison of the fatigue lives of hollow specimens with solid specimens. The multiaxial stress effect from the internal pressure has been investigated as well.

Microstructural analyses of the hollow specimens after the corrosion fatigue tests have been conducted by use of scanning electron microscopy (SEM) and electron backscatter diffraction (EBSD) to identify initiation areas as well as mechanisms of corrosion fatigue. The characterization of the oxidation and damage process at the crack tip will give microstructural explanations and indications for the corrosion fatigue process. The main purpose of the microstructural analyses is to gain insight for modelling corrosion fatigue.

A local continuum damage mechanics (CDM) corrosion model has been developed based on electrochemical kinetics, Gutman's mechano-chemical coupling and Faraday's law. The corrosion model is integrated into an elastoplastic framework together with a neighbour element search algorithm to simulate corrosion fatigue initiation for metal components with geometrical discontinuities. The corrosion fatigue model will be further integrated with crystal plasticity to simulate corrosion fatigue of metal pipes by use of Voronoi cells representing crystal grains, see Figure 2.

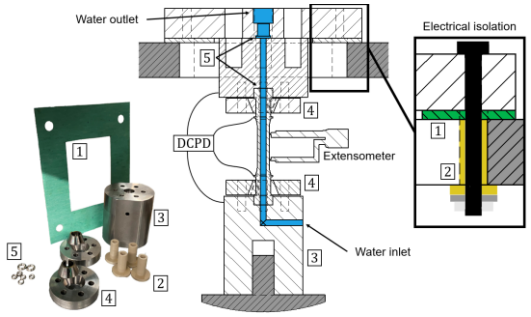

Figure 1: Experimental setup for corrosion fatigue tests electrically isolated from the testing machine (marked in grey) to enable DCPD measurements.

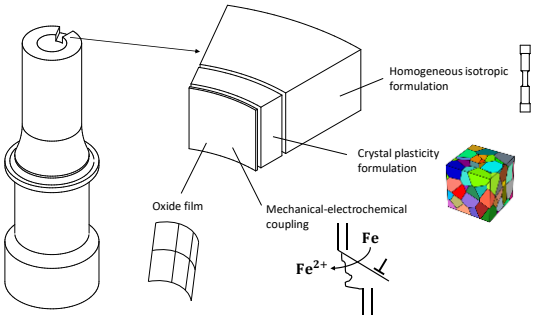

Figure 2: Corrosion fatigue model of metal pipes.

Corresponding author email: msubasic@kth.se

SIMULATION METHODOLOGY FOR PREDICTING INITIATION OF SURFACE CRACKS IN RAILWAY RAILS

N. Talebi[1], B. Andersson[1], M. Ekh[1], K. A. Meyer[2]

[1]*Department of Industrial and Materials Science, Chalmers University of Technology, Gothenburg, Sweden*
[2] *Institute of Applied Mechanics, TU Braunschweig, Germany*

Rolling Contact Fatigue (RCF) cracks in rails cause high maintenance costs and can reduce traffic safety. Hence, accurate predictions of RCF crack initiation are highly needed. Such predictions require reliable fatigue crack initiation criteria, depending on stress and strain histories. Thus, it is essential to use plasticity models that can provide estimations of the stress and strain states in rails, whose material properties evolve during rolling contact loading.

In this contribution, a small strain cyclic plasticity model with an anisotropic yield surface, (based on the large deformation material model formulated by Meyer and Menzel [1]) is used, see Eq. (1).

$$\phi = \sqrt{\sigma_{\text{red}}^{\text{dev}} : \hat{\mathbf{C}} : \sigma_{\text{red}}^{\text{dev}}} - Y \leq 0 \qquad (1)$$

where $\hat{\mathbf{C}}$ is the anisotropy tensor, $\sigma_{\text{red}}^{\text{dev}}$ is the reduced deviatoric Cauchy stress, and Y is the isotropic hardening. The material model is calibrated against previously conducted experiments with railway-like cyclic loading (compression and shear) on pearlitic R260 steel specimens. In these experiments, solid test bars were first twisted under a compressive stress of -600 MPa to obtain different degrees of anisotropy (predeformation). They were then re-machined into thin-walled tubular test bars and subjected to multiaxial cyclic loading. Based on the test results, material parameters for different depths of a highly deformed rail surface layer are identified. Figure 1 shows a comparison between the normal stress-strain results from simulations and tests for cycle number 500.

The calibrated plasticity model is then used in finite element simulations of realistic traffic situations to obtain stress and strain histories in the surface layer of rails. The over-rolling simulations are done using a 2D generalized plane strain model developed by Andersson et al. [2]. The stress and strain histories are employed to predict the number of cycles to macroscopic crack initiation in the rail surface layer using a newly developed RCF crack initiation criterion by Talebi et al. [3]. This criterion accounts for the inhomogeneous stress-strain field in the surface layer and has been calibrated against three groups of experiments: Large shear increments under different amounts of axial stresses (predeformation), predeformation tests with subsequent uniaxial or proportional multiaxial cyclic loadings, and stress-controlled axial high cycle fatigue experiments to identify the fatigue damage limit.

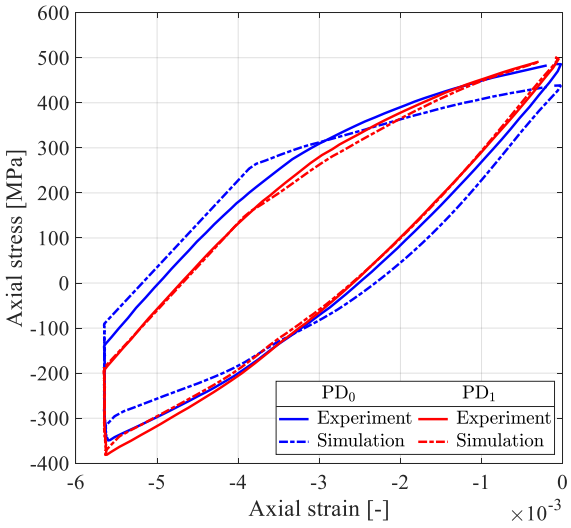

Figure 1: Normal stress-strain behavior from test and simulation for loading cycle 500 for specimens with predeformation levels of 0 (PD_0) and 0.21 (PD_1) shear strain.

References

[1] K. A., Meyer, A., Menzel, a distortional hardening model for finite plasticity. *Int. J. Solids and Struct.*, 232, 111055, (2021)

[2] B., Andersson, M., Ekh, B. Lennart, Josefson, computationally efficient simulation methodology for railway repair welding: Cyclic plasticity, phase transformations, and multi-phase homogenization, *J. of Thermal Stresses*, 47(2), 164-88, (2024)

[3] N., Talebi, J., Ahlström, M., Ekh, K. A., Meyer, evaluations and enhancements of fatigue crack initiation criteria for steels subjected to large shear deformations. *Int. J. Fatigue,* 182, 108227, (2024)

Corresponding author email: nasrin.talebi@chalmers.se

Four-point bending in paper-based sandwich beams: Experimental and modelling aspects

Marcus Vinícius Tavares da Costa[1], Mikael Perstorper[1], Johan Vessby[1]

[1]*Karlstad University, Department of Engineering and Chemical Sciences, Karlstad, Sweden*

In the Värmland region, Sweden, an innovative sandwich structural element has been designed by the cooperation of pulp and paper companies for possible use in indoor products, such as tables, shelves, doors, and furniture in general [1]. The element, lightweight and strong, has facesheets of laminated paperboards made of recycled and/or virgin wood fibres. The core, made of paper pulp, has a unique shape like a cup box with staggered positions between the cups, see [1]). At the Department of Engineering and Chemical Science at Karlstad University, the mechanical performance and properties of the elements have been investigated via experimental tests and finite element (FE) models for different applications. Recently, four-point bending tests have been conducted in sandwich beams from the element, see Fig. 1(a). The facesheets of the beams were made of virgin and/or hybrid (virgin + recycled fibres) paper materials. Results from quasistatic experimental tests were evaluated by means of digital image correlation technique for accurate measurements of the beam deflection.

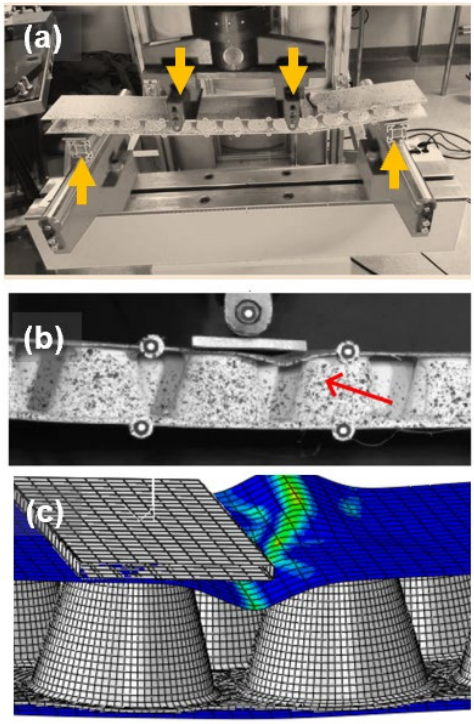

Figure 1: (a) Four-point bending experimental setup, (b) failure in the top facesheet during the tests and (c) FE simulation showing the same failure as in the tests.

In this presentation, we will address aspects of flexural and shear rigidities of the tested samples [2, 3], as well as main observations of failures, which occurred at the top facesheets (c.f. Fig 1(b)). A parametric FE model will also be presented along with its calibration, capability of predicting the failure (c.f. Fig 1(c)), and possibilities for structural optimization.

References

[1] Ecopals AB, Hållbar möblekonstruktion till en bråkdel av vikten/Durable furniture construction at a fraction of the weight. Retrieved March 03, 2024, https://ecopals.se/

[2] Howard, G.A., Analysis and design of structural sandwich panels, *Pergamon*, (1969)

[3] Lorna, J.G., Michael, F.A., The design of sandwich panels with foam cores. In: Cellular Solids: Structure and Properties. *Cambridge University Press*, 345-386, (1997)

Corresponding author email: marcus.tavares@kau.se

IMPACT STRESS IN A ROCK DRILLING MACHINE PISTON

A. Tkachuk[1], M. Sadek[1,2], M. Grehk[1]

[1]*Department of Engineering and Physics, Karlstad University, Karlstad, Sweden*
[2]*Engineering Solutions, Etteplan, Lund, Sweden*

Pistons inside percussive rock drilling machines are subject to impact loads with frequencies 10–120 Hz and velocities up to 12 m/s. High impact stress is one of the reasons for the limited service life of the pistons. It is difficult to access a piston during operation to measure impact stress values and understand important factors influencing the stress histories on the impact surface. Analytical and semi-analytical solutions are limited to the normal incidence angle of pistons, see [**1**] and references there. However, experimental studies and previous simulations show that a misalignment angle during the impact is important [**2**, **3**]. Furthermore, the specific dimensions of the piston head for each manufacturer influence the values of stress. Therefore, a series of simulations for specific geometries is carried out to find characteristics of the impact stress. These simulations are coupled with a fractography of real piston heads made of two low alloy steel grades to complete an engineering failure analysis, reported in [**4**].

A simplified setup for the impact of the piston head against a shank adapter is shown in figure 1. An isotropic elastic material model is used for both parts with parameters $E = 210$ GPa, $\nu = 0.3$ and $\rho = 7850$ kg/m^3. The piston has an initial velocity of $v_0 = 10$ m/s. Three misalignment angle values $0°$, $0.11°$ and $0.22°$ are compared. These values correspond to tolerances of guiding surfaces for the piston, and similar values were used in [**3**]. The termination time for the simulation is 44 μs. A model with ca. 6.5 million C3D8R finite elements is used for an explicit dynamics simulation in Abaqus R2020. Default values for bulk viscosity and hourglass control are used. In the contact pair, a dry friction model with $\mu = 0.1$ and "hard" formulation is used. A reference amplitude of the primary compressive wave for zero misalignment is $\sigma_z = -\frac{v_0 E}{c_1} \approx -350$ MPa, where c_1 is the speed of longitudinal waves.

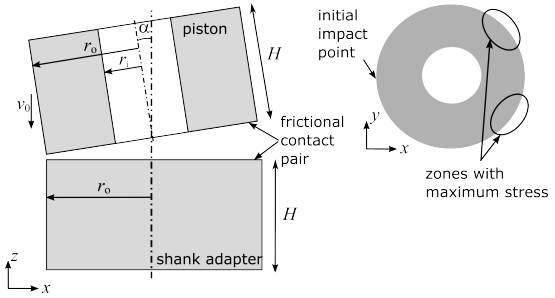

Figure 1: Simulation setup for misaligned impact of the piston head with the shank adapter. Dimensions: $r_o = 18$ mm, $r_i = 6$ mm, $H = 45$ mm.

Stress values for zero misalignment cannot describe the crack pattern on the surface (max. principal stress 232 MPa). For the misalignment angle of $0.11°$, the maximum principal stress is 372 MPa and it is reached at the point on the outer radius with ca 165° offset from the initial impact point. For the misalignment angle of $0.22°$, the maximum principal stress is 773 MPa and it is reached at the point on the outer radius with ca 120° offset from the initial impact point. The tensile stress is along the hoop direction and explains the crack opening at the outer radius. Similar observations are made in [**3**] for a misalignment angle $0.22°$, but a different geometry of the piston head. The location of the maximum stress values is due to the superposition of the impact stress waves propagating along the surface. The qualitative behavior differs for the misalignment angles: the sign of surface stress wave is negative for $0.11°$ and positive for $0.22°$ (figure 2).

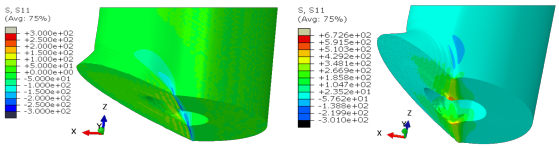

Figure 2: Stress σ_{xx} in the piston head for misalignment angles $0.11°$ (left) and $0.22°$ (right) at time 6.3 μs.

References

[1] Cerv, J., Adamek, V., Vales, F., Gabriel, D., Plesek, J. Wave motion in a thick cylindrical rod undergoing longitudinal impact. Wave Motion, 66, 88-105 (2016)

[2] Hawkes, I., Burks, J. A. Investigation of noise and vibration in percussive drill rods. International Journal of Rock Mechanics and Mining Sciences, 16, 362-376, (1979)

[3] Wang, J., Han, B., Wang, C., Gong, Y., Li, Y., Neville, A., Morina, A. Failure analysis of the piston used in a pneumatic down the hole impactor. Engineering Failure Analysis, 127, 105561, (2021)

[4] Bakhshandi R.K., Tkachuk A., Sadek M., Bergstrom J., Grehk M. Failure analysis of two cylindrical impact pistons subjected to high velocity impacts in drilling applications, Engineering Failure Analysis, 140, 106623, (2022)

Corresponding author: anton.tkachuk@kau.se

DISCRETE NETWORK MODEL FOR IRREVERSIBLE DEFORMATION OF NEEDLE-PUNCHED NONWOVEN FABRICS

M. Tkachuk[1,2], A. Biel[1], A. Tkachuk[1]

[1] *Department of Engineering and Physics, Karlstad University, Karlstad, Sweden*
[2] *Institute of Education and Science in Mechanical Engineering and Transport, National Technical University "Kharkiv Polytechnical Institute", Kharkiv, Ukraine*

Needle-punched nonwoven textiles can undergo large irreversible deformations. This response can be primarily attributed to relative sliding of fibers at the entangled knots [1]. We have developed a new discrete network model [2] for this type of materials. It is based on the following simplifying assumptions:

- the fibers are considered as inextensible cables composing a central force network; there is no elastic elongation when fibers are loaded in tension; when compressed the segments become slack and produce no axial force;
- the fibers slide relative to each other at the connecting knots as shown in Figure 1 when the force difference on the opposite sides of the knot overcomes the frictional limit; the yield limits do not change during the deformation process.

The rate-independent sliding and the quasi-static equilibrium loading of such network structure are constituted within the theory of standard dissipative systems. A minimum principle for incremental potential is formulated with respect to the displacement-based variables: nodal coordinates, segment end-to-end vectors, segment lengths and incremental fiber slidings. It takes the form of second-order cone programming (SOCP) similarly to the case of elastic cable networks [3]. A pure complementary energy principle is derived as the dual formulation in terms of stress-like variables: nodal reactions, fiber force vectors, axial forces and friction forces. Both SOCP problems can be solved numerically by interior-point methods.

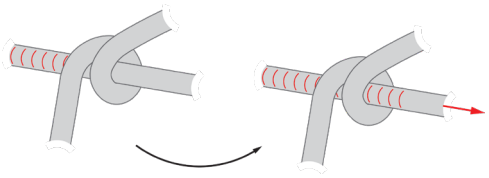

Figure 1: Relative sliding of entangled fibers.

Fiber pill-out is incorporated to the model as the microscopic failure mechanism. It is detected at the end of each loadstep when the slip in the terminal knots exceeds the free tail length at the beginning of the loading. This allows to capture the behavior of the fiber networks in the entire macroscopic specimens as shown in Figure 2 and the characteristic material response shown in Figure 3.

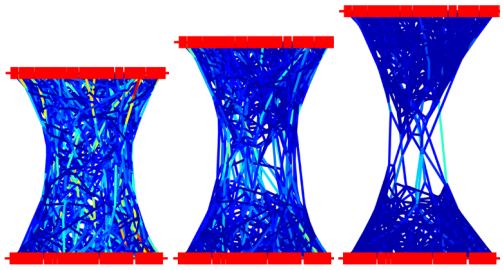

Figure 2: Deformation of a fiber network.

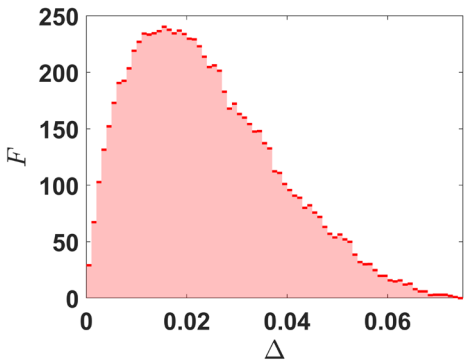

Figure 3: Clamp force for a rectangular specimen.

We study various specimen geometries, including notched specimens. The simulation results are validated by the known and newly obtained experimental data.

References

[1] Martínez-Hergueta, F., Ridruejo, A., González, C., & LLorca, J., Deformation and energy dissipation mechanisms of needle-punched nonwoven fabrics: A multiscale experimental analysis. *International Journal of Solids and Structures*, 64(65), 120-131, (2015).

[2] Tkachuk, M., & Tkachuk, A., Large Deformation of Cable Networks with Fiber Sliding as a Second-Order Cone Programming. *Available at SSRN 4620591* , preprint (2023).

[3] Kanno, Y., Nonsmooth mechanics and convex optimization (pp. 61-63). CRC Press (2011)

Corresponding author email: Mykola.Tkachuk@kau.se

TOWARD SIMULATING FRACTURE IN LARGE PARTICLE SYSTEMS

V. Tojaga[1], L. Suarez[2], E. Olsson[2], A. Bilock[3], K. Jareteg[3], J. Quist[1]

[1]*Department of Computational Engineering and Design, Fraunhofer-Chalmers Centre for Industrial Mathematics, Gothenburg, Sweden*
[2]*Division of Solid Mechanics, Luleå University of Technology, Luleå, Sweden*
[3]*Industrial Path Solutions Sweden AB, Gothenburg, Sweden*

We need more metals and minerals for the green transition of our society. The mining sector, which consumes around 6% of the world's total energy, sees about 40% of this energy used in the grinding process of the ore to extract minerals. Sustainability begins with the materials you extract through mining. This project is committed to creating a virtual platform that facilitates the development of eco-efficient rock processing solutions aimed at reducing energy consumption. The challenge in crushing simulations is to improve the accuracy and reliability of the rock geometry and the dynamic fracture model, ensuring precise predictions while also scaling up to an industrial level.

The explicit Discrete Element Method (DEM) is the preferred tool for modeling processes involving granular materials, particularly with parallel computing on Graphics Processing Units (GPUs), it offers efficient and scalable solutions for industrial-sized problems. In DEM, Newton's second law governs the movement of pseudo-rigid particles, meaning they can overlap, provided the overlap distance is small compared to the particles' size such that the particles' deformation is negligible. We present a cohesive zone model for mixed-mode fracture [1] in bonded GPU-accelerated Voronoi-based DEM implemented in the commercial software Demify developed at Fraunhofer-Chalmers Centre (FCC). This model introduces virtual, yet removable, cohesive bonds between Voronoi-shaped particles, mimicking the natural bonds found between grains in a rock, thereby simulating rock fracture. We model the bond as a truss-bar, exhibiting Hookean behavior until failure initiation. At that point, we integrate the Mohr-Coulomb failure criterion in shear with a maximum stress criterion in tension, utilizing a quadratic nominal stress criterion followed by a linear softening traction-separation law within the framework of classical damage mechanics. In compression, a penalty method, represented by a linear truss-bar, is employed, while the dilated polyhedron approach with the Hertz-Mindlin-Deresiewicz (HMD) no-slip contact model for simple spheres kicks in after bond breakage [2].

The DEM model is calibrated against a Brazilian disc test of glimmingen and limestone, followed by validation against a Single Particle Breakage (SPB) test of the same material (see Figure 1). A comparison is made with a Finite Element Method (FEM) model utilizing the KST-DFH constitutive description of the rock material. As the last step, it is applied in cone crusher simulations of large particle systems (see Figure 1), completing the transition from rock fracture mechanics to minerals engineering.

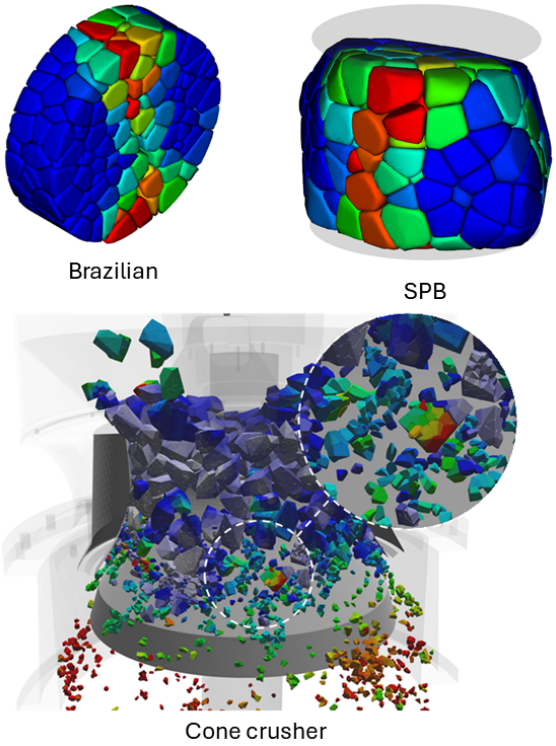

Figure 1: DEM simulations of a Brazilian disc test, Single Particle Breakage (SPB), and a cone crusher.

References

[1] Ma, G., Zhao, W., Chang, X.L., Modeling the particle breakage of rockfill materials with the cohesive crack model. Computers and Geotechnics, 61, 132-143, (2014)

[2] Liu, L., Ji, s., Bond and fracture model in dilated polyhedral DEM and its application to simulate breakage of brittle materials. Granular Matter, 21, 41, (2019)

Corresponding author: vedad.tojaga@fcc.chalmers.se

MODELLING OF INDUSTRIAL APPLICATIONS WITH A DEM-FEM COUPLING ALGORITHM

A. Ullrich[1], J. Quist[1], C. Cromvik[1], G. Kettil[1]

[1]*Department for Computational Engineering and Design, Fraunhofer-Chalmers Centre, Gothenburg, Sweden*

In the modelling of industrial processes, multi-physics co-simulations become increasingly prevalent. In many industrial applications, various components and subsystems are interacting and affecting each other. Thus, to accurately model the components, different modelling and simulation methods must be combined to capture the correct interactions and behaviours of each component.

The Finite Element Method (FEM) is a common simulation method for solid structures to study for instance deformations due to external loads. In many industrial applications, FEM is even applied to simulate granular materials, e.g. for railroad infrastructure simulations [2]. However, it is important to consider the granular materials as dynamic particle systems for accurate modelling, which is commonly done with the Discrete Element Method (DEM). The combination of the simulation of solid structures and particle systems is presented with the co-simulation of a DEM-FEM surface coupling.

To exemplify the value of the DEM-FEM coupling, it is evaluated in different industrial applications, two of them are given in the following.

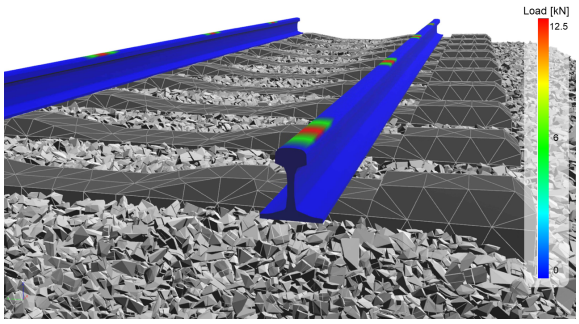

Figure 1: Snapshot of a railroad simulation with a moving point load pattern. The sleepers and rails are simulated with FEM and the ballast particles with DEM.

In the first industrial application of railroad simulations, the sleepers and rails are modelled with FEM and the ballast layer consisting of rock particles with DEM to evaluate the interaction between the sleepers and the ballast material. An example of a simulation can be seen in Figure 1. In this case, a moving point load is applied on the rails representing train axles and the settlement of the track can be evaluated. The inclusion of DEM in the DEM-FEM coupling facilitates to evaluate different size distributions or shapes of the material, i.e. rounded particles versus highly irregular particles.

In the second industrial application, a wheel loader bucket is simulated with a FEM model and interacts with a pile of rock particles represented in DEM. A visualisation of this application is shown in Figure 2, where nodes on the FEM mesh are coloured by the von Mises stress. Here, the DEM-FEM coupling facilitates to analyse the fatigue and wear on the bucket, especially the tip, when interacting with the rock pile, considering the difficulties of varying size distributions or material properties of the rocks. Thus, varying bucket designs and their resistance and stability can be evaluated in more detail.

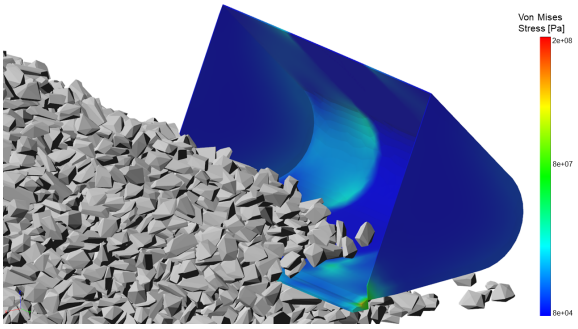

Figure 2: Snapshot of a simulation of a wheel loader bucket represented as a FEM object interacting with a pile of rocks simulated with DEM.

The DEM-FEM coupling bridges the gap of understanding the behavior and effects in granular materials for solid mechanics applications, such as simulations of infrastructure. With FEM the solid structures can be simulated accurately and their deformations and strain due to external loads can be analysed. Furthermore, with the representation of the individual rock particles in DEM with various details, e.g. their exact shape, the coupling facilitates the evaluation of the dynamics inside the particle population due to the movement of solid structures.

References

[1] Anita Ullrich. “Development of a DEM-FEM framework for infrastructure simulations”, master thesis, 2022

[2] Yahia Alabbasi and Mohammed Hussein. “Geomechanical Modelling of Railroad Ballast: A Review”. In: Archives of Computational Methods in Engineering 28.3 (Dec. 2019), pp. 815–839

Corresponding author: anita.ullrich@fcc.chalmers.se

STUDYING HYDROMECHANICS OF HETEROGENOUS POROUS SANDSTONE USING ADVANCED EXPERIMENTS AND DIGITAL TWIN MODELLING

F. Vieira Lima[1], S. Hall[1], F. Prada[2], J. Engqvist[1], E. Tudisco[1], Robin Woracek[3]

[1]*Department of Construction Sciences, Lund University, Lund, Sweden;* [2]*Department Department of Civil and Architectural Engineering, Aarhus University, Aarhus, Denmark;* [3]*European Spallation Source, Lund, Sweden*

Enhancing our comprehension of localized deformation and heterogeneity within rocks and their consequent impact on fluid flow is paramount for optimizing various geoenergy applications. Recent advancements in 3D imaging techniques, notably X-ray and neutron tomography, have significantly advanced our ability to tackle this challenge.

In this study, we employed a multidisciplinary approach combining advanced imaging technologies with numerical simulations to investigate the hydromechanical behavior of rocks at both macro and micro scales. Specifically, we conducted coupled triaxial permeability tests on Idaho Gray sandstone samples using the state-of-the-art NeXT instrument [1] at ILL (Institut Laue Langevin). This allowed us to capture detailed 3D images of the samples with exceptional spatial resolution and track rapidly fluid flow dynamics within the porous rock matrix. From the X-ray image data, porosity fields were generated to characterize the internal structure of the samples. Additionally, Digital Volume Correlation (DVC) using the SPAM algorithm [2] was performed on pairs of in situ tomograms to quantify strain fields. A custom algorithm was developed to process neutron tomograms generating fluid flow speed fields.

Furthermore, we performed numerical finite element (FE) simulations to complement our experimental observations and delve deeper into the underlying mechanics governing rock-fluid interactions. Mechanical constitutive models, including a logarithmic-based porous elasticity model and a critical state plasticity model [3], were calibrated from experimental data from Bedford et al. [4]. Then numerical analyses based on a homogeneous idealization (material-point simulations) were conducted to ratify the mechanical behavior. Finally, we simulated the mechanical response of the replicated heterogeneous samples under the same boundary conditions of the experiments. To simulate hydraulic behavior, we adopted the Carma-Kozeny model, which accounts for permeability dependence on pore size and porosity. This model allowed us to replicate fluid flow through the samples at axial displacements equivalent to those observed in experiments, providing valuable insights into the hydraulic dynamics within the heterogeneous rock matrix.

A novel aspect of our study involved the incorporation of field heterogeneities into our numerical models, derived from the high-resolution tomographic images. We began by binarizing images of the intact sample and then delineating regions of different porosity levels. Utilizing this data, we generated representative volume elements (RVEs), taking into account the coordinates and area of each element within the finite element mesh. To correlate porosity variations with material behavior, we adjusted the yield surface size and elastic constants of each RVE based the normal consolidation line. The variables were assigned to the elements using field subroutines.

The experimental and numerical results show that heterogeneity significantly influenced both global and local failure mechanisms. Deviatoric and dilative volumetric strain seems to concentrate in the least porous zones, contributing to the on-set of failure. Fluid flow exhibited faster rates in more porous zones, with rock deformation influencing the flow path; dilation facilitated fluid transmissibility, while contraction reduced it. Numerical analysis indicated that, although there are challenges in replicating exact full-field deformation with the adopted constitutive model, the distribution of deviatoric and volumetric strain across different porosity regions was aligned with experimental observations. Additionally, the fluid flow fields were relative aligned with what noted in the neutron image series.

References

[1] Tengattini, A., Lenoir, N., Andò, E., Giroud, B., Atkins, D., Beaucour, J., & Viggiani, G. NeXT-Grenoble, the Neutron and X-ray tomograph in Grenoble. *Nuclear Inst and Methods in Physics Research*, 968, 163939. (2020).

[2] Stamati, O., Andò, E., Roubin, E., Cailletaud, R., Wiebicke, M., Pinzon, G., ... & Birmpilis, G. Spam: software for practical analysis of materials. *Journal of Open Source Softwar*e, 5(51), 2286. (2020).

[3] Schofield, A. N., & Wroth, P. Critical state soil mechanics (Vol. 310). London: McGraw-hill. (1968).

[4] Bedford, J. D., Faulkner, D. R., Wheeler, J., & Leclère, H. High-resolution mapping of yield curve shape and evolution for high-porosity sandstone. *Journal of Geophysical Research: Solid Earth*, 124(6), 5450-5468. (2019).

Corresponding author email: fernando.vieira.lima@solid.lth.se

A NON-LOCAL GURSON MODEL WITH TWO FRACTURE-MECHANISM ASSOCIATED LENGTH SCALES

Shuyue Wang[1] and Jonas Faleskog[1]
[1]*Department of Engineering Mechanics, KTH Royal Institute of Technology, Stockholm, Sweden*

A viable method to predict the initiation and propagation of cracks in ductile materials is using a Gurson model [1], which accounts for void nucleation, growth, and coalescence. A non-local treatment of suitable internal variables, involving one or several length scales, is preferable when numerically analysing failure processes based on damage constitutive models. In this way, a pathological dependence on the discretization of the numerical model and strain localization can be avoided. [2]

In this study, an integral approach that utilizes two different length scales is applied, in which the integration is carried out in spatial configuration motivated by the observation that ductile failure typically is preceded by finite deformation [3]. To address ductile failure in the full range, low to high triaxial stress states, the Gurson model modified for shear failure is employed [4]. A model for void nucleation is also included, which was observed to be a necessity to enable the development of cup-cone fracture in uniaxial tension. With this model, the progression of shear failure may be separated from the progression of flat dimple rupture, by assuming that the contribution to the evolution of the effective void volume fraction can be split into a deviatoric part in addition to the dilatational part. It is assumed that these failure mechanisms are governed by different characteristic length parameters, a deviatoric R_s and a dilatational length R_h, respectively.

The influence on the failure of the two length parameters (R_s, R_h) is numerically investigated using different benchmark loading conditions and physical material parameters. These benchmark problems constitute a set of discriminating tests, from which the two length parameters can be estimated for practical purposes. It is shown that the introduction of an additional deviatoric length parameter has a significant effect on the deformation to failure in shear-dominated geometries with strong plastic strain gradients, as well as on the appearance of the classic cup-cone failure and shear band formation leading to slant fracture in tension-dominated geometries. Fig.1 presents failure modes for a round smooth bar (RSB) loaded in uniaxial tension, where a smaller R_s facilitates the development of cup-cone fracture and L_e denotes the element size.

Experiments are carried out on test specimens similar to the numerically analysed benchmark problems on material A508. Model parameters are systematically estimated using the experimental outcomes. Fig.2 presents the load deformation response and the JR curve for single edged bend specimen (SENB) with initial deep and shallow crack, respectively.

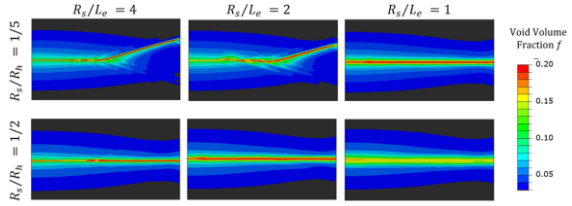

Figure 1: Cup-cone failure modes in RSB shown in the undeformed configuration. Iso-contours of the effective void volume fraction are shown.

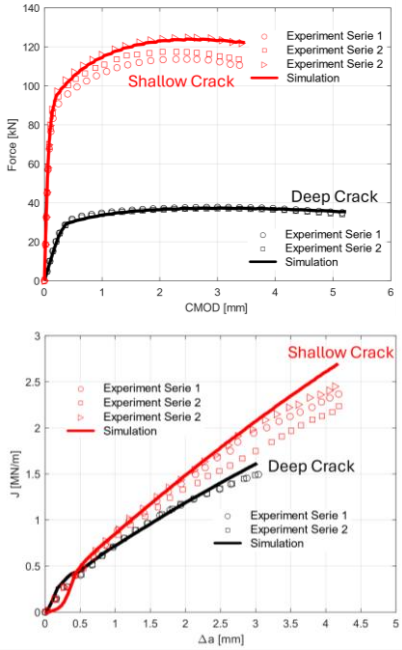

Figure 2: Calibration of SENB with initial deep and shallow crack.

References

[1] Gurson, A. L. Continuum theory of ductile rupture by void nucleation and growth: Part I—Yield criteria and flow rules for porous ductile media, *J. Eng. Mater. Technol.*, 99(1): 2-15. (1977)

[2] Wang, S., & Faleskog, J., A non-local GTN model with two length scales – Application to ductile failure in a wide range of stress triaxiality, *Eur. J. Mech. A/Solids.*, 105056. (2023)

[3] Bergo, S., Morin, D., & Hopperstad, O. S. Numerical implementation of a non-local GTN model for explicit FE simulation of ductile damage and fracture. *Int. J. Solids Struct.*, 219, 134-150. (2021)

[4] Nahshon, K., & Hutchinson, J. Modification of the Gurson model for shear failure, *Eur. J. Mech. A/Solids.*, 27(1), 1-17. (2008)

Corresponding author email: shuyue@kth.se

ULTRASONIC ATTENUATION IN POLYCRYSTALLINE MATERIALS

A. Boström[1], A. Jafarzadeh[1], P.D. Folkow[1]

[1]*Department of Mechanics and Maritime Sciences, Chalmers University of Technology, Gothenburg, Sweden*

When an ultrasonic wave propagates through a polycrystalline material, typically a metal, it undergoes grain scattering and it therefore becomes dispersive and attenuated. The grains are usually anisotropic but in many cases their orientation is random so the effective properties become isotropic. A classical approach to study such media is to replace the micro-inhomogeneous elastic material with a continuous random material characterized by a local elastic stiffness tensor with mean isotropic stiffness and random fluctuations [1]. A volume integral approach is then employed which is solved by a perturbative method assuming weak elastic fluctuations (the method is often called the second order approximation (SOA)).

More recently FEM has been used to estimate the effective wavenumbers [2]. This modelling of a polycrystalline material raises questions about the size of the model and its boundary conditions, grain and mesh generation, the statistical approach, and computer running times.

Here a very different approach is taken. First the scattering by a single anisotropic sphere in an infinite isotropic surrounding is solved, and this leads to an explicit algebraic solution for low frequencies [3]. To model a polycrystalline material each grain is assumed to be a sphere and to act as a scatterer in the average material of all the other grains. Multiple scattering is disregarded and the grains are assumed to completely fill the material in the sense that the total volume of all the grains equals the volume of the material. The grains are also randomly located and oriented.

The effective wave propagation in a material consisting of a matrix with a distribution of scatterers is a classical subject in mathematical physics. For the scattering in elastic media Gubernatis and Domany [4] give the following equation for the effective wavenumber K_i

$$K_i^2 = k_i^2 + 4\pi n \langle f_i \rangle, \tag{1}$$

where i determines the type of wave, compressional or shear. Here n is the number densities of scatterers and $\langle f_i \rangle$ is the ensemble averaged (with respect to orientation) forward scattering amplitude of a single grain. All together this means that the effective wavenumber can be given in closed algebraic form.

A final important issue is how to choose the matrix material in which the scattering by a single grain is taken place and similarly for SOA how the mean elasticity properties are chosen relative which the deviations are given. Traditionally the Voigt average is used [1,2], but it appears [3] that a better choice may be to take the static-consistent average.

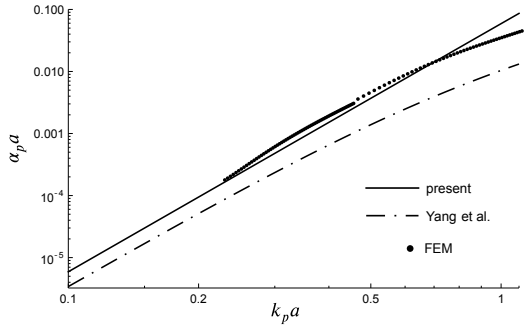

Figure 1: Attenuation of zinc as a function of frequency.

As an example Figure 1 shows the attenuation of zinc as a function of frequency on a log-log scale for the present approach, FEM, and the SOA method of Yang et al. [5]. Both axes are made dimensionless by the sphere radius (and a similar length for FEM and SOA). The low frequency range where the present approach is valid is roughly $k_p a < 0.5$. Zinc is a strongly anisotropic material and that is the reason for SOA underestimating the attenuation as compared to the other two methods which show a reasonable agreement.

References

[1] Sha, G., Huang, M., Lowe, M.J.S., Rokhlin, S.I., Attenuation and velocity of elastic waves in polycrystals with generally anisotropic grains: Analytical and numerical modeling, J. Acoust. Soc. Am. 147, 2442–2465 (2020)

[2] Huang, M., Rokhlin, S.I., Lowe, M.J.S., Appraising scattering theories for polycrystals of any symmetry using finite elements, Trans. R. Soc. A 380, 20210382 (2022)

[3] Jafarzadeh, A., Folkow, P.D., Boström, A., Scattering of elastic waves by a sphere with orthorhombic anisotropy and application to polycrystalline material characterization, Ultrasonics 138, 107199 (2024)

[4] Gubernatis, J.E., Domany, E., Effects of microstructure on the speed and attenuation of elastic waves in porous materials, Wave Motion 6, 579–589 (1984)

[5] Yang, L., Lobkis, O.I., Rokhlin, S.I., Explicit model for ultrasonic attenuation in equiaxial hexagonal polycrystalline materials, Ultrasonics 51, 303–309 (2011)

Corresponding author: anders.bostrom@chalmers.se

NONLINEAR DYNAMICS OF MULTILAYER GRAPHENE CONSIDERING SIZE EFFECTS

Bo Yang and Mahmoud Mousavi

Division of Applied Mechanics, Department of Materials Science and Engineering, Uppsala University, 75103 Uppsala, Sweden

This research numerically investigates wave propagation within two-dimensional defect-free multilayer graphene. It incorporates geometric nonlinearity using second strain gradient elasticity. We analyze the dynamic characteristics of multilayer graphene, including band structures, employing periodic structures theory [1]. The numerical findings demonstrate that incorporating nonlinearity enables more accurate predictions of higher frequency values, resulting in a stiffness hardening effect in graphene. At elevated frequencies, a substantial portion of energy becomes confined to a single direction, and the nonlinear model demonstrates enhanced wave-controlling capabilities.

As depicted in Fig.1, the configuration of carbon atoms includes interactions through out-of-plane π-bonds and in-plane σ-bonds. The multilayer graphene under consideration is assumed to be free of defects. The primary emphasis here is on exploring the continuum mechanics of graphene, employing a geometrically nonlinear continuous beam model to capture the interaction dynamics between two carbon atoms.

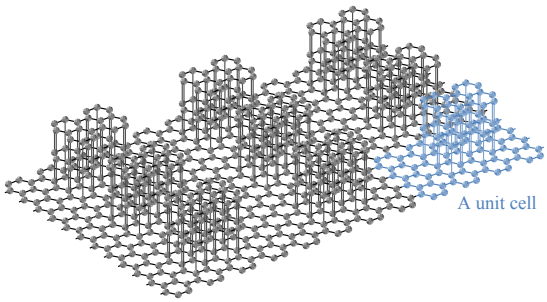

Figure 1: The schematic of a resonator constructed from the multilayer graphene-based waveguide.

In order to confirm the mechanical model of the graphene, the strain energy density through the SSG theory [2] is introduced, as below:

$$\bar{\mathcal{U}} = \bar{\mathcal{U}}_0 + \bar{\mathcal{U}}_1 + \bar{\mathcal{U}}_2 + \bar{\mathcal{U}}_3 + \bar{\mathcal{U}}_4, \tag{1}$$

where $\bar{\mathcal{U}}_0$ represents the classical strain energy density component, $\bar{\mathcal{U}}_1$ signifies the strain energy density associated with the second gradient of displacement, $\bar{\mathcal{U}}_2$ denotes the strain energy density linked to the third gradient of displacement, $\bar{\mathcal{U}}_3$ indicates the coupled portion of strain energy density, and $\bar{\mathcal{U}}_4$ relates to the cohesion modulus b_0 in terms of force dimension. The corrected frequency ω is determined by combining the solutions of the linear zero-order system and the perturbed system [3], resulting in the following expression:

$$\omega = \omega_0 + \beta\omega_1, \tag{2}$$

in which ω_0 stands for the linear frequency, ω_1 means the frequency from perturbed system, β is a quantifier for the degree of nonlinearity inherent in the system. Fig. 2 displays the first five branches of the normalized frequency spectrum along the boundary O-A-B-O of the irreducible first Brillouin zone.

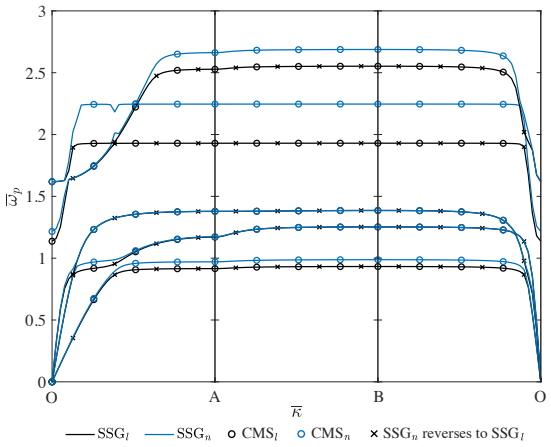

Figure 2: Band structures of defect-free multilayer graphene

Acknowledgements

This work is funded by the European Union's Horizon Europe Programme (NANOWAVE) under the Marie Skłodowska-Curie Actions grant agreement No. 101105373.

References

[1] Mead, D., A general theory of harmonic wave propagation in linear periodic systems with multiple coupling, Journal of Sound and Vibration, 27, 235-260, (1973)

[2] Mindlin, R. D., Second gradient of strain and surface tension in linear elasticity, International Journal of Solids and Structures, 147-438, (1965)

[3] Ramos, J. I., On Linstedt–Poincaré techniques for the quintic Duffing equation, Applied Mathematics and Computation, 2, 303–310, (2007)

Corresponding author: boyang-chn@hotmail.com

MIXED REALITY FOR EDUCATING MECHANICAL ENGINEERS

Kaveh Amouzgar[1], Mahmoud Mousavi[2]

[1]*Department of Civil and Industrial Engineering, Division of Industrial Engineering and Management, Uppsala University, Uppsala, Sweden*

[2]*Department of Materials Science and Engineering, Division of Applied Mechanics, Uppsala University, Uppsala, Sweden*

The Many engineering concepts in higher education involve 3D descriptions of objects, such as structures within Mechanical Engineering. Understanding such concepts can be challenging for students in the absence of proper visualization [1].

Immersive technologies such as Virtual Reality (VR), Augmented Reality (AR), and Mixed Reality (MR) can offer a novel teaching tool as a virtual lab for teachers and students to address these challenges. [2]. In MR, users can interact with digital objects in the real world typically with a headset with transparent lenses. MR can also make it possible to explore inside a 3D object, which is not feasible in real experiment labs. As an example, MR can help students better understand mechanical structures and their responses by providing a 3D immersive environment to explore and interact with the structure and capture concepts such as stress (internal force) and strain (deformation). Furthermore, it has been proven to reduce the cognitive load on the brain and improve students' focus and attention. MR can also simulate complex engineering systems and scenarios, reducing the need for costly physical prototypes and minimizing risks associated with real-world testing. Employing MR for setting up virtual labs can also remove the logistical hindrances of a physical lab and even promote an internet-based learning platform [3].

HoloMech is an MR-based application developed at Uppsala University to enhance the education in Solid Mechanics. The HoloMech application has been demonstrated and used for several study programs including Mechanical Engineering, Construction Engineering, and Engineering Physics, receiving positive feedback from the students.

In this talk, HoloMech will be presented, and there will also be opportunity for hands-on experience with HoloMech, allowing the participants to explore the possibilities of immersive technology within the context of higher education pedagogy. During this session, we will share the results of evaluation of HoloMech based on the feedback collected from the students. Furthermore, the potential benefits and innovative ways of integrating MR technology into the learning process will be discussed.

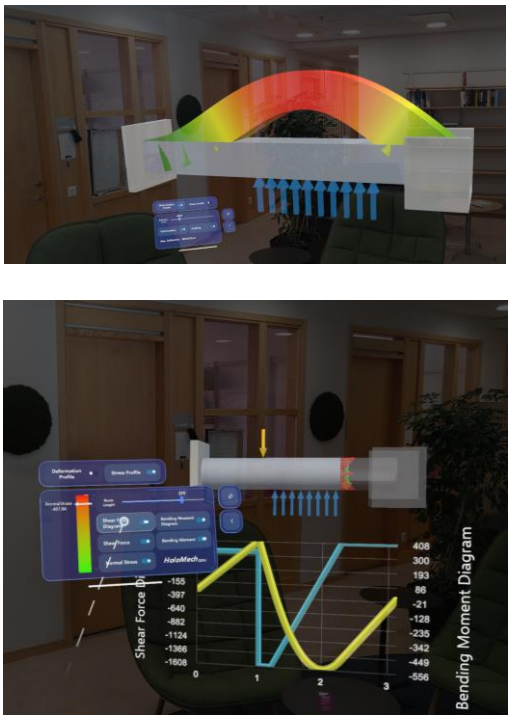

Figure 1: HoloMech: Beam bending with deformation and internal forces including stress resultants and stress components

References

[1] Dan, A. and Reiner, M. (2017). Reduced mental load in learning a motor visual task with virtual 3D method. Journal of Computer Assisted Learning, 34(1), pp.84-93.

[2] Lu, S. and Liu, Y. (2014). Integrating augmented reality technology to enhance children's learning in marine education. Environmental Education Research, 21(4), pp.525-541.

[3] Tuli, N., Singh, G., Mantri, A., & Sharma, S. (2022). Augmented reality learning environment to aid engineering students in performing practical laboratory experiments in electronics engineering. Smart Learning Environments, 9(1), 1-20.

Corresponding author email:
mahmoud.mousavi@angstrom.uu.se
kaveh.amouzgar@angstrom.uu.se

Acknowledgment:

The authors acknowledge the financial support by the Uppsala University project grant for educational development (PUMA).

MATERIAL CHARACTERIZATION OF A HIGH PRESSURE DIE CAST SECONDARY ALUMINUM ALLOY

B. Dalai[1], S. Jonsson[1], M. da Silva[2], L. Yu[3], J. Kajberg[1]

[1]*Division of Solid Mechanics, Department of Engineering Sciences and Mathematics, Luleå University of Technology, 97187, Luleå, Sweden*

[2]*Eurecat, Centre Tecnològic de Catalunya, Unit of Metallic and Ceramic Materials, 08290, Cerdanyola del Vallès, Spain*

[3]*Chemical Technology, Department of Civil, Environmental and Natural Resources Engineering, Luleå University of Technology, 97187, Luleå, Sweden*

The current structural castings used in the automotive industry are exteremely thin walled (of the order of 2.5 mm) and of large dimensions, and therefore require to be processed through high pressure die casting (HPDC) [1]. The conventional HPDC alloys possess high Fe content up to around 1.5 wt% [2], which promotes the formation of brittle platelets of β-Al_5FeSi phase during the casting process [3], thereby severely affecting the ductility of the component. This has led to the development of primary AlSi10MnMg alloy by adding Mn in a range of 0.4-0.8 wt% and restricting Fe content to 0.2 wt%. Addition of Mn bypasses the formation of deleterious β-Fe phase via evolution of less problematic α-Fe phase. However, limiting the Fe content in the material significantly increases the production cost. In addition, the current era calls for production of sustainable materials that are more environment friendly with respect to industrial applications. Thus, there is a growing interest for recycled secondary alloys to be used in the HPDC process for manufacturing the structural parts of automobiles. The usage of secondary alloys, which usually contain a little higher Fe content than primary AlSi10MnMg alloy, can significantly reduce the production cost and CO_2 emission and arguably still be able to exhibit mechanical properties within a range that are desirable in the cast components [4,5].

Thus, the aim of the current work is to investigate the microstructure evolution in a 2 mm thick casting of a novel recycled secondary Al alloy (denoted as AlSi10MnMg(Fe)) processed by vacuum assisted HPDC and the resultant mechanical properties and deformation behavior. First, the microstructure of the as-cast part was analyzed, revealing 3 constituents: (i) α-Al primary phases, (ii) α-Fe/Mn intermetallic compounds, and (iii) Al-Si eutectic clusters. The microstructure evolution starting from the surface layer through the depth up to the center of the casting could be divided into 3 regions with distinct features: (i) "skin" layer at the surface, indicated by very fine α-Al phases, (ii) a mixture of same amount of α-Al and Al-Si phases next to the skin layer, and (iii) gradual increase in the amount of α-Al primary phases with simultaneous decrease in that of Al-Si eutectic phase towards the center of the casting. The hardness distribution profile of the cast part corroborated well with the microstructure evolution through the thickness. Having said that, the formation of skin on the casting surface was found to be relatively irregular in the as-cast parts, which is supposed by the inhomogeneous molten metal flow inside the die cavity. Finally, the tensile properties of the cast parts were measured through uniaxial tensile tests at room temperature with 0.001 s^{-1} strain rate. The results from the tests manifested that the yield strength of the secondary alloy used in the current study is comparable with that expected by the primary alloy [5]. In terms of total elongation, our secondary alloy showed a large variation for the tested samples. The subsequent fracture surface analysis revealed that the restricted ductility is due to the presence of cold flakes (defects that are imparted during the HPDC process) at the casting surface which promoted undesirable crack initiation during the tensile tests.

References

[1] F. Bonollo, N. Gramegna, G. Timelli, High-Pressure Die-Casting: Contradictions and Challenges, JOM. 67 (2015) 901–908.

[2] J.A. Taylor, Iron-Containing Intermetallic Phases in Al-Si Based Casting Alloys, Procedia Mater. Sci. 1 (2012) 19–33.

[3] G. Gustafsson, T. Thorvaldsson, G.L. Dunlop, The influence of Fe and Cr on the microstructure of cast Al-Si-Mg alloys, Metall. Trans. A. 17 (1986) 45–52.

[4] A. Niklas, A. Baquedano, S. Orden, E. Noguès, M. Da Silva, A.I. Fernández-Calvo, Microstructure and Mechanical Properties of a New Secondary AlSi10MnMg(Fe) Alloy for Ductile High Pressure Die Casting Parts for the Automotive Industry, Key Eng. Mater. 710 (2016) 244–249.

[5] Trimal®-05 data sheet, Trimet-05: Die cast alloy for crash-relevant applications, (2008). https://www.trimet.eu/en/products/foundry-alloys/trimal-05.

Corresponding author email: biswajit.dalai@ltu.se